

**A Fluidized Immunoabsorption Device for Removing  
Beta-2-Microglobulin from Whole Blood:  
A Potential Treatment for Dialysis-Related Amyloidosis**

by

**Eric A. Grovender**

B.S. Chemical Engineering  
Iowa State University, 1996

SUBMITTED TO THE DEPARTMENT OF CHEMICAL ENGINEERING IN PARTIAL  
FULFILLMENT OF THE REQUIREMENTS FOR THE DEGREE OF

**DOCTOR OF PHILOSOPHY**  
AT THE  
**MASSACHUSETTS INSTITUTE OF TECHNOLOGY**

JUNE 2003

© 2003 Massachusetts Institute of Technology. All rights reserved.

Signature of Author \_\_\_\_\_

Department of Chemical Engineering  
April 14, 2003

Certified by \_\_\_\_\_

Robert Langer  
Germeshausen Professor of Chemical and Biomedical Engineering  
Thesis Supervisor

Accepted by \_\_\_\_\_

Daniel Blankschtein  
Professor of Chemical Engineering  
Chairman, Department Graduate Committee



This Doctoral Thesis has been examined by the following Thesis Committee:

**Robert Langer, Sc.D.**

**Thesis Supervisor**

Germeshausen Professor of Chemical and Biomedical Engineering  
Department of Chemical Engineering  
Massachusetts Institute of Technology  
Cambridge, Massachusetts

**Charles Cooney, Ph.D.**

Professor  
Department of Chemical Engineering  
Massachusetts Institute of Technology

**Hidde Ploegh, Ph.D.**

Professor  
Department of Pathology  
Harvard Medical School  
Boston, Massachusetts

**Maria Rupnick, M.D., Ph.D.**

Division of Cardiovascular Medicine  
Brigham and Women's Hospital  
Boston, Massachusetts



# **A Fluidized Immunoabsorption Device for Removing Beta-2-microglobulin from Whole Blood: A Potential Treatment for Dialysis-Related Amyloidosis**

by

**Eric A. Grovender**

Submitted to the Department of Chemical Engineering on  
April 14, 2003 in partial fulfillment of the requirements for the degree of  
Doctor of Philosophy in Chemical Engineering

## **Abstract**

Dialysis-related amyloidosis (DRA) is a frequent complication of end-stage renal disease that has been associated with the accumulation of  $\beta_2$ -microglobulin ( $\beta_2$ m). Excluding transplantation, existing kidney replacement technologies are believed to remove insufficient quantities of  $\beta_2$ m for the prevention of DRA, as they are non-specific and based on size-exclusion. A proposed DRA therapy is to use immunoabsorptive particles within an extracorporeal Vortex Flow Plasmapheretic Reactor (VFPR) to specifically remove  $\beta_2$ m from blood. The compartmental design of the VFPR allows for the use of small adsorbent particles ( $\sim 100\ \mu\text{m}$ ) that possess inherent mass-transfer advantages over the larger ones ( $>400\ \mu\text{m}$ ) that are required for safe contact with whole blood for this application. Demonstrating the efficacy of this technology as a therapy for DRA would support its tailored application for treating other pathologies that are caused by circulating compounds such as sepsis, liver failure, autoimmune disease, drug overdoses, and genetic disorders.

Whole anti- $\beta_2$ m antibodies (BBM.1) were immobilized onto agarose beads and used within a VFPR to remove donor baseline and defined quantities of recombinant  $\beta_2$ m from whole human blood, *in vitro*. A dynamic immunoabsorption model was developed for the VFPR that was based upon the independent characterization of the mass-transfer processes within the VFPR and the thermodynamics of the immunoabsorbent. The experimentally-observed and model-predicted dynamics of  $\beta_2$ m clearance from the blood indicate that the process controlling the rate of  $\beta_2$ m removal was the hemofiltration rate (50 mL-plasma/min),

which was on the order of the reported supply rate of  $\beta_2m$  into the vasculature (70 mL-plasma/min).

Single-chain variable region (scFv) antibody fragments offer several potential advantages over whole antibodies due to their size and genetic definition, as well as their amenability for microbial expression and *in vitro* evolution. Hence, a BBM.1 scFv was expressed by a yeast display vector and its affinity was quantified with a fluorescence-activated cell sorter ( $K_D = 0.008 \pm 0.004$  mg- $\beta_2m/L$ ). Soluble scFv was secreted by yeast and immobilized onto agarose beads (adsorption site density of  $0.41 \pm 0.01$  mg- $\beta_2m/mL$ -settled-gel). These results support the feasibility of using the proposed therapy to treat and/or prevent DRA.

*Thesis Supervisor: Robert Langer*

*Title: Germeshausen Professor of Chemical and Biomedical Engineering*

## Acknowledgements

I would like to thank my thesis advisor, Professor Robert Langer, for providing me with the opportunity and privilege of working in his laboratory on this project. Throughout my tenure, the faith that Bob has exhibited in my abilities as a researcher has encouraged and inspired me as an engineer and scientist. There are many members of the Langer Laboratory who have been very helpful over the years, but it is not feasible for me to thank them all here by name. However, I would like to specifically thank Guillermo Ameer, who is now an Assistant Professor of Biomedical Engineering at Northwestern University, for being my friend and mentor over the past five or six years. His support and advice have been an invaluable part of my graduate school experience. I am also grateful for the work that has been performed on this project by several undergraduate researchers at MIT, specifically: David Ting, Helen Lee, Amy Kittredge, Angela Won, and Eric Lau.

I am thankful for the support and guidance that I have received from the members of my Thesis Committee. This research project would have never occurred without Dr. Maria Rupnick, as she was its original champion. Meanwhile, Professor Charlie Cooney provided valuable advice regarding the mathematical modeling of the Vortex Flow Plasmaphoretic Reactor. Professor Hidde Ploegh has graciously contributed his expertise in the field of immunology to the project, while several members of his research group have been very helpful with the production of recombinant human  $\beta_2$ -microglobulin, including: Madelone Maurice, Ben Gewurz, Evelyn Wang, and Fleur Sernee.

While they did not serve my Thesis Committee, two other MIT professors also have been extremely helpful. The development of the scFv-based immunoadsorbent may not have been possible without the collaboration of Professor K. Dane Wittrup (Chemical Engineering) and several members of his laboratory, including: Brenda Kellogg, Andy Yeung, Jeffrey Swers, and Katarina Midelfort. The refolding yield of the recombinant human  $\beta_2$ -microglobulin was drastically increased by following the advice of Professor Jonathan King (Biology) and his post-doc, Stephen Raso.

I had several outstanding professors as an undergraduate at Iowa State University whom I would like to thank for their teaching, mentorship, and guidance. I would like to specifically acknowledge Professor Richard Seagrave who was the most dynamic and

engaging lecturer one could imagine and inspired me to earn my Ph.D. Furthermore, I am forever grateful to Dr. Carole Heath, now at Immunex, for introducing me to the field of bioengineering as a sophomore and providing me with the opportunity to conduct my undergraduate independent research project. There are two teachers at Woodbury Senior High School (Minnesota) whose courses I believe laid the foundation for the success that I experienced at ISU and MIT. They are Judy Trepka and Brian Bonfig who taught Advanced Placement Chemistry and Advanced Placement Calculus, respectively. America desperately needs more teachers such as them.

I would like to thank my entire family and all of my friends for supporting me throughout my 24-year education. I am particularly grateful to both of my parents for always caring about and encouraging my academic success and achievement. I can still remember experimenting with electric circuits and chemistry sets at a very young age (well under 10 years old) with my Father. I also appreciate all of the support I received and time invested in me by my Mother throughout my competitive swimming career, which I believe has helped me more with my academic career than any single course that I have ever taken.

Finally, I would like to thank Kim Bigelow, my girlfriend throughout most of my graduate education, for all of her love, friendship, support and understanding.

**Eric A. Grovender**  
**April 2003**

*This material is based on work supported under a National Science Foundation Graduate Fellowship as well as a National Institutes of Health Biotechnology Training Grant.*

# Biographical Sketch (Curriculum Vitae)

for

**Eric A. Grovender**

## Education

***Ph.D. Chemical Engineering, Massachusetts Institute of Technology, Spring 2003***

GPA: 4.50/5.00

Thesis Advisor: Robert S. Langer

Thesis Title: “A Fluidized Immunoabsorption Device for Removing Beta-2-Microglobulin from Whole Blood: A Potential Treatment for Dialysis-Related Amyloidosis”

Thesis Description: Developed a biotherapeutic device to remove a specific protein ( $\beta_2$ -microglobulin) from blood that forms solid deposits throughout the bodies of kidney dialysis patients

- Engineered a single-chain variable region (scFv) antibody fragment via yeast display
  - Purified immunoglobulin proteins secreted by yeast and hybridoma cells
  - Scaled-up production (>100 mg) of recombinant human  $\beta_2$ -microglobulin expressed in *E. coli*
  - Tested the feasibility of the proposed therapy through in vitro experimentation with human blood
  - Characterized the mass-transfer and thermodynamic behavior of the novel biomedical device
  - Developed a mathematical device model, based on chemical engineering fundamentals
- Biology Minor: Courses in immunology, genetics, biochemistry, cell/tissue engineering, and controlled release drug delivery

***B.S. Chemical Engineering, Iowa State University, Ames, IA, 1996***

GPA: 3.99/4.00

Independent Tissue Engineering Research Project: “Estimation of the Specific Oxygen and Glucose Uptake Rates of Chondrocytes Living in Cartilage Grown *In Vitro*.”

Biology Elective Courses: Biochemistry, Bioprocess Engineering

Extracurricular: Men’s Intercollegiate Swimming Team (Division I)

## Industrial

***Medtronic MiniMed, Northridge (Los Angeles), CA***

Position: Senior Scientist, Sensor Research and Development, starting May 19, 2003

***Abbott Laboratories, Chemical and Agricultural Products Division, North Chicago, IL***

Position: Intern with the Tissue Culture Department, summer 1996

- Identified glutamine as the potential limiting nutrient in the culture of Chinese hamster ovary (CHO) cells
- Presented research findings to the department, including management (oral and written)

***3M Company, Engineering Systems and Technology Group, St. Paul, MN***

Positions: Graduate Intern, Jan-July 1997; Contract Employee, summer 1995

- Designed and built the graphical user interface (GUI) for a drying process simulation program which enabled its distribution to manufacturing facilities
- Created a shareware database of coating solution physical parameters for the drying process simulation program

***Cargill, Oilseeds Division, Des Moines, IA***

Position: Process Engineering Intern, summer 1994

- Performed an energy balance on the refining process which discovered that the majority of the oil feed stream was bypassing a key heat exchanger
- Supervised plant operators and contractors

<b>Leadership</b>	Teaching Assistant, MIT Chemical Engineering Senior Design Course, 2001 Assistant Coach, Boy's Varsity Swimming Team, St. Paul Central H.S. (MN), 1995-1997
<b>Biology Lab Skills</b>	Tissue culture, yeast & bacterial fermentation, PCR, inclusion body refolding, yeast display of proteins, size exclusion and affinity chromatography, antibody/protein engineering, FACS, radioimmunoassay, protein and DNA electrophoresis, Western blots
<b>Hobbies</b>	Wilderness camping, fishing, canoeing, backpacking, cycling, running, triathlons, SCUBA diving
<b>Computer Skills</b>	Visual Basic for Applications, FORTRAN, Lotus Notes, Word, Excel, PowerPoint, Windows/DOS, software & hardware maintenance
<b>Awards</b>	National Institutes of Health Biotechnology Training Grant, 2000-2003 National Science Foundation Graduate Fellowship, 1997-2000 ISU Engineering College Senior Scholastic Award (one of top 3 graduates), 1997 Iowa State University Chemical Engineering Department Junior and Senior of the Year, 1995 AIChE Donald F. Othmer Sophomore Academic Excellence Award, 1994 NCAA Academic All-Big 8 Conference Swimming Team, 1993 & 1994
<b>Papers</b>	<p>“Single-Chain Antibody Fragment-Based Adsorbent for the Extracorporeal Removal of <math>\beta_2</math>-microglobulin.” In Preparation.</p> <p>“Immunoabsorption Model for a Novel Fluidized-bed Blood Detoxification Device.” EA Grovender, CL Cooney, R Langer, and GA Ameer. <i>AIChE Journal</i> 48 (2002): 2357-2365.</p> <p>“Modeling the Mixing Behavior of a Novel Fluidized Extracorporeal Immunoabsorber.” EA Grovender, GA Ameer, CL Cooney and RS Langer. <i>Chemical Engineering Science</i> 56 (2001): 5437-5441.</p> <p>“A Novel Immunoabsorption Device for Removing <math>\beta_2</math>-microglobulin from Whole Blood.” GA Ameer &amp; EA Grovender, H Ploegh, D Ting, WF Owen, M Rupnick, and R Langer. <i>Kidney International</i> 59 (2001): 1544-1550.</p> <p>“RTD Analysis of a Novel Taylor-Couette Flow Device for Blood Detoxification.” GA Ameer, EA Grovender, B Obradovic, CL Cooney, and R Langer. <i>AIChE Journal</i> 45 (1999): 633-638.</p>
<b>Patent</b>	“Apparatus for Treating Whole Blood Comprising Concentric Cylinders Defining an Annulus There Between.” G Ameer, RS Langer, M Rupnick, HL Ploegh and EA Grovender, <i>US Patent No. 6,099,730</i> (2000).
<b>Presentations</b>	<p>“Mixing Behavior of a Novel Fluidized-bed Blood Detoxification Device.” <i>International Society for Blood Purification Annual Meeting</i>, Tokyo (2001).</p> <p>“Dynamic Modeling of a Fluidized Bed Immunoabsorber for Therapeutic Blood Detoxification.” <i>American Institute of Chemical Engineers National Meeting</i>, Los Angeles (2000).</p> <p>“Therapeutic Blood Detoxification via an Immunoabsorptive Fluidized Bed.” <i>Biomedical Engineering Society National Meeting</i>, Seattle (2000).</p>

# Table of Contents

<b>Title Page</b> .....	<b>1</b>
<b>Committee Page</b> .....	<b>3</b>
<b>Abstract</b> .....	<b>5</b>
<b>Acknowledgements</b> .....	<b>7</b>
<b>Biographical Sketch (Curriculum Vitae)</b> .....	<b>9</b>
<b>Table of Contents</b> .....	<b>11</b>
<b>List of Figures</b> .....	<b>15</b>
<b>List of Tables</b> .....	<b>17</b>
<b>Chapter 1: Introduction</b> .....	<b>19</b>
1.1 MOTIVATION .....	19
1.2 SPECIFIC AIMS .....	23
1.3 THE VORTEX FLOW PLASMAPHERETIC REACTOR (VFPR) .....	24
1.4 REFERENCES.....	27
<b>Chapter 2: In Vitro Removal of <math>\beta_2</math>-Microglobulin from Human Blood with an Immunoabsorptive VFPR</b> .....	<b>31</b>
2.1 INTRODUCTION .....	31
2.2 METHODS .....	31
2.2.1 Assays .....	31
2.2.2 Protein Immobilization.....	32
2.2.3 Recombinant $\beta_2$ m Preparation .....	32
2.2.4 Capacity of the Immunoabsorptive Media .....	33
2.2.5 Clearance of $\beta_2$ m from Whole Blood by a VFPR in a Closed-Loop Circuit ..	34
2.2.6 Statistical Analysis .....	35
2.3 RESULTS .....	35
2.3.1 Protein Immobilization.....	35
2.3.2 Capacity of the Immunoabsorptive Media .....	35
2.3.3 Clearance of $\beta_2$ m from Human Blood with an Immunoabsorptive VFPR.....	36
2.4 DISCUSSION .....	38
2.5 REFERENCES.....	42

<b>Chapter 3: Macroscopic Mixing Model for the VFPR.....</b>	<b>45</b>
3.1 INTRODUCTION .....	45
3.2 METHODS .....	45
3.2.1 Reactor Prototypes.....	45
3.2.2 Residence Time Distribution Experiments.....	46
3.2.3 Mathematical Modeling.....	47
3.3 RESULTS AND DISCUSSION .....	49
3.4 REFERENCES.....	57
<b>Chapter 4: Immunoadsorption Model for the VFPR .....</b>	<b>59</b>
4.1 INTRODUCTION .....	59
4.2 IMMUNOADSORPTIVE GEL.....	59
4.2.1 Solute Partitioning .....	59
4.2.2 Adsorption Isotherm.....	60
4.2.3 Adsorption Site Distribution.....	61
4.2.4 Effective Diffusivity .....	62
4.3 DEVICE MODEL.....	62
4.3.1 Blood Compartment .....	62
4.3.2 Active Plasma Compartment (APC) .....	63
4.3.3 Plasma Line, Collection Chamber, and Blood Outlet Port.....	65
4.4 RESERVOIR MODEL.....	65
4.5 CHARACTERIZATION OF MASS-TRANSFER TO THE SURFACE OF SUSPENDED PARTICLES.....	66
4.6 COMPUTATIONAL METHODS.....	67
4.7 RESULTS AND DISCUSSION .....	67
4.8 REFERENCES.....	78

<b>Chapter 5: ScFv-Based Immunoabsorbent .....</b>	<b>79</b>
5.1 INTRODUCTION .....	79
5.2 METHODS .....	79
5.2.1 Labeling of $\beta_2m$ .....	79
5.2.2 Cloning of $V_H$ and $V_L$ genes .....	80
5.2.3 Display of scFv fragment by yeast.....	81
5.2.3.1 <i>Insert Assembly</i> .....	81
5.2.3.2 <i>Plasmid Construction</i> .....	82
5.2.3.3 <i>Yeast Transformation, Growth, and Induction</i> .....	82
5.2.3.4 <i>Yeast Labeling</i> .....	83
5.2.3.5 <i>FACS Analysis</i> .....	83
5.2.3.6 <i>Mathematical Modeling</i> .....	84
5.2.4 Secretion of scFv fragment by yeast.....	85
5.2.4.1 <i>Plasmid Construction</i> .....	85
5.2.4.2 <i>Yeast Transformation, Growth, and Induction</i> .....	86
5.2.4.3 <i>Protein Purification</i> .....	87
5.2.5 Immunoabsorbent based on scFv fragment .....	87
5.2.5.1 <i>Protein Immobilization</i> .....	87
5.2.5.2 <i>Characterization</i> .....	88
5.2.6 Statistical Analysis .....	90
5.3 RESULTS .....	90
5.3.1 Cloning of $V_H$ and $V_L$ genes .....	90
5.3.2 Display of scFv fragment by yeast.....	91
5.3.3 Secretion of scFv fragment by yeast.....	91
5.3.4 Immunoabsorbent based on scFv fragment .....	91
5.4 DISCUSSION .....	93
5.5 REFERENCES.....	102
<b>Chapter 6: Afterword.....</b>	<b>105</b>
6.1 SUMMARY AND CONCLUSIONS .....	105
6.2 RECOMMENDATIONS FOR FUTURE WORK.....	110
6.2.1 Optimization of ScFv Production .....	110
6.2.2 Optimization of ScFv Purification.....	111
6.2.3 Optimization of ScFv Immobilization .....	111
6.3 REFERENCES.....	113
<b>Appendix: Immunoabsorption Model FORTRAN 77 Program.....</b>	<b>115</b>



## List of Figures

Figure 1.1 Structural comparison of whole antibodies and single-chain variable region antibody fragments (scFv).....	25
Figure 1.2 The Vortex Flow Plasmapheretic Reactor (VFPR).....	26
Figure 2.1 Diagram of the circuit used to study the clearance $\beta_2m$ of from human blood. ....	41
Figure 2.2 Dynamics of $r\beta_2m$ clearance from human blood with a BBM.1-loaded VFPR, <i>in vitro</i> .....	41
Figure 3.1 Photograph of the new, larger VFPR prototype.....	53
Figure 3.2 Schematic diagram of the experimental setup used to obtain RTDs from the plasma port. ....	54
Figure 3.3 The compartmental mixing model for the VFPR. ....	54
Figure 3.4 Blood port residence time distribution functions for the small (top: a,b) and large (bottom: c,d) VFPR prototypes at plasma pump flowrates of 50 (left: a,c) and 100 (right: b,d) mL/min.....	55
Figure 3.5 Plasma port RTD curves for the small (top: a,b) and large (bottom: c,d) VFPR prototypes at plasma pump flowrates of 50 (left: a,c) and 100 (right: b,d) mL/min.....	56
Figure 4.1 Schematic diagram of the dynamic VFPR adsorption model. ....	71
Figure 4.2 Closed-loop blood detoxification with the VFPR. ....	72
Figure 4.3 Apparatus used to conduct the dissolution studies.....	73
Figure 4.4 Equilibrium adsorption behavior of the immunoadsorptive media. ....	74
Figure 4.5 Confocal micrograph of the immunoadsorptive gel: center cross-section of a typical bead (a) and an atypical bead (b).....	75
Figure 4.6 The predicted and observed dynamics of $\beta_2m$ clearance from whole blood by an immunoadsorptive VFPR, <i>in vitro</i> .....	76
Figure 4.7 Sensitivity analysis results for the model parameters $k_m$ (a), $R$ (b), $D_e$ (c), and $\Phi$ (d).....	77
Figure 5.1 Schematic diagram of yeast display.....	97
Figure 5.2 Custom primers used for PCR. ....	98

<b>Figure 5.3 V<sub>H</sub> and V<sub>L</sub> Genes Cloned from the BBM.1 Hybridoma.....</b>	<b>99</b>
<b>Figure 5.4 Titration of BBM.1-scFv displaying yeast with fluorescent <math>\beta_2m</math>.....</b>	<b>100</b>
<b>Figure 5.5 The scFv fragment secreted by YVH10 yeast transformed with pEAG3. ..</b>	<b>101</b>
<b>Figure 5.6 SDS-PAGE of the secreted BBM.1-scFv fragment after nickel affinity purification. ....</b>	<b>101</b>
<b>Figure 6.1 Immunoabsorption model-predicted clearance of <math>\beta_2m</math> from whole blood by the large VFPR prototype loaded with the hypothetical scFv-based adsorbent...</b>	<b>109</b>

## List of Tables

Table 2.1 Capacity of the Immunoadsorptive Media .....	35
Table 2.2 Clearance of $\beta_2m$ from Human Blood by the VFPR, <i>In Vitro</i> . .....	36
Table 2.3 Complete Blood Count Data for the BBM.1 VFPR Experiments ( $N=4$ ).....	37
Table 2.4 Total Protein Data for the VFPR BBM.1 Experiments and BSA Controls....	37
Table 3.1 Comparison of the compartmental volumes of the two VFPR Prototypes....	46
Table 3.2 Comparison of the pertinent length scales of the two VFPR Prototypes.....	46
Table 3.3 Model parameters calculated from the blood port RTD data for the small VFPR prototype. ....	50
Table 3.4 Model parameters calculated from the blood port RTD data for the large VFPR prototype. ....	50
Table 3.5 Model Parameters calculated from the plasma port RTD data for the small VFPR prototype. ....	51
Table 3.6 Model Parameters calculated from the plasma port RTD data for the large VFPR prototype. ....	52
Table 4.1 Model input parameters. ....	69
Table 5.1 $\beta_2m$ -Adsorption Site Density of the Immunoadsorptive Media ( $\rho'_s$ )......	92
Table 6.1 Immunoadsorption model input parameters for the large VFPR prototype loaded with the hypothetical scFv-based adsorbent. ....	108



# Chapter 1: Introduction

## 1.1 MOTIVATION

A frequent complication of end-stage renal disease (ESRD) is dialysis-related amyloidosis (DRA), a debilitating disorder associated with the long-term accumulation of  $\beta_2$ -microglobulin ( $\beta_2m$ ) [Gejyo *et al.*, 1985; Drueke, 2000]. Symptoms are caused by the formation of amyloid deposits and include chronic pain, carpal tunnel syndrome, nerve compressions, and cystic bone lesions with associated fractures.  $\beta_2m$ , the primary constituent of DRA amyloid, is a highly conserved globular protein (11.8 kD) that is secreted by all nucleated cells and is specifically removed from the blood plasma by healthy kidneys. Presently, there are no widely available treatments to prevent this chronic and debilitating disease, short of a kidney transplant. Conventional kidney function replacement technologies such as hemodialysis, hemodiafiltration, and peritoneal dialysis are believed to remove insufficient quantities of  $\beta_2m$ , as they are non-specific and based on size-exclusion [Ameer, 2001]. Even so, research has revealed a correlation between the removal of  $\beta_2m$  from the circulation and a delay in the occurrence of symptoms [Miyata *et al.*, 1998; Drueke, 2000; Lornoy *et al.*, 2000]. In recent years, adsorbents that are based on hydrophobic adsorption and size-exclusion (Lixelle® and Betasorb®) have been developed for the extracorporeal removal of  $\beta_2m$  [Furuyoshi *et al.*, 1998; Davankov *et al.*, 2000]. However, their specificity and/or affinity for  $\beta_2m$  remains in question, complicating the evaluation of patient outcome due to their use [Tsuchida *et al.*, 1998; Reiter *et al.*, 2002; Tsuchida *et al.*, 2002].

Ideally, an adsorbent material for the extracorporeal removal of  $\beta_2m$  should be highly specific, so as to prevent the significant loss of proteins and other molecules that are beneficial to the patient. Furthermore, a highly specific  $\beta_2m$ -adsorbent material could also serve as a valuable tool for research. It could potentially be used to study the therapeutic efficacy of  $\beta_2m$  clearance independent of the removal of other molecules that have also been implicated in the pathogenesis of DRA, such as inflammatory cytokines [Miyata *et al.*, 1994; Matsuo *et al.*, 2000; Niwa, 2001]. The optimal  $\beta_2m$ -adsorbent should possess an affinity for  $\beta_2m$  that is strong enough to bring the concentration to a level that is well below normal (1 mg/mL [Floege and Ketteler, 2001]). This high affinity would serve to increase the rate of  $\beta_2m$  removal from the patient by maximizing the concentration gradient that drives the mass-

transfer rate of  $\beta_2m$  to the adsorption sites. Along these lines, the adsorbent material should consist of small porous particles in order to minimize the time-scales of convective and diffusive mass-transport.

Antibodies are a logical choice as the active species (or ligand) on which to base a  $\beta_2m$ -adsorbent material, as they can be highly specific and possess a high affinity for their target molecules. In the past, antibodies immobilized onto small porous beads have been used to clear  $\beta_2m$  from human plasma [Mogi *et al.*, 1989; Nakano *et al.*, 1991; Vallar *et al.*, 1995; Shabunina *et al.*, 2001]. However, this research did not address the challenge using of small (i.e. 100  $\mu m$ ) immunoadsorbent particles for the removal of  $\beta_2m$  from whole blood in a clinically feasible system. It is necessary to perform plasmapheresis (the separation of plasma from blood cells) before using small (< 400  $\mu m$ ) beads for the extracorporeal removal of  $\beta_2m$  because unacceptably high levels of blood cell lysis occur when packed beds of this type are perfused with whole blood (direct hemoperfusion or DHP) under these conditions [Furuyoshi *et al.*, 1998]. While packed beds of relatively large (> 400  $\mu m$ ) beads (Lixelle® and Betasorb® columns) have been safely used for this application [Furuyoshi *et al.*, 1998; Davankov *et al.*, 2000], they possess inherent mass-transfer limitations. In fact, due to the low surface area to volume ratio of such large particles, the rate of toxin removal is directly proportional to the volume of adsorbent. Hence, increasing the volume of adsorbent used for DHP can increase the rate of blood detoxification, but this comes at the expense of additional blood hold-up (a biocompatibility issue). This is why the volumes of DHP columns used to date (Lixelle® and Betasorb®) for the extracorporeal removal of  $\beta_2m$  have been kept below 350 mL [Furuyoshi *et al.*, 1998; Ronco *et al.*, 2001].

As immunoadsorption ligands, single-chain variable region antibody fragments (scFv, Figure 1.1) offer several potential advantages over whole polyclonal or monoclonal antibodies. The transfer of antibody genes to a defined expression vector provides the opportunity to eliminate the production of unwanted immunoglobulins. ScFv fragments are also smaller in size, which should theoretically allow for higher effective  $\beta_2m$  adsorption site densities (steric argument). This would reduce the volume of adsorbent required for therapeutic efficacy, thereby minimizing the retention of blood components during operation. Additionally, the properties (affinity, stability, expression yield) of scFv fragments can be engineered through *in vitro* evolution in a yeast display format [Boder and Wittrup, 1997;

Boder and Wittrup, 1998; Boder and Wittrup, 2000]. The fact that scFv fragments can be produced through microbial expression vectors provides greater flexibility for the optimization of the production process economics [Datar *et al.*, 1993]. Furthermore, very high yields (3.1 g-scFv/L-culture) of properly folded scFv fragments have been expressed in and purified from the cytoplasm of *E. coli* [Martineau *et al.*, 1998].

The Vortex Flow Plasmapheretic Reactor (VFPR, refer to Figure 1.2 and Section 1.3) is a multi-compartment extracorporeal device that was originally developed to carry out the safe and efficient enzymatic neutralization of heparin in whole blood [Ameer, Barabino *et al.*, 1999; Ameer, Raghavan *et al.*, 1999]. The VFPR is the first device designed to use Taylor vortices and a fluidized bed of particles to conduct a heterogeneous reaction or adsorption process on whole blood. A major advantage of fluidized beds over packed beds is that they exhibit lower pressure drops (when all other specifications are held constant) [Kunii and Levenspiel, 1977]. The fluidized bed of the VFPR also possesses an unusually high aspect ratio (length of the mesh divided by the radial distance between the membrane and mesh), which also contributes to its low-pressure drop (generally less than 20 mmHg). Most importantly, however, the compartmental design of the VFPR allows for the use of relatively small (approximately 100  $\mu\text{m}$ ) active particles that possess inherent mass-transfer advantages over larger ones. The relatively high surface area to volume ratio of these smaller particles could potentially allow for a significant reduction in the volume of the adsorbent required for the effective extracorporeal removal of  $\beta_2\text{m}$ , which would represent an improvement in biocompatibility.

The research presented herein investigates the feasibility of using the VFPR design for the immunoabsorptive extracorporeal removal of  $\beta_2\text{m}$  through experiments with whole human blood, *in vitro*. Initially, immobilized whole monoclonal antibodies and a device prototype are investigated as a model system. A mathematical model that describes the dynamic behavior of the immunoabsorptive VFPR is presented that is intended to serve as a design tool for future device prototypes, experiments, and potential clinical trials. Finally, a new type of immunoabsorbent for the extracorporeal removal of  $\beta_2\text{m}$  is developed that is based upon scFv antibody fragments. The goal of this research is to lay a foundation for a new extracorporeal  $\beta_2\text{m}$ -removal technology that is more specific, biocompatible, and effective than existing methods. Demonstrating the efficacy of this technology as a therapy

for DRA would support its tailored application for treating other pathologies that are caused by circulating compounds such as sepsis, liver failure, autoimmune disease, drug overdoses, and genetic disorders.

## 1.2 SPECIFIC AIMS

This thesis investigates feasibility of using the VFPR design with immobilized antibodies for the extracorporeal removal of  $\beta_2\text{m}$  as a potential therapy for DRA. More specifically, this thesis aims to:

1. Evaluate the biocompatibility and efficacy of an immunoadsorptive VFPR for this application through experimentation with recombinant human  $\beta_2\text{m}$ , monoclonal antibodies, and a reservoir of whole human blood, *in vitro*. Here, biocompatibility will be assessed in terms of the effect that the immunoadsorptive device has on blood components (complete cell count, total protein, and plasma free hemoglobin). The efficacy of the device is defined as its ability to bring the  $\beta_2\text{m}$  concentration down to a level that is below the normal range of healthy individuals (1.0-3.0 mg/L [Floege and Ketteler, 2001]) at a clinically relevant flowrate (on the order of 70 mL-plasma/min, the approximate flowrate of extravascular  $\beta_2\text{m}$  into the circulation [Floege *et al.*, 1991]).
2. Develop a mathematical model for the immunoadsorptive VFPR that is based upon the independent characterization of the mass-transfer processes within the device and the thermodynamic behavior of a model immunoadsorbent.
3. Create and characterize a novel  $\beta_2\text{m}$ -adsorbent material that is based upon high-affinity scFv antibody fragments and possesses a mass ratio of adsorbed  $\beta_2\text{m}$  to immobilized antibody that is at or above the theoretical limit for bivalent whole antibodies (0.16 mg- $\beta_2\text{m}$ /mg-antibody). For this application, a high-affinity scFv fragment is defined as one that has an equilibrium dissociation constant that is well below the lower limit of  $\beta_2\text{m}$  concentrations found in healthy individuals ( $K_D \ll 1$  mg- $\beta_2\text{m}$ /L  $\approx$  100 nM). Creating an immunoadsorbent with a high mass ratio of adsorbed  $\beta_2\text{m}$  to immobilized antibody (under saturating conditions) would support the future development an immunoadsorbent with the highest  $\beta_2\text{m}$  adsorption site density reported to date ( $> 0.9$  mg- $\beta_2\text{m}$ /mL-settled-gel [Vallar *et al.*, 1995]).

### 1.3 THE VORTEX FLOW PLASMAPHERETIC REACTOR (VFPR)\*

A VFPR is constructed by counter-boring two concentric chambers within the outer cylinder wall of a Taylor-Couette vortex flow device (Figure 1.2). The collection chamber is sealed with a polyester mesh filter (15  $\mu\text{m}$  opening) to keep the fluidized bed of particles within the active plasma chamber. These particles are typically gel beads that are approximately 100  $\mu\text{m}$  in diameter, are highly porous, and have the active species immobilized onto them (i.e. an antibody or enzyme). The active plasma compartment is sealed with a 1  $\mu\text{m}$  pore-size, track-etched polyester membrane to prevent contact between blood cells and the gel beads. Compartmentalization in this novel Taylor-Couette flow device eliminates red cell lysis due to particle fluidization and prevents white cell and platelet activation due to contact with the active gel beads [Ameer, Harmon *et al.*, 1999].

During operation, whole blood is pumped into the inlet port (typically 200-400 mL/min) and channeled through the innermost annular, or “blood”, compartment. A dedicated peristaltic pump (“plasma pump”) controls the plasma flowrate through the microporous membrane, the active plasma compartment, and the plasma collection chamber (typically 50-75 mL/min). The rotation of the solid inner cylinder (usually at about  $1.2 \times 10^3$  rpm) is achieved via magnetic coupling and serves to create the Taylor vortices [Donnelly, 1991] in the blood compartment. These flow instabilities induce undulations throughout the unsupported microporous membrane, fluidizing the gel beads in the active plasma compartment. The cleansed plasma exits the active plasma compartment via the collection chamber, which retains the gel beads. The cleansed plasma is returned to the top of the device where it mixes with bypassed cells and plasma prior to exiting the VFPR via the blood outlet port. These mechanisms enable the VFPR to perform high-flux plasmapheresis in series with a fluidized bed reaction or adsorption process. The More detailed descriptions of specific device prototypes are provided Chapters 2 and 3 of this document and have been published elsewhere [Ameer, Barabino *et al.*, 1999; Ameer, Raghavan *et al.*, 1999].

---

\* This section has appeared in a research article originally published in the *AICHE Journal* [Grosvender *et al.*, 2002]. It has been reproduced with permission of the American Institute of Chemical Engineers. Copyright © 2002 AIChE. All rights reserved.

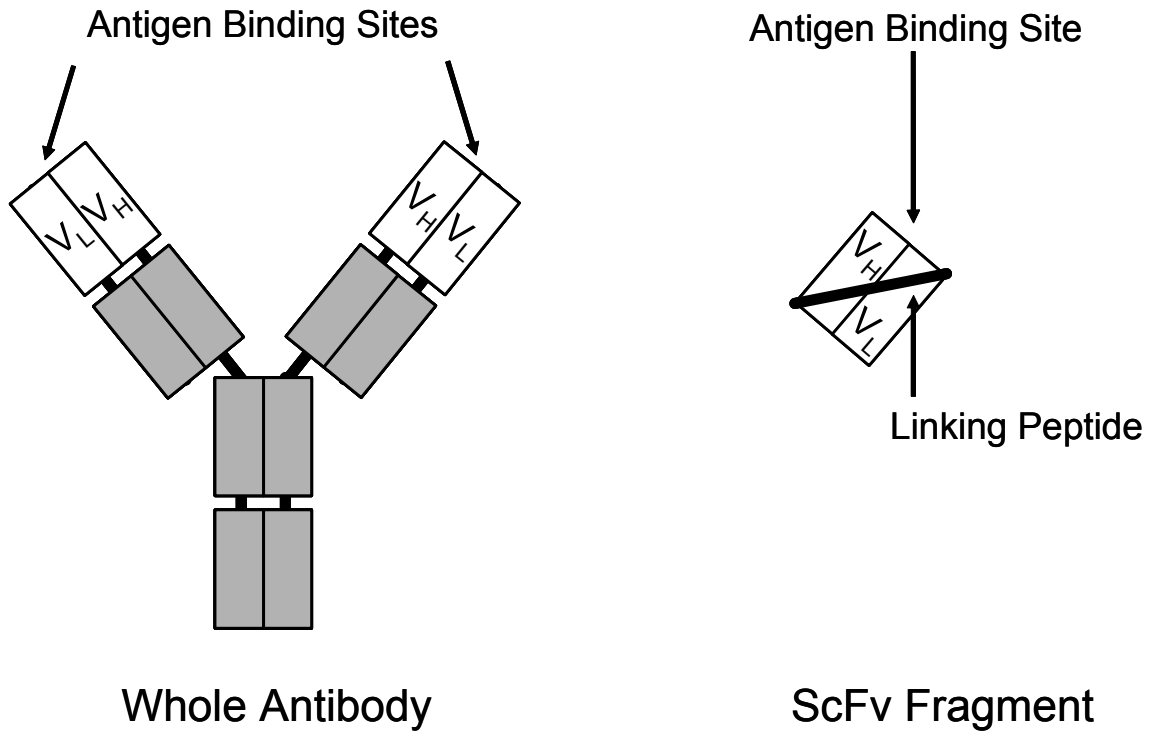


**Figure 1.1 Structural comparison of whole antibodies and single-chain variable region antibody fragments (scFv).** Whole antibodies are approximately 150 kD, while scFv fragments are generally 25-30 kD. The scFv fragment shown is assembled in a V<sub>H</sub>-linker-V<sub>L</sub> configuration.

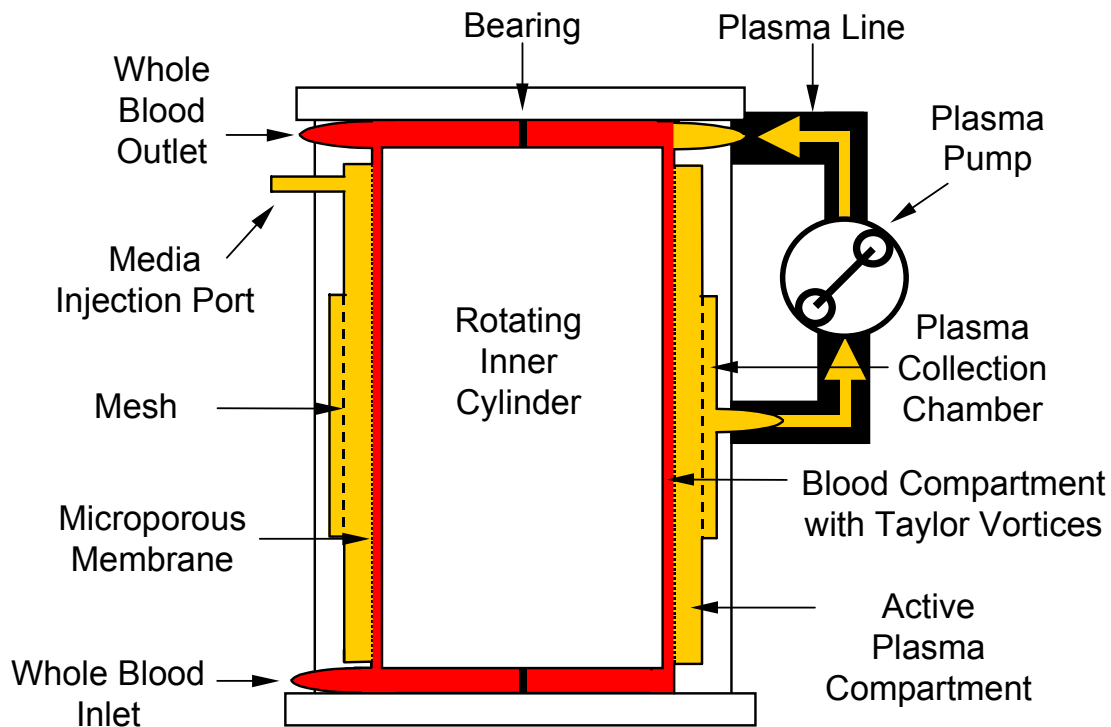


**Figure 1.2 The Vortex Flow Plasmapheretic Reactor (VFPR).**\* The whole blood path is shown in red, while the regions accessible only to plasma are shown in gold. The Taylor vortices in the blood compartment reduce the cell polarization layer formed at the surface of the membrane (allowing for higher blood filtration rates) and induce periodic undulations in the unsupported microporous membrane. These membrane undulations drive the mixing and fluidization of the active plasma compartment.

\* This figure has been previously published in *Kidney International* [Ameer *et al.*, 2001]. It has been used with permission from Blackwell Publishing. Copyright © 2001 Blackwell Publishing. All rights reserved.

## 1.4 REFERENCES

- Ameer GA (2001) "Modalities for the Removal of Beta-2-Microglobulin from Blood." *Semin Dial.* 14: 103-6.
- Ameer GA, G Barabino, R Sasisekharan, W Harmon, CL Cooney and R Langer (1999) "Ex Vivo Evaluation of a Taylor-Couette Flow, Immobilized Heparinase I Device for Clinical Application." *Proc Natl Acad Sci USA.* 96: 2350-5.
- Ameer GA, EA Grovender, H Ploegh, D Ting, WF Owen, M Rupnick and R Langer (2001) "A Novel Immunoabsorption Device for Removing Beta2-Microglobulin from Whole Blood." *Kidney Int.* 59: 1544-50.
- Ameer GA, W Harmon, R Sasisekharan and R Langer (1999) "Investigation of a Whole Blood Fluidized Bed Taylor-Couette Flow Device for Enzymatic Heparin Neutralization." *Biotechnol Bioeng.* 62: 602-8.
- Ameer GA, S Raghavan, R Sasisekharan, W Harmon, CL Cooney and R Langer (1999) "Regional Heparinization Via Simultaneous Separation and Reaction in a Novel Taylor-Couette Flow Device." *Biotechnol Bioeng.* 63: 618-24.
- Boder ET and KD Wittrup (1997) "Yeast Surface Display for Screening Combinatorial Polypeptide Libraries." *Nat Biotechnol.* 15: 553-7.
- Boder ET and KD Wittrup (1998) "Optimal Screening of Surface-Displayed Polypeptide Libraries." *Biotechnol Prog.* 14: 55-62.
- Boder ET and KD Wittrup (2000) "Yeast Surface Display for Directed Evolution of Protein Expression, Affinity, and Stability." *Methods Enzymol.* 328: 430-44.
- Datar RV, T Cartwright and CG Rosen (1993) "Process Economics of Animal Cell and Bacterial Fermentations: A Case Study Analysis of Tissue Plasminogen Activator." *Bio-Technology.* 11: 349-57.
- Davankov V, L Pavlova, M Tsyurupa, J Brady, M Balsamo and E Yousha (2000) "Polymeric Adsorbent for Removing Toxic Proteins from Blood of Patients with Kidney Failure." *J Chromatogr B Biomed Sci Appl.* 739: 73-80.
- Donnelly R (1991) "Taylor-Couette Flow: The Early Days." *Physics Today.* 44: 32-9.
- Drueke TB (2000) "Beta-2-Microglobulin and Amyloidosis." *Nephrol Dial Transplant.* 15: 17-24.
- Floege J, A Bartsch, M Schulze, S Shaldon, KM Koch and LC Smeby (1991) "Clearance and Synthesis Rates of Beta-2-Microglobulin in Patients Undergoing Hemodialysis and in Normal Subjects." *J Lab Clin Med.* 118: 153-65.
- Floege J and M Ketteler (2001) "Beta-2-Microglobulin-Derived Amyloidosis: An Update." *Kidney Int.* 59 Suppl 78: S164-71.
- Furuyoshi S, M Nakatani, J Taman, H Kutsuki, S Takata and N Tani (1998) "New Adsorption Column (Lixelle) to Eliminate Beta-2-Microglobulin for Direct Hemoperfusion." *Ther Apher.* 2: 13-7.
- Gejyo F, T Yamada, S Odani, Y Nakagawa, M Arakawa, T Kunitomo, H Kataoka, M Suzuki, Y Hirasawa, T Shirahama and et al. (1985) "A New Form of Amyloid Protein Associated with Chronic Hemodialysis Was Identified as Beta 2-Microglobulin." *Biochem Biophys Res Commun.* 129: 701-6.

- Grovender EA, CL Cooney, R Langer and GA Ameer (2002) "Immunoabsorption Model for a Novel Fluidized-Bed Blood Detoxification Device." *AIChE Journal*. 48: 2357-65.
- Kunii D and O Levenspiel (1977) *Fluidization Engineering*, Robert E. Krieger Publishing Company, Huntington, New York.
- Lornoy W, I Beaus, JM Billiow, L Sierens, P Van Malderen and P D'Haenens (2000) "On-Line Haemodiafiltration. Remarkable Removal of Beta-2-Microglobulin. Long-Term Clinical Observations." *Nephrol Dial Transplant*. 15 Suppl 1: 49-54.
- Martineau P, P Jones and G Winter (1998) "Expression of an Antibody Fragment at High Levels in the Bacterial Cytoplasm." *Journal of Molecular Biology*. 280: 117-27.
- Matsuo K, TA Ikizler, RL Hoover, M Nakamoto, C Yasunaga, LB Pupim and RM Hakim (2000) "Transforming Growth Factor-Beta Is Involved in the Pathogenesis of Dialysis-Related Amyloidosis." *Kidney International*. 57: 697-708.
- Miyata T, R Inagi, Y Iida, M Sato, N Yamada, O Oda, K Maeda and H Seo (1994) "Involvement of Beta(2)-Microglobulin Modified with Advanced Glycation End-Products in the Pathogenesis of Hemodialysis-Associated Amyloidosis - Induction of Human Monocyte Chemotaxis and Macrophage Secretion of Tumor-Necrosis-Factor-Alpha and Interleukin-1." *Journal of Clinical Investigation*. 93: 521-8.
- Miyata T, M Jadoul, K Kurokawa and C Van Ypersele de Strihou (1998) "Beta-2-Microglobulin in Renal Disease." *J Am Soc Nephrol*. 9: 1723-35.
- Mogi M, M Harada, T Adachi, K Kojima and T Nagatsu (1989) "Selective Removal of Beta-2-Microglobulin from Human Plasma by High-Performance Immunoaffinity Chromatography." *J Chromatogr B Biomed Sci Appl*. 496: 194-200.
- Nakano H, H Gomi, T Shibasaki, F Ishimoto and O Sakai (1991) "An Experimental Study on Selective Elimination of Beta-2-Microglobulin Using Immunoabsorption Method in Patients with Chronic Renal Failure." *Biomater Artif Cells Immobilization Biotechnol*. 19: 61-9.
- Niwa T (2001) "Dialysis-Related Amyloidosis: Pathogenesis Focusing on Age Modification." *Semin Dial*. 14: 123-6.
- Reiter K, V Bordoni, G Dall'Olio, MG Ricatti, M Soli, S Ruperti, G Soffiati, E Galloni, V D'Intini, R Bellomo and C Ronco (2002) "In Vito Removal of Therapeutic Drugs with a Novel Adsorbent System." *Blood Purification*. 20: 380-8.
- Ronco C, A Brendolan, JF Winchester, E Golds, J Clemmer, HD Polaschegg, TE Muller, G La Greca and NW Levin (2001) "First Clinical Experience with an Adjunctive Hemoperfusion Device Designed Specifically to Remove Beta-2-Microglobulin in Hemodialysis." *Blood Purification*. 19: 260-89.
- Shabunina IV, OI Afanas'eva and SN Pokrovskii (2001) "Immunoabsorbent for Removal of Beta-2-Microglobulin from Human Blood Plasma." *Bulletin of Experimental Biology and Medicine*. 4: 984-6.
- Tsuchida K, Y Takemoto, T Nakamura, O Fu, C Okada, S Yamagami and T Kishimoto (1998) "Lixelle Adsorbent to Remove Inflammatory Cytokines." *Artif Organs*. 22: 1064-7.
- Tsuchida L, Y Takemoto, K Sugimura, R Yoshimura, K Yamamoto and T Nakatani (2002) "Adsorption of Endotoxin by Beta(2)-Microglobulin Adsorbent Column (Lixelle): The New Approach for Endotoxemia." *Therapeutic Apheresis*. 6: 116-8.

Vallar L, PM Costa, A Teixeira, M Pfister, R Barrois, PP Costa and C Rivat (1995) "Immunoabsorption Procedure as a Potential Method for the Specific Beta 2-Microglobulin Removal from Plasma of Patients with Chronic Renal Failure." *J Chromatogr B Biomed Appl.* 664: 97-106.



# Chapter 2: In Vitro Removal of $\beta_2$ -Microglobulin from Human Blood with an Immunoabsorptive VFPR\*

## 2.1 INTRODUCTION

High plasma levels of  $\beta_2$ -microglobulin ( $\beta_2m$ ) have been implicated in the formation of the severely destructive and potentially fatal amyloid deposits that are characteristic of dialysis-related amyloidosis (DRA) [Gejyo *et al.*, 1985; Drueke, 2000]. Conventional renal replacement technologies remove insufficient quantities of  $\beta_2m$  to normalize plasma levels [Ameer, 2001]. This limitation arises due to non-specific adsorptive qualities and reliance on size exclusion, which can also remove other middle molecular weight proteins. These non-specific approaches also make it difficult to evaluate the role and contribution of middle molecular weight molecules to the pathology of DRA and other morbidities of end stage renal disease. A high affinity and biologically specific approach could target a protein, prevent significant loss of other important molecules, and improve the apparent adsorption rate within an extracorporeal device. This chapter describes the use of agarose-immobilized murine anti-human  $\beta_2m$  monoclonal antibodies in a Vortex Flow Plasmapheretic Reactor (VFPR) to remove donor baseline and controlled amounts of human  $\beta_2m$  from human blood *in vitro*.

## 2.2 METHODS

### 2.2.1 Assays

Serum and plasma  $\beta_2m$  concentrations were assayed with the  $\beta_2$ -micro RIA (radioimmunoassay) kit available from Pharmacia-Upjohn (MI), while the buffer  $\beta_2m$  concentrations were determined by using an extinction coefficient of  $20,065 \text{ M}^{-1} \text{ cm}^{-1}$  at 280 nm. This value was derived from the published amino acid sequence of human  $\beta_2m$  [Suggs *et al.*, 1981] and the equation reported by Pace and co-workers [Pace *et al.*, 1995]. Bradford protein assays were performed according to the dye manufacturer's instructions (Bio-Rad, CA), using a bovine gamma globulin standard (Pierce, IL). Plasma free hemoglobin assays were performed according to the instructions of a kit purchased from Sigma Chemical (MO).

---

\* This chapter is a revised version of a research article previously published in *Kidney International* [Ameer *et al.*, 2001]. It has been used with permission from Blackwell Publishing. Copyright © 2001 Blackwell Publishing. All rights reserved.

Complete blood counts and total protein assays were performed at the MIT Medical Laboratory.

### **2.2.2 Protein Immobilization**

BBM.1 monoclonal antibody (hybridoma purchased as ATCC HB-28) [Brodsky *et al.*, 1979; Parham *et al.*, 1983] and bovine serum albumin (BSA) were each immobilized onto 48 mL settled-volumes of Sepharose CL-4B agarose gel beads (Amersham-Pharmacia, Sweden) using a modified version of a method previously described [Cuatrecasas *et al.*, 1968].

The gel beads were rinsed with 1 L of ultrapurified water, and then combined with 50 mL of ultrapurified water and 100 mL of 2 M sodium carbonate. After being chilled on ice, the agarose gel suspension was activated for 5 minutes with 20% w/v cyanogen bromide (each gram pre-dissolved in 1.5 mL acetonitrile). The activated gel was rinsed sequentially with 1 L of each of the following ice-chilled fluids: ultrapurified water, 1 mM hydrochloric acid, and bicarbonate buffer (0.5 M sodium chloride, 0.1 sodium bicarbonate, pH 8.3). The fluid in the gel void volume was removed and the activated agarose was combined with the protein to be immobilized (167 mg of BBM.1 via Bradford dye assay and 174 mg BSA by dry weight) in 82 mL of phosphate buffered saline, pH 7.4 (PBS). The protein was allowed to bind to the activated agarose suspension for 40 hours at 4°C with gentle mixing. The buffer was removed from the agarose gel and assayed for its residual protein concentration (Bradford assay for BBM.1 and change in absorbance at 280 nm for BSA). The activated gel was quenched by mixing it with a lysine buffer (0.2 M lysine, 0.5 M sodium chloride, 0.1 M sodium bicarbonate, pH 8.3) for one hour at 4°C. The gel was rinsed quickly with 500 mL PBS and rinsed overnight with 200 mL PBS at 4°C. The following day, the overnight rinse was replaced with fresh PBS. A sample was incubated for one hour at 37 °C to check the thermal stability of the immobilized protein (Bradford assay). Coomassie stained SDS-PAGE was used to check for protein in the lysine quenching buffer and PBS rinses.

### **2.2.3 Recombinant $\beta_2m$ Preparation**

The  $\beta_2m$  *E. coli* expression vector [Garboczi *et al.*, 1992] was a generous gift from the Wiley Laboratory (Cambridge, MA) and the recombinant protein was produced in a

fashion similar to those previously described [Buchner and Rudolph, 1991; Fan *et al.*, 1996]. Each liter of Luria-Bertani medium (fortified with 0.4% w/v glucose and 0.100 mg/mL ampicillin) was inoculated with frozen stock, incubated at 37°C, and induced with 0.5 mM isopropyl  $\beta$ -D-thiogalactopyranoside during the log growth phase. The bacteria was centrifuged at 5k x g for 20 minutes and resuspended in 50 mM Tris-HCl, 25% w/v sucrose, 1 mM sodium ethylenediaminetetraacetic acid (EDTA), 10 mM dithiothreitol (DTT), pH 8.0. Cell lysis and DNA degradation were effected through the addition of 1 mg/mL lysozyme, 0.1 mg/mL DNase I (Sigma DN-25), 5 mM magnesium chloride, 1% Triton X-100, 1% sodium deoxycholate, 10 mM DTT, and 70 mM sodium chloride. The insoluble protein was rinsed several times with 50 mM Tris-HCl, 100 mM sodium chloride, 1 mM EDTA, 0.5% Triton X-100, 1 mM DTT, pH 8.0 and one final time with 50 mM Tris-HCl, 1mM EDTA, pH 8.0. The washed inclusion body protein was solubilized in 8 M urea, 25 mM 2-[N-morpholino]ethanesulfonic acid (MES), 10 mM EDTA, 0.1 mM DTT, pH 6.0 and ultracentrifuged for 30 minutes at 25°C and 186,000 x g. The denatured protein was refolded through dilution into 100 mM Tris-HCl, 400 mM L-arginine-HCl, 2 mM EDTA, 0.5 mM oxidized glutathione, 5 mM reduced glutathione, pH 8.0. The refolded  $\beta_2m$  was purified via size-exclusion chromatography using prep-grade Superose® 12 resin (Amersham-Pharmacia), eluted with 20 mM Tris-HCl, 150 mM sodium chloride, pH 8.0. In order to remove residual refolding buffer, the  $\beta_2m$  was dialyzed against the elution buffer with a 6-8 kD membrane (Spectrum Laboratories, CA).

#### 2.2.4 Capacity of the Immunoabsorptive Media

Porcine serum, loaded with three different saturating concentrations of r $\beta_2m$ , was used to quantify the capacity of the immunoabsorptive media. Briefly, 10 mL of 50% gel/PBS suspension, 30 mL of 5 micron-filtered Porcine serum (GIBCO BRL, MD), and either 0.23, 0.31, or 0.40 mg of r $\beta_2m$  (stock: 0.94  $\pm$  0.02 mg/mL in elution buffer) were combined in 50 mL polypropylene tubes (Corning, NY). The tubes were equilibrated under well-mixed conditions for at least 1 hour at 37°C. The r $\beta_2m$ -adsorptive capacity of the agarose-immobilized monoclonal antibody was calculated using Equation 2.1, where  $\rho'_s$  is the adsorption site density on a settled bed volume basis (mg-r $\beta_2m$ /L-settled-gel),  $V_{total}$  is the total volume of the system (mL),  $V_{gel}$  is the settled-volume of gel (mL),  $C_0$  is the initial

diluted concentration of  $r\beta_2m$  in the system (mg/L), and  $C_{eq}$  is the equilibrium concentration of desorbed  $r\beta_2m$  (mg/L).

$$\rho'_s = \frac{V_{total}}{V_{gel}} (C_0 - C_{eq}) \quad [2.1]$$

### 2.2.5 Clearance of $\beta_2m$ from Whole Blood by a VFPR in a Closed-Loop Circuit

The MIT Committee on the Use of Humans as Experimental Subjects approved all experiments with human blood. Healthy, volunteer blood donors read and signed informed consent forms. The staff at the Children's Hospital Blood Donor Center (Boston, MA) performed the phlebotomies. Each donation (450 mL nominal volume) was used the same day it was received and had 63 mL of citrate phosphate dextrose adenine solution added as an anti-coagulant (Baxter, IL). The VFPR and circuit tubing were primed with 0.9% w/v sodium chloride (USP grade, Abbott Laboratories, IL) and the agarose gel was injected into the adsorptive compartment. The blood bag was placed on a shaker and connected to the VFPR in a closed-loop circuit (Figure 2.1). Before the plasma pump and VFPR cylinder were turned on, the main circuit pump was run for 5 minutes to mix the blood with the saline outside of the plasma chambers and plasma line. During the first 60 minutes of a two-hour hemoperfusion, the native donor  $\beta_2m$  was cleared from the circuit by running the plasma pump and the inner VFPR cylinder. Samples were taken before and after this period, and the adsorptive chamber was flushed with 0.9% w/v sodium chloride (BBM.1 gel only).

The immunoadsorptive media (but not the BSA gel) was regenerated with 1.5 L of 0.3 M glycine-HCl, pH 2.8. The regenerated BBM.1 gel was rinsed with 1.5 L of PBS and re-injected into the adsorptive chamber of the VFPR. Recombinant human  $\beta_2m$  (1.5 mg in elution buffer) was injected into the circuit, allowed to mix with the blood for 5 minutes, and samples were taken. The recombinant  $\beta_2m$  was cleared from the circuit by turning on the plasma pump and VFPR cylinder. Samples were taken over a period of 60 minutes and the media was regenerated as before (both BBM.1 and BSA). The samples collected were assayed for their total protein, plasma free hemoglobin, complete blood count, and  $\beta_2m$  concentration. System efficacy was quantified by calculating the conversion of  $\beta_2m$  adsorption,  $X_{adsorption}$ , as shown by Equation 2.2 (dimensionless). Here  $M_{initial}$  and  $M_{final}$  are the initial and final masses (mg) of desorbed  $\beta_2m$  in the system, respectively.

$$X_{adsorption} = 1 - \frac{M_{final}}{M_{initial}} \quad [2.2]$$

## 2.2.6 Statistical Analysis

Observed variables are reported as the mean  $\pm$  SEM (standard error of the mean). All experiments were performed in triplicate ( $N=3$ ), unless otherwise noted. Analysis of variance (ANOVA) was used to determine the significance of the differences among three or more means, while the student's two-sample t-test was used to compare pairs of means. The criterion for significance was a two-tailed p-value of 0.05.

## 2.3 RESULTS

### 2.3.1 Protein Immobilization

Most of the BBM.1 (92%) and the BSA (97%) bound to the activated agarose gel, yielding immobilization densities of 3.0 and 3.5 mg/mL-settled-gel, respectively. The lysine quenching buffer and the PBS rinses did not show significant amounts of BBM.1 on SDS-PAGE as compared to equal volume samples of BBM.1 in PBS from before and after activated substrate contact. Protein leaching, after 1 hour of 37°C incubation, in the BBM.1 and BSA 1 samples was found to be only  $2.9 \pm 0.7$  and  $0.5 \pm 0.2$  mg/L-PBS, respectively.

### 2.3.2 Capacity of the Immunoabsorptive Media

Table 2.1 shows the results from the adsorption capacity measurements. The  $r\beta_2m$  binding capacity of the immunoabsorptive media,  $\rho'_s$ , was calculated to be  $30 \pm 2$  mg- $r\beta_2m$ /L-settled-gel. Assuming bivalent BBM.1- $\beta_2m$  binding, this value corresponds to a BBM.1 efficiency of 6%. There was no apparent effect of the 0.3 M glycine stripping buffer on the binding capacity.

**Table 2.1 Capacity of the Immunoabsorptive Media**

Initial Concentration $C_0$ [mg/L, $N=4$ ]	Final Concentration $C_{eq}$ [mg/L]	Binding Site Density $\rho'_s$ [mg- $\beta_2m$ /L-settled-gel]
$5.8 \pm 0.1$	$2.1 \pm 0.0$	$30. \pm 0.$
$7.7 \pm 0.2$	$3.8 \pm 0.2$	$32. \pm 1.$
$10. \pm 0.$	$6.4 \pm 0.3$	$29. \pm 2.$

### 2.3.3 Clearance of $\beta_2m$ from Human Blood with an Immunoadsorptive VFPR

The average total volume, native  $\beta_2m$  concentration, and hematocrit of the anticoagulated human blood was  $529 \pm 6$  mL,  $1.3 \pm 0.1$  mg/L, and  $0.38 \pm 0.01$ , respectively (N=7). The final native  $\beta_2m$  concentration of the BSA circuit was  $0.5 \pm 0.0$  mg/L, while that of the BBM.1 circuit was below detectable limits. Table 2.2 presents the observed native and recombinant  $\beta_2m$  adsorption conversions for the BBM.1 antibody and BSA control protein matrices. The dynamics of r $\beta_2m$  removal by the VFPR, loaded with BBM.1 gel, are illustrated by Figure 2.2. The relatively low plasma line concentration ( $< 0.4$  mg/L) indicates that the apparent  $\beta_2m$  adsorption rate within the plasma chamber was not limiting. Furthermore, the time-scale of  $\beta_2m$  clearance from the blood bag was in agreement with that obtained by dividing the total blood path volume (445 mL) by the plasma flow rate (50 mL/min). The initial and final recombinant  $\beta_2m$  concentrations in the BBM.1 circuit were  $3.2 \pm 0.2$  and  $0.2 \pm 0.1$  mg/L, respectively. This observed initial value was in agreement with the value (3.4 mg/L) predicted by dividing the mass of injected r $\beta_2m$  (1.5 mg) by the cell-free volume of the blood bag, circuit tubing, and VFPR blood chamber (445 mL). The mass of r $\beta_2m$  adsorbed by the BBM.1 was  $28 \pm 2$  mg/L-gel (settled volume), which was not significantly different from the value of  $\rho'_s$  measured *a priori*.

**Table 2.2 Clearance of  $\beta_2m$  from Human Blood by the VFPR, *In Vitro*.**

	Native			Recombinant		
	$M_{initial}$ [mg]	$M_{final}$ [mg]	$X_{adsorption}$	$M_{initial}$ [mg]	$M_{final}$ [mg]	$X_{adsorption}$
<b>BBM.1 [g] (N=4)</b>	0.48±0.07	*	100%±6%	1.43±0.08	0.10±0.02	92%±2%
<b>BSA [g] (N=3)</b>	0.37±0.04	0.26±0.01	29%±6%	1.80±0.05	1.89±0.11	*
<b>Significance</b>	p>0.05	p<0.002	p<0.0005	p < 0.02	†	†

Table 2.3 and Table 2.4 report the effects of the VFPR circuit on cellular blood elements and total protein, respectively. The donor bag plasma free hemoglobin level (HbP)

\* Below detectable limits.

† Values were not compared due to the significant difference in the initial conditions.

was  $4.3 \pm 1.1$  mg/dL, while HbP at the end of native  $\beta_2m$  removal (1 hour) was  $8.9 \pm 2.2$  g/dL. This increase corresponded to 0.33 mg/dL per circuit pass. A HbP of 0.6 mg/dL per pass through a hemodialyzer is generally considered acceptable [Ameer, Barabino *et al.*, 1999].

**Table 2.3 Complete Blood Count Data for the BBM.1 VFPR Experiments (N=4).**

	Native			Recombinant	
	Diluted Bag <sup>*</sup>	Initial	Final	Initial	Final
Erythrocyte [M/ $\mu$ L] <sup>†</sup>	3.39 $\pm$ 0.08	3.23 $\pm$ 0.20	3.26 $\pm$ 0.08	3.18 $\pm$ 0.11	3.51 $\pm$ 0.15
Leukocyte [k/ $\mu$ L] <sup>†</sup>	4.2 $\pm$ 0.5	4.2 $\pm$ 0.5	3.9 $\pm$ 0.5	4.0 $\pm$ 0.5	4.3 $\pm$ 0.5
Platelet [k/ $\mu$ L] <sup>†</sup>	164 $\pm$ 13	175 $\pm$ 15	162 $\pm$ 13	161 $\pm$ 18	172 $\pm$ 20

**Table 2.4 Total Protein Data for the VFPR BBM.1 Experiments and BSA Controls.**

	Native			Recombinant	
	Bag	Initial	Final	Initial	Final
BBM.1 (N=4) <sup>‡</sup>	19.3 $\pm$ 0.4	18.1 $\pm$ 0.5	19.7 $\pm$ 1.4	14.8 $\pm$ 0.4	15.8 $\pm$ 0.3
BSA (N=3) <sup>§</sup>	19.1 $\pm$ 0.5	17.7 $\pm$ 0.4	18.5 $\pm$ 0.54	**	19.7 $\pm$ 0.6
Significance <sup>††</sup>	p>0.8	p>0.5	p>0.5	N.A.	p<0.005

\* Values were not compared due to the significant difference in the initial conditions. Concentrations determined by multiplying the donor blood bag measurement by the dilution factor resulting from the saline priming volume.

† No significant differences were found among the mean observed values for each count type over the two hour period (ANOVA, p>0.4).

‡ No significant differences were found among the mean observed values during the native phase (ANOVA, p>0.4). A significant decrease was found between the native and recombinant phases (ANOVA, p<0.001), which was due to the flushing of the adsorptive compartment and the regeneration of the media.

§ No significant differences were found among the mean observed values (ANOVA, p>0.1).

\*\* This sample was equivalent to the "Final Native" sample because the BSA gel was not regenerated.

†† Two-sample t-test.

## 2.4 DISCUSSION

Although the clinical pathology of DRA is not fully understood, it has been shown that removal of  $\beta_2\text{m}$  can apparently delay the onset of the disease and improve symptoms [Furuyoshi *et al.*, 1998; Drueke, 2000; Lornoy *et al.*, 2000]. For the first time, we have shown the feasibility of removing  $\beta_2\text{m}$  from whole blood within a single device via immunoadsorption. As a first step, agarose-immobilized murine anti-human  $\beta_2\text{m}$  monoclonal antibodies (BBM.1) were used in a Vortex Flow Plasmapheretic Reactor (VFPR) to remove both native and recombinant human  $\beta_2\text{m}$  from human blood, *in vitro*. The characteristics and advantages of the VFPR have been previously shown for the enzymatic neutralization of heparin, to potentially make heparin anticoagulation during open-heart surgery and dialysis safer [Bernstein *et al.*, 1987; Leaver *et al.*, 1992; Ameer, Barabino *et al.*, 1999]. Porous agarose gel beads were suspended within the adsorptive/reactive compartment and did not come into contact with the blood cells, thereby minimizing hemolysis. The agarose gel beads used in this study were hydrophilic and did not have any significant net surface charge, which could result in ion exchange phenomena. Furthermore, the common use of agarose gel beads in size exclusion chromatography also reflects its low protein-binding characteristic. Our results demonstrated that a VFPR is able to clear low concentrations of  $\beta_2\text{m}$  from whole blood at a clinically relevant flow rate, without any deleterious effects on the cellular blood components, total protein, or plasma free hemoglobin. Other factors, such as complement activation could potentially be an issue with agarose gel beads. However, the immobilization chemistry and support used in the study was a model system to establish feasibility. The ability of the VFPR to perform adsorption, without a separate plasma filter, should potentially render the device convenient for use during dialysis. Furthermore, the relatively low whole blood priming volume of 50 mL should minimize hemodilution.

Our approach offers several potential advantages. The VFPR design overcomes the hemolysis and mass-transfer limitations associated with fluidized and packed columns when they are used for direct hemoperfusion [Ameer, Harmon *et al.*, 1999]. The high affinity of the antibodies could potentially reduce patient  $\beta_2\text{m}$  concentrations below those obtainable with a low-affinity, hydrophobic adsorbent. The larger  $\beta_2\text{m}$ -concentration difference between the plasma and the adsorptive surface should result in an apparent increased rate of

adsorption. The high specificity of the antibodies should avoid the indiscriminate loss of desirable molecules. In addition, immunoadsorption could potentially be used in clinical trials as a diagnostic tool to help determine whether or not  $\beta_2m$  clearance is the underlying mechanism responsible for the therapeutic response of non-specific treatments. Some investigators have shown that a hydrophobic adsorbent, thought to be selective for  $\beta_2m$ , removed various cytokines [Tsuchida *et al.*, 1998]. Therefore, defined immunoadsorbents could be targeted towards these molecules to help understand their role in the pathogenesis of DRA or other morbidities associated with ESRD.

It is very difficult, and at times not practical, to reproduce *in vitro* all of the parameters that are characteristic of an *in vivo* or *ex vivo* situation. Pathologic  $\beta_2m$  levels and larger  $\beta_2m$  distribution volumes were not tested due to the limited available quantities of the BBM.1 monoclonal antibody. However, the dynamics of  $\beta_2m$  removal from blood with the VFPR using the immobilized BBM.1 antibody as a model system could be evaluated. The lower than expected immobilization yield of BBM.1 using the CNBr activated agarose beads was also observed with agarose immobilized protein A, which specifically binds the Fc region of an IgG antibody. This phenomenon could potentially be attributed to the expression of an additional immunoglobulin (impurity) in the hybridoma culture, or simply an inherent inability of immobilized BBM.1 to retain its binding activity. Even though our initial  $\beta_2m$  concentrations were relatively low, the adsorption kinetics of our system should not be negatively affected by higher initial  $\beta_2m$  concentrations. Provided a high-capacity immunoadsorbent media is used,  $\beta_2m$  concentrations that are characteristic of ESRD should be cleared. Vallar and co-workers have reported high immobilization efficiencies (67%,  $\rho'_s = 0.9$  mg- $\beta_2m$ /mL-settled-gel) of other Sepharose® CL-4B-immobilized anti-human  $\beta_2m$  monoclonal antibodies [Vallar *et al.*, 1995]. A VFPR containing an immunoadsorbent media of 0.9 mg- $\beta_2m$ /mL-settled-gel should remove clinically relevant quantities of  $\beta_2m$  within the allotted treatment time. A VFPR containing 300 mL of gel is potentially capable of removing 270 mg of  $\beta_2m$ . Depending on the initial plasma  $\beta_2m$  levels, session duration, and the type of dialysis membrane used, up to 250 mg  $\beta_2m$  /session can be removed via filtration and non-specific adsorption (about 100 mg/4-hr-session on average) [van Ypersele de Strihou *et al.*, 1994]. However, the key difference is the high affinity and specificity of

immunoabsorption. High affinity is important because it helps maintain a high apparent adsorption rate within the VFPR.

To date, the emphases of attention to remove  $\beta_2m$  from blood under clinically relevant conditions have been filtration and hydrophobic interactions between the  $\beta_2m$  and the adsorptive media [Furuyoshi *et al.*, 1998; Kay, 1999; Davankov *et al.*, 2000; Druke, 2000]. However, the specificity and affinity of these approaches continue to be a concern. We overcame these obstacles by using monoclonal antibody technology. The BBM.1 antibody, produced by mammalian cell culture, had the required affinity to lower  $\beta_2m$  concentrations below the detectable limit of the radioimmunoassay. We anticipate that this kind of affinity and specificity can be obtained using single chain antibody fragments (scFv) [Raag and Whitlow, 1995], which offer several potential advantages over whole antibodies (refer to Section 1.1). Future research will focus on the development of anti- $\beta_2m$  scFv fragments and various immobilization chemistries to achieve a higher  $\beta_2m$  binding site density. Furthermore, the efficacy of the VFPR suggests that this technology could be tailored for the treatment of a range of pathologies characterized by elevated circulating concentrations of unwanted compounds, such as genetic disorders, liver failure, autoimmune disease, sepsis, or drug overdoses.

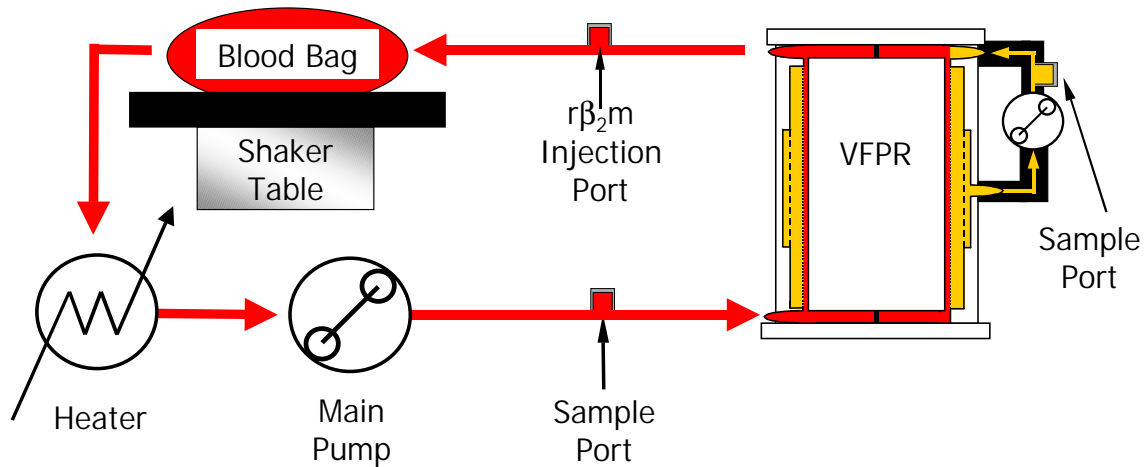


**Figure 2.1 Diagram of the circuit used to study the clearance  $\beta_2m$  of from human blood.** The whole blood path is shown in red, while regions accessible only to plasma are shown in gold. The overall circulation flow rate was set at 200 mL/min, the plasma pump was calibrated to 50 mL/min, and the rotation rate was set at 1150 rpm. The volume of the tubing running from the blood bag to the VFPR was 60 mL, while the return tubing was 5 mL. The total reactor volume was 125 mL, which was distributed among the whole blood, adsorptive plasma, and plasma collection chambers as 50, 70, and 5 mL, respectively. The volume of the plasma tubing was 10 mL. The settled-volume of agarose gel beads was 48 mL. The blood temperature at the VFPR inlet and outlet was 35°C during the clearance of  $r\beta_2m$ . The dimensions of this device prototype are given in Section 3.2.1.

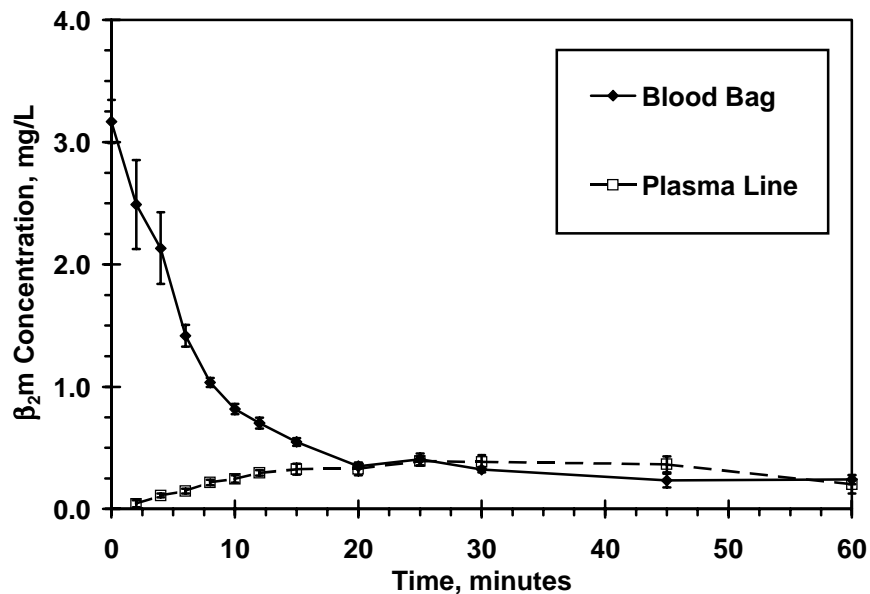


**Figure 2.2 Dynamics of  $r\beta_2m$  clearance from human blood with a BBM.1-loaded VFPR, *in vitro*.** Error bars represent the standard error of the mean (SEM,  $N=4$ ).

## 2.5 REFERENCES

- Ameer GA (2001) "Modalities for the Removal of Beta-2-Microglobulin from Blood." *Semin Dial.* 14: 103-6.
- Ameer GA, G Barabino, R Sasisekharan, W Harmon, CL Cooney and R Langer (1999) "Ex Vivo Evaluation of a Taylor-Couette Flow, Immobilized Heparinase I Device for Clinical Application." *Proc Natl Acad Sci USA.* 96: 2350-5.
- Ameer GA, EA Grovender, H Ploegh, D Ting, WF Owen, M Rupnick and R Langer (2001) "A Novel Immunoabsorption Device for Removing Beta2-Microglobulin from Whole Blood." *Kidney Int.* 59: 1544-50.
- Ameer GA, W Harmon, R Sasisekharan and R Langer (1999) "Investigation of a Whole Blood Fluidized Bed Taylor-Couette Flow Device for Enzymatic Heparin Neutralization." *Biotechnol Bioeng.* 62: 602-8.
- Bernstein H, VC Yang, D Lund, M Randhawa, W Harmon and R Langer (1987) "Extracorporeal Enzymatic Heparin Removal: Use in a Sheep Dialysis Model." *Kidney Int.* 32: 452-63.
- Brodsky FM, WF Bodmer and P Parham (1979) "Characterization of a Monoclonal Anti-Beta-2-Microglobulin Antibody and Its Use in the Genetic and Biochemical Analysis of Major Histocompatibility Antigens." *Eur J Immunol.* 9: 536-45.
- Buchner J and R Rudolph (1991) "Renaturation, Purification and Characterization of Recombinant Fab-Fragments Produced in Escherichia Coli." *Bio/Technology.* 9: 157-61.
- Cuatrecasas P, M Wilchek and CB Anfinsen (1968) "Selective Enzyme Purification by Affinity Chromatography." *Proc Natl Acad Sci USA.* 61: 636-43.
- Davankov V, L Pavlova, M Tsyurupa, J Brady, M Balsamo and E Yousha (2000) "Polymeric Adsorbent for Removing Toxic Proteins from Blood of Patients with Kidney Failure." *J Chromatogr B Biomed Sci Appl.* 739: 73-80.
- Drueke TB (2000) "Beta-2-Microglobulin and Amyloidosis." *Nephrol Dial Transplant.* 15: 17-24.
- Fan QR, DN Garboczi, CC Winter, N Wagtmann, EO Long and DC Wiley (1996) "Direct Binding of a Soluble Natural Killer Cell Inhibitory Receptor to a Soluble Human Leukocyte Antigen-Cw4 Class I Major Histocompatibility Complex Molecule." *Proc Natl Acad Sci USA.* 93: 7178-83.
- Furuyoshi S, M Nakatani, J Taman, H Kutsuki, S Takata and N Tani (1998) "New Adsorption Column (Lixelle) to Eliminate Beta-2-Microglobulin for Direct Hemoperfusion." *Ther Apher.* 2: 13-7.
- Garboczi DN, DT Hung and DC Wiley (1992) "Hla-A2-Peptide Complexes: Refolding and Crystallization of Molecules Expressed in Escherichia Coli and Complexed with Single Antigenic Peptides." *Proc Natl Acad Sci USA.* 89: 3429-33.
- Gejyo F, T Yamada, S Odani, Y Nakagawa, M Arakawa, T Kunitomo, H Kataoka, M Suzuki, Y Hirasawa, T Shirahama and et al. (1985) "A New Form of Amyloid Protein Associated with Chronic Hemodialysis Was Identified as Beta 2-Microglobulin." *Biochem Biophys Res Commun.* 129: 701-6.
- Kay J (1999) In *Dialysis and Transplantation*(Ed, Owen WD Jr, PB, Sayegh MH) WB Saunders Company, Philadelphia: pp. 237-52.
- Leaver G, JA Howell and JR Conder (1992) "Adsorption Kinetics of Albumin on a Cross-Linked Cellulose Chromatographic Ion Exchanger." *J Chromatog.* 509: 101.

Lornoy W, I Beaus, JM Billiow, L Sierens, P Van Malderen and P D'Haenens (2000) "On-Line Haemodiafiltration. Remarkable Removal of Beta-2-Microglobulin. Long-Term Clinical Observations." *Nephrol Dial Transplant*. 15 Suppl 1: 49-54.

Pace CN, F Vajdos, L Fee, G Grimsley and T Gray (1995) "How to Measure and Predict the Molar Absorption Coefficient of a Protein." *Protein Sci*. 4: 2411-23.

Parham P, MJ Androlewicz, NJ Holmes and BE Rothenberg (1983) "Arginine 45 Is a Major Part of the Antigenic Determinant of Human Beta-2-Microglobulin Recognized by Mouse Monoclonal Antibody Bbm.1." *J Biol Chem*. 258: 6179-86.

Raag R and M Whitlow (1995) "Single-Chain Fvs." *Faseb J*. 9: 73-80.

Suggs SV, RB Wallace, T Hirose, EH Kawashima and K Itakura (1981) "Use of Synthetic Oligonucleotides as Hybridization Probes: Isolation of Cloned Cdna Sequences for Human Beta-2-Microglobulin." *Proc Natl Acad Sci USA*. 78: 6613-7.

Tsuchida K, Y Takemoto, T Nakamura, O Fu, C Okada, S Yamagami and T Kishimoto (1998) "Lixelle Adsorbent to Remove Inflammatory Cytokines." *Artif Organs*. 22: 1064-7.

Vallar L, PM Costa, A Teixeira, M Pfister, R Barrois, PP Costa and C Rivat (1995) "Immunoabsorption Procedure as a Potential Method for the Specific Beta 2-Microglobulin Removal from Plasma of Patients with Chronic Renal Failure." *J Chromatogr B Biomed Appl*. 664: 97-106.

van Ypersele de Strihou C, J Floege, M Jadoul and KM Koch (1994) "Amyloidosis and Its Relationship to Different Dialysers." *Nephrol Dial Transplant*. 9 Suppl 2: 156-61.



## Chapter 3: Macroscopic Mixing Model for the VFPR<sup>\*</sup>

### 3.1 INTRODUCTION

Effective extracorporeal removal of  $\beta_2m$  from a patient will require the VFPR to exhibit favorable mass-transfer rates and to possess a sufficient binding capacity for  $\beta_2m$  (up to 500 mg). An accurate description of the macroscopic mixing pattern within the active plasma compartment (APC) of the VFPR is required if the mass-transfer characteristics of the fluidized particles are to be understood. A macroscopic mixing model, previously developed to characterize the enzymatic degradation of heparin in the VFPR [Ameer *et al.*, 1999], has been unable to accurately describe the  $\beta_2m$ -immunoabsorption data presented in Chapter 2. Therefore, in this chapter, improved experimental methods and mathematical analyses are presented which provide a better understanding of the macroscopic mixing pattern within the VFPR. These methods are used to characterize the mixing behavior of the prototype studied in Chapter 2 and a new, larger VFPR prototype. By comparing the results from the two different device prototypes, the effect of increasing the size of the APC on mixing is assessed. These results provide a better understanding of the VFPR as well as a framework for the development of a dynamic immunoabsorption model for the device, which is described in Chapter 4.

### 3.2 METHODS

#### 3.2.1 Reactor Prototypes

The small-scale prototype was identical to the one used in Chapter 2 and in the previous heparinase I experiments conducted by Ameer and co-workers [1999]. The new, larger VFPR prototype was constructed with a 22% longer and 90% thicker active compartment (Figure 3.1). The compartmental volumes and pertinent length-scales of the two VFPR prototypes are compared by Table 3.1 and Table 3.2, respectively.

---

<sup>\*</sup> Some of the material in this chapter has been reprinted from *Chemical Engineering Science*, Vol. 56, No. 18, "Modeling the mixing behavior of a novel fluidized extracorporeal immunoabsorber," E. A. Grovender, C. L. Cooney, G. A. Ameer, R. S. Langer, 5437-5441, Copyright 2001, with permission from Elsevier [Grovender *et al.*, 2001] (<http://www.sciencedirect.com/science/journal/00092509>). Single copies of this chapter can be downloaded and printed only for the reader's personal research and study.

**Table 3.1 Comparison of the compartmental volumes of the two VFPR Prototypes.**

Prototype	Blood Compartment Volume [mL]	Active Plasma Compartment [mL]	Plasma Collection Chamber [mL]
Small	50	70	5
Large	60	175	10

**Table 3.2 Comparison of the pertinent length scales of the two VFPR Prototypes.**

Prototype	Shaft Radius [cm]	Membrane Radius [cm]	Mesh Radius [cm]	Membrane Length [cm]	Mesh Length [cm]
Small	2.70	2.86	3.20	11	6.4
Large	2.70	2.86	3.49	14	6.4

### 3.2.2 Residence Time Distribution Experiments

The RTD experiments were conducted by injecting a pulse of dye into the VFPR inlet, as depicted in Figure 3.2. The outlet dye concentration measurements were taken from the blood and plasma ports during separate experiments and normalized to obtain the RTD function,  $E(t)$ . The injections of dye ranged from 0.5-2.0 mL, depending on the outlet port and prototype considered. The dye was a 50 mg/mL aqueous solution of blue dextran (2,000 kD). The dye concentration measurements were made by reading the absorbance at 620 nm in a flow-cell cuvette using a spectrophotometer capable of real-time data acquisition (Shimatzu UV-1601). The tubing connecting the VFPR to the spectrophotometer was treated as an ideal plug and was accounted for by subtracting the calculated residence time from the RTD data.

In accordance with the  $\beta_2$ m-immunoabsorption experiments presented in Chapter 2, the main pump flowrate was set to 200 mL/min, the plasma pump flowrate was set to 50 ml/min, and the shaft rotation rate was set at  $1.2 \times 10^3$  rpm. Additional RTD experiments were conducted with the plasma pump set at 100 mL/min. To determine the effect of the fluidized particles on the mixing of the device, experiments were conducted at both plasma pump flowrates with and without of swollen polyacrylamide gel beads (90-180  $\mu$ m diameter, Bio-Rad No. 150-4140). This type of bead was selected because it effectively excludes blue

dextran from its pores. The same 69% suspended volume fraction of gel beads was used in both prototypes (48 mL and 120 mL on a settled bed volume basis for the small and large prototypes, respectively).

### 3.2.3 Mathematical Modeling

The macroscopic mixing behavior of each physical compartment within the VFPR is described using the standard “tanks-in-series” model [Levenspiel, 1999]. This model assumes that the real mixing pattern of a compartment can be described as a series of ideally well-mixed control volumes, or CSTRs (constant stirred tank reactors). The residence times of fluid exiting the blood and plasma ports,  $\tau_{bport}$  and  $\tau_{pport}$ , are calculated by integrating the empirical RTD functions. The number of CSTRs in the blood compartment,  $N_{BC}$ , is determined by regressing the tanks-in-series analytical solution [Levenspiel, 1999] to the RTD of the blood port,  $E_{bport}(t)$ . A key assumption of the standard tanks-in-series model is that the CSTRs have equal residence times. Typically in this model the volumetric flowrate of fluid between CSTRs is constant, yielding a series of equal volume CSTRs. However, the axial flowrate varies with axial position within the VFPR’s blood compartment, due to the loss of flow across the microporous membrane. Therefore, each theoretical CSTR in the blood compartment has a unique inlet flowrate, membrane surface area, and volume as shown by Figure 3.3.

It then follows that the residence time of each CSTR in the blood compartment,  $\tau_{BC,i}$ , is described by Equation 3.1.

$$\tau_{BC,i} = \frac{\tau_{bport}}{N_{BC}} = \frac{V_{BC,i}}{Q_{m,i} + Q_{BC,i}} = \frac{V_{1,i}}{Q_{BC,i-1}} \quad [3.1]$$

Here  $V_{BC,i}$  is the volume,  $Q_{m,i}$  is the transmembrane volumetric flowrate, and  $Q_{BC,i}$  is the non-transmembrane outlet volumetric flowrate of an arbitrary blood compartment CSTR. The flow across the microporous membrane is assumed to be uniformly distributed, which yields Equation 3.2.

$$Q_{m,i} = \left( \frac{Q_m}{V_{BC}} \right) V_{BC,i} \quad [3.2]$$

Here  $Q_m$  is the total transmembrane, or plasma pump flowrate, and  $V_{BC}$  is the total volume of the blood compartment, defined by Equation 3.3 (total conservation of volume within the

blood compartment). The non-transmembrane outlet volumetric flowrate of an arbitrary blood compartment CSTR,  $Q_{BC,i}$ , is calculated by Equation 3.4 (incompressible flow).

$$V_{BC} = \sum_{i=1}^{N_{BC}} V_{BC,i} \quad [3.3]$$

$$Q_{BC,i} = Q_{BC,0} - \sum_{j=1}^i Q_{m,j} \quad [3.4]$$

Here  $Q_{BC,0}$  is the VFPR inlet volumetric flowrate. Equations 3.1, 3.2 and 3.4 are combined to yield Equation 3.5,

$$V_{BC,i} = \tau_{BC,i} \left( Q_{BC,0} + Q_{m,i} - \frac{Q_m}{V_{BC}} \sum_{j=1}^i V_{BC,j} \right) \quad [3.5]$$

Equations 3.3 and 3.5 are used to calculate the blood compartment CSTRs in an iterative fashion.

The number of CSTRs in the active plasma compartment (APC),  $N_{APC}$ , is determined by regressing Equations 3.6-3.12 to the empirical RTD of the plasma port,  $E_{pport}(t)$ .

$$\frac{dC_{BC,i}}{dt} = \frac{1}{\tau_{BC,i}} (C_{BC,i-1} - C_{BC,i}) \quad [3.6]$$

$$\frac{dC_{APC,i}}{dt} = \frac{1}{\tau_{APC,i}} (C_{APC,i-1} - C_{APC,i}) \quad [3.7]$$

$$\frac{dC_{PCC}}{dt} = \frac{1}{\tau_{PCC}} (C_{APC,N_{APC}} - C_{PCC}) \quad [3.8]$$

Here  $C_{BC,i}$  and  $C_{APC,i}$  are the dye concentrations of arbitrary blood and plasma compartment CSTRs, respectively.  $C_{PCC}$  is the dye concentration in the plasma collection chamber, which is assumed to be one CSTR. Thus,  $C_{PCC}$  is also the dye concentration exiting the plasma port.  $\tau_{APC,i}$  is the residence time of an arbitrary plasma compartment CSTR, while  $\tau_{PCC}$  is the residence time of the plasma collection chamber. These residence times are defined by Equations 3.9 and 3.10.

$$\tau_{APC,i} = \frac{\tau_{APC}}{N_{APC}} = \frac{V_{APC}^{bulk}}{N_{APC} Q_m} \quad [3.9]$$

$$\tau_{PCC} = \frac{V_{PCC}}{Q_m} \quad [3.10]$$

Here  $V_{APC}^{bulk}$  and is the volume of the active plasma compartment minus the volume of the bead spheres, while  $V_{PCC}$  is the volume of the plasma collection chamber.  $\tau_{APC}$  is the residence time of the entire APC (assuming that the dye is excluded from the gel bead pores). The average dye concentration flowing across the microporous membrane,  $\bar{C}_m$ , and the mean residence time of fluid flowing across the microporous membrane,  $\tau_m$ , are defined by Equations 3.11 and 3.12.

$$\bar{C}_m(t) = C_{APC,0} = \frac{1}{Q_m} \sum_{i=1}^{N_{BC}} [Q_{m,i} C_{BC,i}(t)] = \frac{1}{V_{BC}} \sum_{i=1}^{N_{BC}} [V_{BC,i} C_{BC,i}(t)] \quad [3.11]$$

$$\tau_m = \frac{\tau_{BC,i}}{V_{BC}} \sum_{i=1}^{N_{BC}} [i V_{BC,i}] \quad [3.12]$$

The value for  $V_{APC}^{bulk}$  is calculated from the specified values of  $V_{PCC}$  and  $Q_m$  and the calculated values of  $\tau_m$  and  $\tau_{pport}$ . The initial conditions of the system of equations are: 1) the first blood compartment CSTR contains a finite amount of dye and 2) the remaining compartments contain no dye. The model differential equations were integrated numerically using a fourth-order Runge-Kutta method.

### 3.3 RESULTS AND DISCUSSION

Analysis of RTD curves can be a powerful tool for characterizing the real mixing patterns within a reaction vessel. Using methods similar to those described in this chapter, two RTD data sets were previously obtained from the blood port of a prototype VFPR (plasma line connections shown in Figure 1.2 and Figure 3.2) [Ameer *et al.*, 1999]. These separate data sets were used to gain preliminary insight into the mixing behavior of the APC during steady-state enzymatic reactions. To mathematically simplify the VFPR model, the APC, collection chamber, and plasma line were treated as one compartment. Furthermore, the RTD of fluid exiting the blood compartment through the microporous membrane was assumed to be identical to that exiting from the blood port. These assumptions were not supported by the  $\beta_2m$ -immunoabsorption data presented in Chapter 2. Therefore, the development of a more rigorous compartmental model for the VFPR was deemed necessary.

In this chapter, experimental and modeling approaches are presented to better understand the mixing pattern within the VFPR and to assess the effects of gel loading and

changes in design specifications on mixing. Figure 3.4 illustrates the mixing behavior of the blood compartments of the two prototypes, while Table 3.3 and Table 3.4 list the model parameters calculated from the blood port RTD data. By comparing the values of  $\tau_{bport}$  and  $N_{BC}$  for the small prototype, it was concluded that the effect of loading gel beads into the APC on the blood compartment's mixing pattern is negligible. The same was assumed to be true for the large prototype, as the only difference in its blood compartment specifications was a 22% increase in membrane length.

**Table 3.3 Model parameters calculated from the blood port RTD data for the small VFPR prototype.**

$Q_m$ [mL/min]	Gel [mL]	$\tau_{bport}$ [s]	$r_{bport}^2$ [-]	$\tau_m$ [s]	$N_{BC}$ [-]	$V_{BC}$ [mL]
50	0	14.6	0.9829	7.9	8	43
50	48	14.0	0.9912	7.6	8	41
100	0	19.0	0.9817	9.8	7	48
100	48	19.2	0.9786	9.9	7	48

**Table 3.4 Model parameters calculated from the blood port RTD data for the large VFPR prototype.**

$Q_m$ [mL/min]	Gel [mL]	$\tau_{bport}$ [s]	$r_{bport}^2$ [-]	$\tau_m$ [s]	$N_{BC}$ [-]	$V_{BC}$ [mL]
50	0	17.8	0.9768	9.6	8	51
75	0	19.2	0.9784	10.4	8	52
100	0	21.1	0.9717	10.7	8	53

Figure 3.5 illustrates the mixing patterns of fluid exiting through the plasma ports of the two prototypes, which were loaded with the same volume fraction of gel. Table 3.5 and Table 3.6 list the model parameters calculated from the plasma port RTD data. For a given prototype and flowrate, loading gel beads into the APC decreases the values of  $V_{APC}^{bulk}$  and  $\tau_{pport}$  because the dye is excluded by the gel. According the model regression, the bulk fluid volumes within the APC of each prototype essentially behave as single CSTRs ( $N_{APC} = 1$ ,  $r_{pport}^2 > 0.98$ ) at the 50 mL/min plasma pump flowrate, regardless of gel loading. Hence, it

was concluded that gel loading does not significantly affect macroscopic mixing at these process conditions. At the 100 mL/min plasma pump flowrate, the bulk fluid volumes within the APC of each prototype essentially behave as single CSTRs ( $N_{APC} = 1$ ,  $r_{pport}^2 > 0.95$ ), provided that gel is not loaded. However, at the 100 mL/min plasma pump flowrate, it was found that gel loading decreases mixing within the APC of each prototype ( $N_{APC} = 2$ , Figure 3.5, flow visualization). Therefore, it was concluded that the time-scale of mixing is modulated by the presence of the gel suspension when the plasma pump flowrate is doubled. The model is able to describe the plasma port RTD data from the large prototype better than that obtained from the small prototype with gel loaded at the 100 mL/min plasma pump flowrate ( $r_{pport}^2 = 0.97$  vs. 0.87, Figure 3.5). This suggests that the increase in the time-scale of mixing, due to the increase in the radial thickness of the active compartment, is more than offset by the associated increase in residence time ( $\tau_{APC}$ ). Hence, the new VFPR prototype is expected to provide additional effective capacity for active gel particles and membrane surface area for increased plasma flowrates during blood detoxification. Meanwhile, the large VFPR design only represents a small (10 mL) increase in the whole blood priming volume.

**Table 3.5 Model Parameters calculated from the plasma port RTD data for the small VFPR prototype.**

$Q_m$ [mL/min]	Gel [mL]	$\tau_{pport}$ [s]	$r_{pport}^2$ [-]	$\tau_{APC}$ [s]	$N_{APC}$ [-]	$V_{APC}^{bulk}$ [mL]
50	0	108	0.9955	95	1	79
50	48	80	0.9966	66	1	55
100	0	59	0.9807	46	1	77
100	48	46	0.8671	33	2	55

Measuring the RTD at a plasma flowrate of 100 mL/min represents an extreme case that may not be clinically feasible for these prototypes; nevertheless, the model describes this condition moderately well. For instance, the  $\beta_2$ m-immunoabsorption experiments were performed with the small prototype at a plasma flowrate of 50 mL/min (Chapter 2) and the plasma separation rate of the device that was used for those studies is limited to approximately 60-70 mL/min. Assuming that the maximum hemofiltration rate is

proportional to the membrane surface area, the expected maximum plasma pump flowrate for the large prototype is 73-85 mL/min.

**Table 3.6 Model Parameters calculated from the plasma port RTD data for the large VFPR prototype.**

$Q_m$ [mL/min]	Gel [mL]	$\tau_{port}$ [s]	$r_{port}^2$ [-]	$\tau_{APC}$ [s]	$N_{APC}$ [-]	$V_{APC}^{bulk}$ [mL]
50	0	226	0.9989	205	1	170
50	120	143	0.9860	122	1	102
75	0	158	0.9761	140	1	175
75	120	103	0.9410	84	1	106
100	0	124	0.9596	107	1	178
100	120	78	0.9711	62	2	103

In summary, RTD data sets were collected from the plasma and blood ports separately for the studies presented in this chapter. The new model treats each physical compartment within the VFPR individually. It also accounts for, at least partially, the differences in RTD of the fluid exiting the blood compartment through the blood port and the microporous membrane. The model regression revealed that the bulk fluid within the APC was well-mixed ( $N_{APC} = 1$ ) at a plasma pump flowrate of 50 ml/min, with or without gel beads. The results of this study will be incorporated into a dynamic adsorption model for the VFPR (Chapter 4).

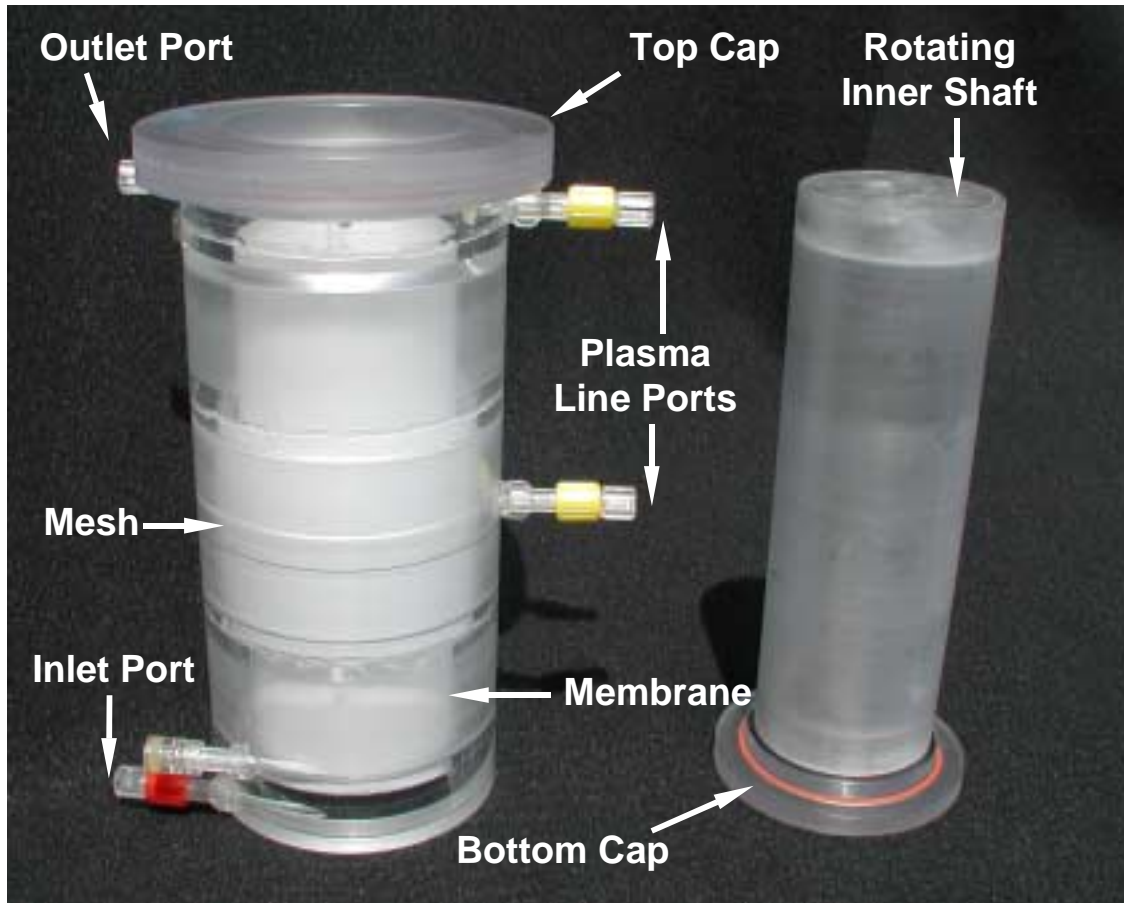


**Figure 3.1 Photograph of the new, larger VFPR prototype.** The device is partially disassembled for display purposes. The compartment volumes and pertinent length scales are provided in Table 3.1 and Table 3.2.

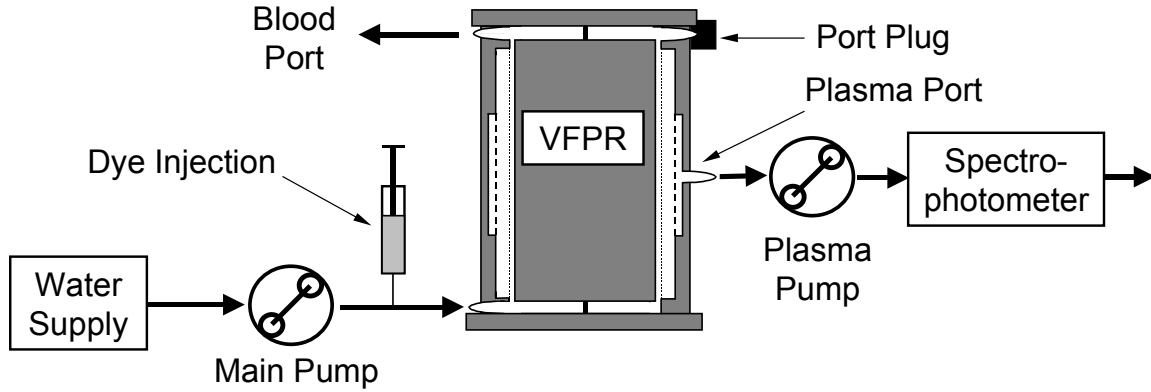


**Figure 3.2 Schematic diagram of the experimental setup used to obtain RTDs from the plasma port.** The spectrophotometer was moved to the blood port to obtain the RTDs of the blood compartment (not shown).

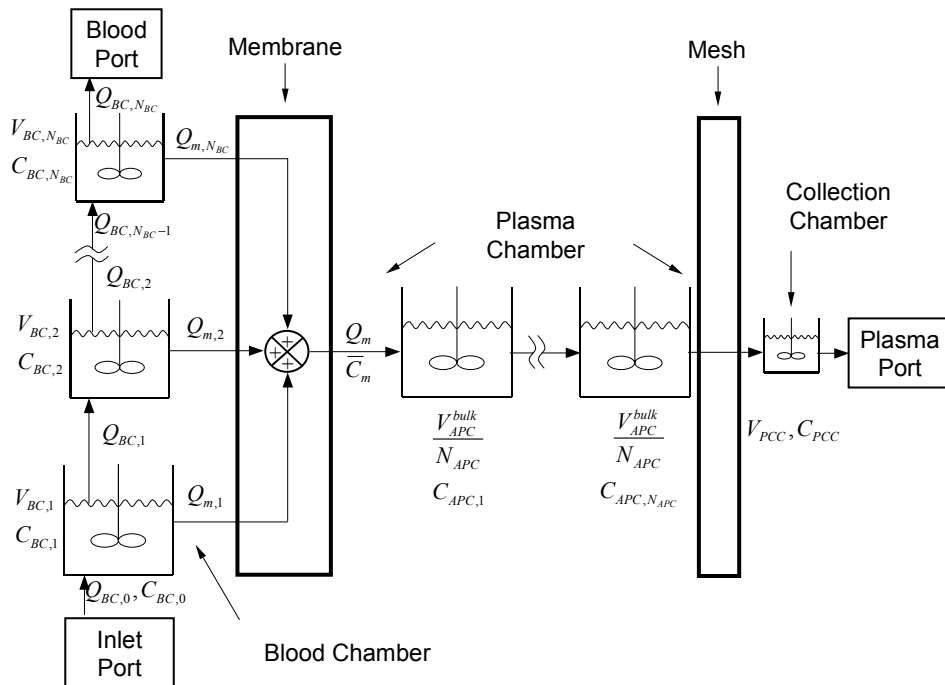


**Figure 3.3 The compartmental mixing model for the VFPR.**

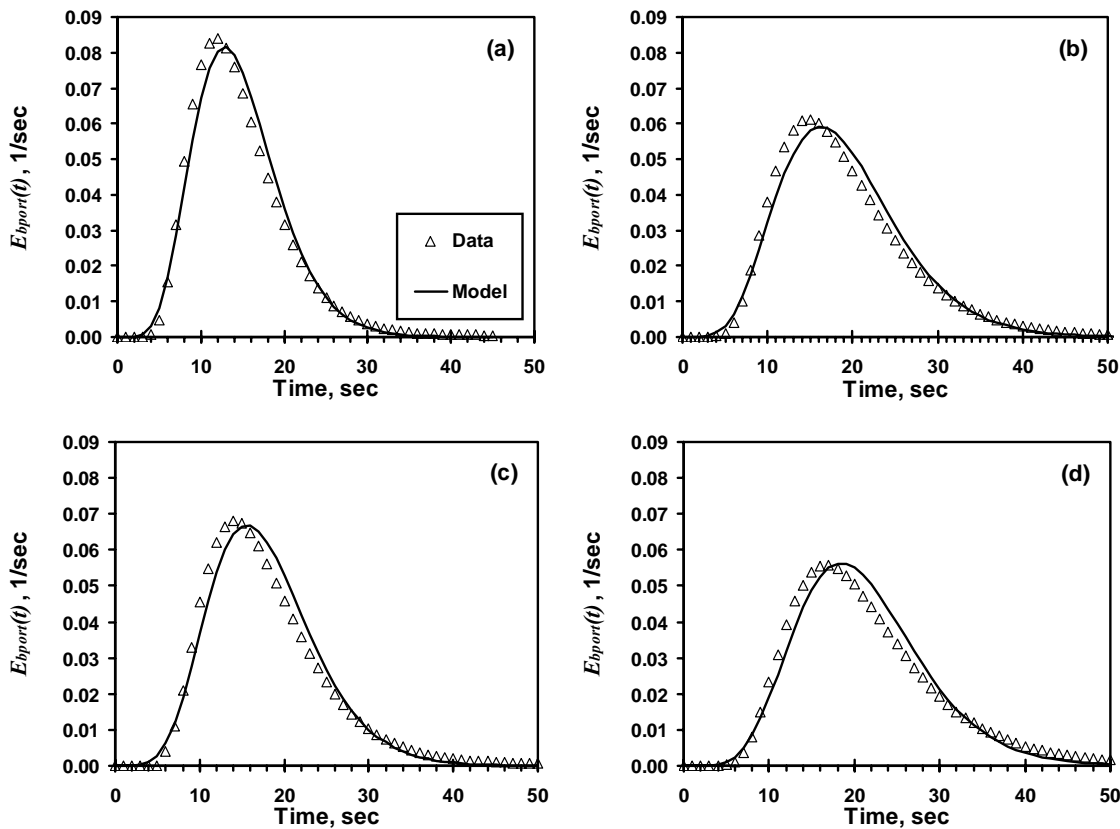


**Figure 3.4** Blood port residence time distribution functions for the small (top: a,b) and large (bottom: c,d) VFPR prototypes at plasma pump flowrates of 50 (left: a,c) and 100 (right: b,d) mL/min. The average data sets ( $N=3$ ,  $SEM < 0.0025 \text{ s}^{-1}$ ) and model curves are shown for the experiments conducted without gel loaded into the active plasma compartment.

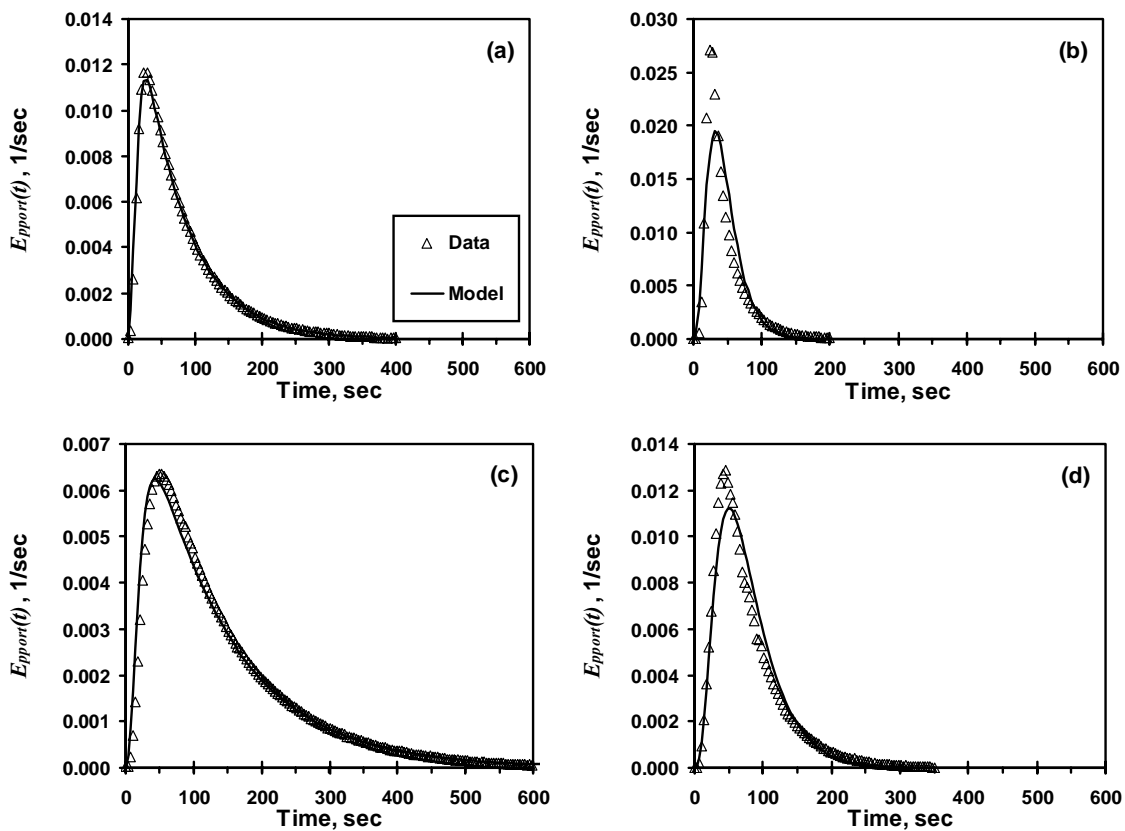


**Figure 3.5 Plasma port RTD curves for the small (top: a,b) and large (bottom: c,d) VFPR prototypes at plasma pump flowrates of 50 (left: a,c) and 100 (right: b,d) mL/min. The average data sets ( $N=3$ ,  $SEM < 0.0005 \text{ s}^{-1}$ ) and model curves are shown for the experiments conducted with gel loaded into the active plasma compartment.**

### 3.4 REFERENCES

Ameer GA, EA Grovender, B Obradovic, CL Cooney and R Langer (1999) "Rtd Analysis of a Novel Taylor-Couette Flow Device for Blood Detoxification." *AIChE Journal*. 45: 633-8.

Grovender EA, CL Cooney, RS Langer and GA Ameer (2001) "Modeling the Mixing Behavior of a Novel Fluidized Extracorporeal Immunoabsorber." *Chem Eng Sci*. 56: 5437-41.

Levenspiel O (1999) *Chemical Reaction Engineering*, John Wiley and Sons, New York.



## Chapter 4: Immunoadsorption Model for the VFPR\*

### 4.1 INTRODUCTION

From an engineering perspective, it would be useful to have a dynamic immunoadsorption model for the VFPR to aid in the design of device prototypes, *in vitro* experiments, and potential clinical trials. To derive such a model, the mass-transfer and adsorption processes within the VFPR need to be described. Towards this end, experimental and mathematical methods for characterizing the macroscopic mixing pattern within an immunoadsorptive VFPR were described in Chapter 3. In this chapter, the equilibrium behavior of immunoadsorptive gel beads is characterized using the Langmuir adsorption isotherm and confocal microscopy. Furthermore, the importance of external mass-transfer resistances within the active plasma compartment (APC) is assessed through dissolution studies conducted with benzoic acid particles. These results are used to develop a dynamic immunoadsorption model that describes the performance of the immunoadsorptive VFPR without using any adjustable parameters.

### 4.2 IMMUNOADSORPTIVE GEL

Thus far, the immunoadsorptive media used with VFPR devices has consisted of anti- $\beta_2m$  monoclonal antibodies immobilized onto 4% agarose gel beads (Chapter 2). In this section, the partitioning, diffusion, and adsorption of  $\beta_2m$  within the immunoadsorptive gel beads is described. These characteristics of the immunoadsorbent are used later in the derivation and solution of the dynamic immunoadsorption model equations for the VFPR.

#### 4.2.1 Solute Partitioning

The partition coefficient of  $\beta_2m$  in the gel ( $\Phi$ ) is defined on a total bead volume basis by Equation 4.1. The value of this parameter is estimated using Equation 4.2, a relation derived by Ogston [1958] for dilute solutions of uncharged, spherical macromolecules in an array of randomly arranged cylindrical fibers.

---

\* This chapter is a revised version of a research article originally published in the *AICHE Journal* [Grosvender *et al.*, 2002]. It has been reproduced with permission of the American Institute of Chemical Engineers. Copyright © 2002 AIChE. All rights reserved.

$$\Phi \equiv \frac{C_{gel}}{C_{bulk}} \quad [4.1]$$

$$\Phi = \exp \left[ -\phi \left( 1 + \frac{r_s}{r_f} \right)^2 \right] \quad [4.2]$$

Here  $C_{bulk}$  is the concentration of desorbed  $\beta_2m$  in the bulk fluid,  $C_{gel}$  is the concentration of desorbed  $\beta_2m$  inside the beads on a total gel volume basis, and  $\phi$  is the volume fraction of polymer fibers within the gel beads ( $\phi = 0.04$ ). The average radius of the agarose fibers,  $r_f$ , is taken to be  $1.9 \times 10^{-9}$  m, which was the value measured by Djabourov and co-workers [1989] using small-angle X-ray scattering. The hydrated radius of  $\beta_2m$ ,  $r_s$ , was estimated to be  $1.7 \times 10^{-9}$  m by assuming that  $\beta_2m$  has the specific volume and degree of hydration of a typical globular protein [Cantor and Schimmel, 1980].

#### 4.2.2 Adsorption Isotherm

The antigen-antibody equilibrium dissociation constant,  $K_D$ , is defined by Equation 4.3, while an adsorption site mass-balance is given by Equation 4.4. The combination of Equations 4.1, 4.3, and 4.4 results in the Langmuir adsorption isotherm, Equation 4.5.

$$K_D \equiv \frac{\rho_s^{eq} C_{gel}^{eq}}{\rho_{\beta_2m}^{eq}} \quad [4.3]$$

$$\rho_s^0 = \rho_s^{eq} + \rho_{\beta_2m}^{eq} \quad [4.4]$$

$$\rho_{\beta_2m}^{eq} = \frac{\rho_s^0 C_{bulk}^{eq}}{\frac{K_D}{\Phi} + C_{bulk}^{eq}} = \frac{\rho_s^0 C_{gel}^{eq}}{K_D + C_{gel}^{eq}} \quad [4.5]$$

On a total gel volume basis  $\rho_s$  and  $\rho_{\beta_2m}$  are the densities of adsorption sites and adsorbed  $\beta_2m$ , respectively. This is in contrast to the settled-bed volume basis that was used to define  $\rho'_s$  for Equation 2.1. The superscripts  $^0$  and  $^{eq}$  refer to the initial and equilibrium values, respectively.

A  $\beta_2m$  mass-balance (Equation 4.6) can be used with Equations 4.1 and 4.5 to obtain Equation 4.7, a form of the Langmuir adsorption isotherm in terms of measurable variables.

$$(1 - \varepsilon)V_{bed} \rho_{\beta_2m}^{eq} = [V_{total} - (1 - \varepsilon)V_{bed}] [C_{bulk}^0 - C_{bulk}^{eq}] + [(1 - \varepsilon)V_{bed}] [C_{gel}^0 - C_{gel}^{eq}] \quad [4.6]$$

$$\left[ \frac{V_{total} - V_{bed}(1-\varepsilon)(1-\Phi)}{V_{bed}} \right] (C_{bulk}^0 - C_{bulk}^{eq}) = \frac{(1-\varepsilon)\rho_s^0 C_{bulk}^{eq}}{\frac{K_D}{\Phi} + C_{bulk}^{eq}} \quad [4.7]$$

Here  $V_{total}$  is the total volume of the system,  $V_{bed}$  is the settled-bed volume of immunoadsorbent, and  $\varepsilon$  is the settled-bed void fraction. For cases when  $\Phi \sim 1$  or  $V_{bed} \ll V_{total}$ , the left hand side of Equation 4.7 can be approximated as in Equation 4.8.

$$\left[ \frac{V_{total} - V_{bed}(1-\varepsilon)(1-\Phi)}{V_{bed}} \right] (C_{bulk}^0 - C_{bulk}^{eq}) \approx \left[ \frac{V_{total}}{V_{bed}} \right] (C_{bulk}^0 - C_{bulk}^{eq}) \quad [4.8]$$

For the values of the parameters considered herein, this approximation represents an error of less than 2%. The adsorption site density ( $\rho_s^0$ ) of the immunoadsorbent gel was determined in Chapter 2 by equilibrating samples with saturating amounts of  $\beta_2m$  (where  $\rho_s' = [1-\varepsilon]\rho_s^0$ ). The same protocol and batch of immunoadsorbent was used with three sub-saturating quantities of  $\beta_2m$  to produce additional data, from which the value of  $K_D$  was regressed by minimizing SSE (Sum Squared Error).

### 4.2.3 Adsorption Site Distribution

Confocal microscopy\* was used to assess the spatial distribution of  $\beta_2m$ -adsorption sites within the immunoadsorbent gel beads. Recombinant human  $\beta_2m$  was prepared using the protocol described in Chapter 2 and labeled with fluorescein-5-EX succinimidyl ester, according to the instructions provided by the manufacturer (Molecular Probes, Eugene, OR). Fluorescein- $\beta_2m$  (6 mg) was equilibrated with a sample of the immunoadsorbent gel (0.20 mL) in phosphate buffered saline (pH 7.4; PBS). The sample was combined with an equal volume of anti-bleaching buffer (10  $\mu$ g p-phenylene diamine, 1.5 mL deionized water, and 1 mL 10x PBS brought to a total volume of 10 mL with glycerol) and studied with a Zeiss LSM 510 confocal microscope (Oberkochen, Germany). Two additional samples were analyzed as controls: 1) gel beads without immobilized antibody, but equilibrated with fluorescein- $\beta_2m$  and 2) gel beads with immobilized antibody, but not equilibrated with fluorescein- $\beta_2m$ .

---

\* This work was conducted utilizing the W. M. Keck Foundation Biological Imaging Facility at the Whitehead Institute.

#### 4.2.4 Effective Diffusivity

The effective diffusivity ( $D_e$ ) of  $\beta_2m$  inside the gel beads was calculated using Equation 4.9, where  $D_w$  is the diffusion coefficient of  $\beta_2m$  in dilute aqueous solution and  $\theta$  is the diffusion hindrance exerted by the gel polymer fibers.

$$D_e = \theta D_w \quad [4.9]$$

The value of  $D_w$  was estimated at 37°C ( $1.8 \times 10^{-10}$  m<sup>2</sup>/s) using a correlation for large molecules including proteins [Polson, 1950] and  $\theta$  was assumed to be the measured value (0.63) reported by Johnson and co-workers [1996] for lactalbumin (a  $1.4 \times 10^4$  g/mol globular protein) in 4% agarose gel.

### 4.3 DEVICE MODEL

#### 4.3.1 Blood Compartment

Figure 4.1 illustrates the dynamic adsorption model for the VFPR. Through residence time distribution studies and mathematical modeling it was shown in Chapter 3 that the macroscopic mixing behavior within the blood compartment can be well represented by a series of  $N_{BC}$  ideally well-mixed tanks. The residence time ( $\tau_{BC,i}$ ) of blood plasma in each tank is constant, but each tank has its own unique volume ( $V_{BC,i}$ ). Equations 4.10-4.14 represent a mass balance of  $\beta_2m$  within the blood compartment, taking into account hemofiltration into the APC.

$$\frac{dC_{BC,i}}{dt} = \frac{1}{\tau_{BC,i}} (C_{BC,i-1} - C_{BC,i}) \quad [4.10]$$

$$\tau_{BC,i} = \frac{(1 - H_{BC,i})V_{BC,i}}{Q_{m,i} + Q_{BC,i}(1 - H_{BC,i})} \quad [4.11]$$

$$H_{BC,i} = \frac{Q_{BC,0}H_{BC,0}}{Q_{BC,0} - \sum_{j=1}^i Q_{m,j}} \quad [4.12]$$

$$Q_{m,i} = V_{BC,i} \left( \frac{Q_m}{V_{BC}} \right) \quad [4.13]$$

$$Q_{BC,i} = Q_{BC,i-1} - Q_{m,i} \quad [4.14]$$

Here  $C_{BC,0}$ ,  $H_{BC,0}$  and  $Q_{BC,0}$  are the inlet plasma  $\beta_2m$  concentration, hematocrit (volume fraction of blood cells), and whole blood volumetric flowrate, respectively. The plasma pump controls the total volumetric flowrate of plasma across the microporous membrane into the active compartment,  $Q_m$ . For the  $i^{\text{th}}$  tank-in-series,  $C_{BC,i}$  is the plasma concentration of  $\beta_2m$ ,  $H_{BC,i}$  is the hematocrit,  $Q_{BC,i}$  is the outlet volumetric flowrate of whole blood, and  $Q_{m,i}$  is the volumetric flowrate of plasma across the membrane. The total volume of the blood compartment is  $V_{BC}$ . The  $\beta_2m$  concentration of plasma crossing the membrane,  $\bar{C}_m$ , is given by Equation 4.15.

$$\bar{C}_m = \frac{1}{V_{BC}} \sum_{i=1}^{N_{BC}} (V_{BC,i} C_{BC,i}) \quad [4.15]$$

### 4.3.2 Active Plasma Compartment (APC)

The APC houses the immunoabsorptive media, which consists of an antibody immobilized onto porous agarose gel beads. The model for the APC incorporates the following assumptions: 1) the intrinsic antibody-antigen association rate is instantaneous, 2) the adsorption sites are uniformly distributed inside the gel beads, 3) the adsorption equilibrium follows the Langmuir isotherm, 4) the bulk fluid within the APC behaves as a single well-mixed control volume (Chapter 3), and 5) the size of the gel beads can be well represented by the volume-average radius,  $R$ .

Equation 4.16 represents a mass balance for  $\beta_2m$  in the bulk fluid of the APC. The first term on the right-hand side of Equation 4.16 accounts for convective flow through the APC; the second term accounts for transport of  $\beta_2m$  to the surface of the active beads.

$$\left[ V_{APC} - V_{bed} (1 - \varepsilon) \right] \frac{dC_{APC}}{dt} = Q_m (\bar{C}_m - C_{APC}) + A_{surface} \bar{k}_m (C_{APC}^{surface} - C_{APC}) \quad [4.16]$$

Here  $V_{APC}$  is the total volume of the APC and  $\bar{k}_m$  is the mass-transfer coefficient for the transport of  $\beta_2m$  from the bulk fluid to the surface of the gel beads. The  $\beta_2m$  concentrations within the bulk fluid and at the outer surface of the gel beads are  $C_{APC}$  and  $C_{APC}^{surface}$ , respectively. The total surface area of the gel,  $A_{surface}$ , is expressed by Equation 4.17 in terms of previously defined parameters, where  $N_{beads}$  is the total number of gel beads in the APC.

$$A_{surface} = N_{beads} (4\pi R^2) = \left[ \frac{(1-\varepsilon)V_{bed}}{(4\pi R^3/3)} \right] (4\pi R^2) = \frac{3(1-\varepsilon)V_{bed}}{R} \quad [4.17]$$

Equations 4.1, 4.16, and 4.17 are combined to yield Equation 4.18 which, along with Equations 4.19 and 4.20, are used to model dynamics of the  $\beta_2m$  concentration of the bulk fluid within the APC.

$$\frac{dC_{APC}}{dt} = \frac{1}{\tau_{APC}} (\bar{C}_m - C_{APC}) + \frac{3V_{bed}(1-\varepsilon)}{\tau_{EMT} [V_{APC} - V_{bed}(1-\varepsilon)]} \left( \frac{C_{gel}^{surface}}{\Phi} - C_{APC} \right) \quad [4.18]$$

$$\tau_{APC} = \frac{V_{APC} - V_{bed}(1-\varepsilon)}{Q_m} \quad [4.19]$$

$$\tau_{EMT} = \frac{R}{k_m} \quad [4.20]$$

Here the characteristic time-scale of external mass-transfer (or the transport of  $\beta_2m$  to the surface of the active beads) is  $\tau_{EMT}$  and  $\tau_{APC}$  is the residence time of the bulk fluid volume.

Using the aforementioned assumptions, the species conservation equation for desorbed  $\beta_2m$  within an immunoabsorptive gel bead is reduced to the form shown by Equation 4.21. The rate of adsorption,  $R_{adsorption}$ , is expressed in the convenient form shown by Equation 4.22.

$$\frac{\partial C_{gel}}{\partial t} = D_e \frac{1}{r^2} \frac{\partial}{\partial r} \left( r^2 \frac{\partial C_{gel}}{\partial r} \right) - R_{adsorption} \quad [4.21]$$

$$R_{adsorption} = \frac{\partial \rho_{\beta_2m}}{\partial C_{gel}} \left( \frac{\partial C_{gel}}{\partial t} \right) \quad [4.22]$$

The Langmuir adsorption isotherm, or Equation 4.5, is combined with Equations 4.21 and 4.22 to yield Equations 4.23 and 4.24 which represent a mass balance for  $\beta_2m$  within a gel bead. Here the characteristic time-scale of internal mass-transfer within the porous beads is  $\tau_{IMT}$ . Equation 4.23 has previously been derived and used to model the adsorption of albumin onto ion exchange resin [Leaver *et al.*, 1992]. Equations 4.25 and 4.26 represent the boundary conditions that were used to solve Equation 4.23, where the superscripts *surface* and *center* refer to their respective radial positions.

$$\frac{\partial C_{gel}}{\partial t} = \frac{R^2}{\tau_{IMT}} \left( 1 + \frac{\rho_S^0 K_D}{(K_D + C_{gel})^2} \right)^{-1} \left( \frac{\partial^2 C_{gel}}{\partial r^2} + \frac{2}{r} \frac{\partial C_{gel}}{\partial r} \right) \quad [4.23]$$

$$\tau_{IMT} = \frac{R^2}{D_e} \quad [4.24]$$

$$\bar{k}_m \left( C_{APC} - \frac{C_{gel}^{surface}}{\Phi} \right) = D_e \left( \frac{\partial C_{gel}}{\partial r} \right)^{surface} \quad [4.25]$$

$$\left( \frac{\partial C_{gel}}{\partial r} \right)^{center} = 0 \quad [4.26]$$

### 4.3.3 Plasma Line, Collection Chamber, and Blood Outlet Port

The plasma line and collection chamber are lumped together as a single well-mixed control volume and modeled by Equations 4.27-4.28. Here  $C_{PLCC}$ ,  $V_{PLCC}$ , and  $\tau_{PLCC}$  are the lumped  $\beta_2m$  concentration, volume, and residence time, respectively. The plasma  $\beta_2m$  concentration of partially cleansed whole blood exiting the VFPR,  $C_{VFPR}$ , is calculated by Equation 4.29.

$$\frac{dC_{PLCC}}{dt} = \frac{1}{\tau_{PLCC}} (C_{APC} - C_{PLCC}) \quad [4.27]$$

$$\tau_{PLCC} = \frac{V_{PLCC}}{Q_m} \quad [4.28]$$

$$C_{VFPR} = \frac{Q_m C_{PLCC} + (Q_{BC,0} - Q_m)(1 - H_{BC,N_{BC}})C_{BC,N_{BC}}}{Q_{BC,0}(1 - H_{BC,0})} \quad [4.29]$$

## 4.4 RESERVOIR MODEL

The VFPR is usually connected to a  $\beta_2m$  reservoir in a closed-loop circuit for blood detoxification (Figure 4.2). This reservoir can be comprised of a bag of donated blood, an animal model, or a human patient. To date,  $\beta_2m$ -immunoabsorption experiments with the VFPR have been limited to bags of whole human blood (Chapter 2). Equations 4.30 and 4.31 represent the mass balance of  $\beta_2m$  in a blood bag (530 mL) and its circuit tubing (65

mL). These two volumes are lumped together as  $V_{BR}$ . Equations 4.32 and 4.33 mathematically connect the reservoir to the VFPR device in a closed-loop circuit.

$$\frac{dC_{BR,i}}{dt} = \frac{1}{\tau_{BR,i}} (C_{BR,i-1} - C_{BR,i}) \quad [4.30]$$

$$\tau_{BR,i} = \frac{\tau_{BR}}{N_{BR}} = \frac{V_{BR}}{N_{BR}Q_{BR}} \quad [4.31]$$

$$C_{BR,0} = C_{VFPR} \quad [4.32]$$

$$C_{BC,0} = C_{BR,N_{BR}} \quad [4.33]$$

Here  $N_{BR}$  is the number of theoretical tanks representing  $V_{BR}$ . For the  $i^{\text{th}}$  tank-in-series,  $C_{BR,i}$  is the plasma  $\beta_2\text{m}$  concentration and  $\tau_{BR,i}$  is the residence time.

#### 4.5 CHARACTERIZATION OF MASS-TRANSFER TO THE SURFACE OF SUSPENDED PARTICLES

The importance of mass-transfer resistance at the external surface of the suspended gel beads ( $\tau_{EMT}$ , Equation 4.20) relative to the mass-transfer resistance associated with the hemofiltration rate ( $\tau_{APC}$ , Equation 4.19) was assessed through dissolution studies conducted with small, non-spherical particles of benzoic acid. These particles were created using a method similar to one previously described by Moore [1994]. Briefly, benzoic acid was melted, solidified into a flat sheet on aluminum foil, and crushed with a ceramic mortar and pestle. Irregularly shaped particles approximately 100  $\mu\text{m}$  in size were obtained by sifting the crushed benzoic acid between 150  $\mu\text{m}$  and 75  $\mu\text{m}$  nominal opening stainless steel sieves (VWR, Westchester, PA).

The dissolution studies were conducted as shown in Figure 4.3. The active plasma compartment was flushed for 5 minutes ( $>3.5$  residence times) to remove most ( $>95\%$ ) of the dissolved benzoic acid that was injected along with the solid particles. During the following 5 minute experimental period, samples were taken every 60 seconds and immediately filtered to remove any remaining fine particles (0.45  $\mu\text{m}$  Millipore catalog number SLHV R04 NL, Bedford, MA). The concentration of benzoic acid was measured by reading the absorbance at 250 nm (diluting the samples as necessary with 0.01% Triton X-100).

## 4.6 COMPUTATIONAL METHODS

Equations 4.10-4.15, 4.18-4.20, and 4.23-4.33 model the dynamics of  $\beta_2m$  adsorption within the VFPR and the subsequent removal of  $\beta_2m$  from a blood reservoir. The Forward-Time Centered-Space (FTCS) method was used to convert Equation 4.23 into a discrete form (200 finite radial sections) and the second-order Runge-Kutta algorithm was applied to integrate the differential equations [Press *et al.*, 1992]. Input parameters (including initial conditions, with superscripts  $t=0$ ) used for the model calculations are listed in Table 1. At each time-step, the total mass-balance error for Equations 4.10-4.15, 4.18-4.20, and 4.23-4.33 was kept below 0.5%. A copy of the FORTRAN program used to perform the model calculations is provided in the Appendix.

## 4.7 RESULTS AND DISCUSSION

The VFPR is a multi-compartment Taylor-Couette flow hemofilter designed to remove toxins from a patient's blood stream via heterogeneous adsorption or reaction. The first immunoadsorption application has been the removal of the amyloid-associated protein  $\beta_2$ -microglobulin from human blood *in vitro*. This technology, we believe, can be used for understanding and treating the progression of Dialysis-Related Amyloidosis, a devastating complication of long-term kidney failure, by targeting a specific macromolecule and monitoring the effect of its removal on the patient via clinical trials. To lay a solid foundation for the derivation of a dynamic model, the equilibrium behavior of the immunoadsorbent and the mass-transfer characteristics of the VFPR were investigated independently.

Over the  $\beta_2m$  concentration range considered, the Langmuir isotherm describes equilibrium  $\beta_2m$  adsorption data (Figure 4.4). The value of the antibody-antigen dissociation constant ( $K_D = 0.1 \pm 0.1$  mg/L) is significantly smaller than the lower limit of the  $\beta_2m$  concentration range (1.0 - 3.0 mg/L) in the circulation of healthy individuals [Floege and Ketteler, 2001]. Therefore, this model immunoadsorbent appears to have sufficient affinity for therapeutic application.

The cross-sectional confocal micrograph of a typical immunoadsorptive gel bead shows that the  $\beta_2m$  adsorption sites are uniformly distributed throughout the polymer (Figure 4.5a). This was a key assumption in the numerical solution of Equation 4.23 (i.e.

$\rho_s^0$  is not a function of radial position). Meanwhile, the defect in the atypical bead demonstrates the ability of the imaging technique to detect regions inside the gel that lack adsorbed  $\beta_2m$  (Figure 4.5b). These results demonstrate the utility of confocal microscopy for the characterization of porous matrices.

During the dissolution studies the observed concentration of benzoic acid ( $3.0 \pm 0.1$  g/L) exiting the VFPR through the plasma line did not significantly differ from the solubility limit (2.9 g/L at 20°C) [Budavari *et al.*, 1989]. This strongly suggests that external mass-transfer resistances within the active plasma compartment are not rate limiting under the process conditions considered. In order to provide flexibility for other process conditions that may arise in the future, the derivation of the VFPR model accounts for the possibility of a rate-limiting external mass-transfer resistance through the mass-transfer coefficient,  $\bar{k}_m$ . In accordance with the findings of the dissolution studies,  $\bar{k}_m$  was assigned a finite value sufficiently large such that  $\tau_{EMT} \ll \tau_{IMT}$  and  $\tau_{EMT} \ll \tau_{APC}$  (Table 4.1 and Equations 4.19, 4.20, and 4.24). Thus, external mass-transfer resistance did not have any appreciable effect on the immunoadsorption dynamics calculated by the model for the experiment considered (refer to the sensitivity analysis below and Figure 4.7a). However, the second term on the right-hand side of Equation 4.18 is required in any case to account for the transport of  $\beta_2m$  to the surface of the gel beads.

The model's ability to describe VFPR performance was tested with a set of input parameters corresponding to a previously conducted  $\beta_2m$ -adsorption experiment (Table 4.1). Without adjusting any of the parameters, the dynamic immunoadsorption model is able to describe the performance of the VFPR (Figure 4.6, Equations 4.10-4.15, 4.18-4.20 and 4.23-4.33). It is important to note that the equilibrium concentration of  $\beta_2m$  is on the order of the antibody-antigen dissociation constant ( $K_D$ ). This is the case because the system was charged, approximately, with a 1:1 stoichiometric ratio of  $\beta_2m$  and adsorption sites. Under clinical operating conditions, an immunoadsorptive VFPR would likely contain an excess number of adsorption sites. In separate  $\beta_2m$  immunoadsorption experiments that were conducted with excess adsorption sites, the equilibrium  $\beta_2m$  concentrations were below detectable limits (Chapter 2).

**Table 4.1 Model input parameters.**

Parameter	Value	Units	Parameter	Value	Units
$C_{APC}^{t=0}$	0	mg/L	$Q_m$	50*	mL/min
$C_{BC,i}^{t=0}$	3.2*	mg/L	$R$	46 <sup>†</sup>	
$C_{BR,i}^{t=0}$	3.2*	mg/L	$V_{BC}$	46.5 <sup>§,††</sup>	mL
$C_{gel}^{t=0}$	0	mg/L	$V_{BC,i}$	6.6, 6.3, 6.1, 5.9	mL
$C_{PLCC}^{t=0}$	0	mg/L		5.7, 5.5, 5.3, 5.1 <sup>§,††</sup>	
$D_e$	1.1 x 10 <sup>-10</sup>	m <sup>2</sup> /s	$V_{APC}$	79 <sup>§</sup>	mL
$H_{BR}$	0.31 <sup>‡</sup>	-	$V_{bed}$	48*	mL
$K_D$	0.1	mg/L	$V_{BR}$	595*	mL
$\bar{k}_m$	10 <sup>-3</sup>	m/s	$V_{PLCC}$	15*	mL
$N_{BC}$	8 <sup>§,††</sup>	-	$\epsilon$	0.4 <sup>**</sup>	-
$N_{BR}$	3 <sup>§,††</sup>	-	$\Phi$	0.87	-
$Q_{BR}$	200*	mL/min	$\rho_s^0$	50 <sup>*,‡‡</sup>	mg/L

A sensitivity analysis was conducted on the external mass-transfer coefficient ( $\bar{k}_m$ ) to confirm that increasing the value of  $\bar{k}_m$  above the arbitrarily assigned value does not have a significant effect on the model predictions (Figure 4.7a). Furthermore, the model's flexibility to account for external mass-transfer resistances is demonstrated by the shape of the plasma line model curve for the low value of  $\bar{k}_m$  ( $\tau_{EMT} \sim \tau_{IMT}$ ). The assumption that the population of gel beads can be well represented by the volume-average radius was tested by a sensitivity analysis on  $R$  (Figure 4.7b). Varying the value of this parameter by one standard of deviation has an effect on the shape of the plasma line concentration curve; however, this

\* Chapter 2 [Ameer *et al.*, 2001]

† Data provided by the manufacturer.

‡ After accounting for dilution by the priming saline.

§ Chapter 3 [Grosvender *et al.*, 2001]

\*\* Calculated from the total and void volumes measured in a packed column (acetone and pore-excluded aggregate protein markers; Bio-Rad #151-1901, Hercules, CA).

†† The mixing behavior was re-characterized through similar RTD studies using a 36% glycerol-in-water solution at 20°C to better account for the viscosity and density of whole blood [Wolf *et al.*, 1984; Fournier, 1999].

‡‡ Value previously reported on a settled-bed volume basis.

effect is reasonably symmetric. Therefore, the assumption appears to be justified. Because their values were estimated from the literature, sensitivity analyses on the hindered effective diffusivity ( $D_e$ ) and the solute partition coefficient ( $\Phi$ ) were performed (Figure 4.7c-Figure 4.7d). The variations considered (refer to Figure 4.7 caption) in  $D_e$  and  $\Phi$  resulted in changes of less than 15% in the calculated values of  $C_{PLCC}$  at all time-points.

The dynamic immunoadsorption model for the VFPR was developed to facilitate the development of the device and the optimization of its potential therapeutic application. With the desire for a model capable of describing the VFPR's performance over a range of conditions, the model was based on fundamental transport theory and guided by the independent characterization of the fluid dynamics and adsorption equilibrium. The model calculations predict that the mass-transfer processes within the active compartment of the VFPR do not control the rate of  $\beta_2m$ -adsorption (Figure 4.7). Hence, we conclude that the process controlling the  $\beta_2m$ -adsorption rate within the VFPR is the hemofiltration rate ( $Q_m = 50$  mL/min), which is on the order of the reported flowrate of extravascular  $\beta_2m$  into the blood stream (approximately 70 mL/min) [Floege *et al.*, 1991]. These two processes are expected to be rate-controlling for  $\beta_2m$  removal from a patient with the immunoadsorbent VFPR. A major goal for the future development of the VFPR will be to increase the hemofiltration rate while maintaining the fast mass-transfer rates within the active plasma compartment. The methods for characterizing the VFPR and the dynamic immunoadsorption model presented herein should prove useful in this endeavor.

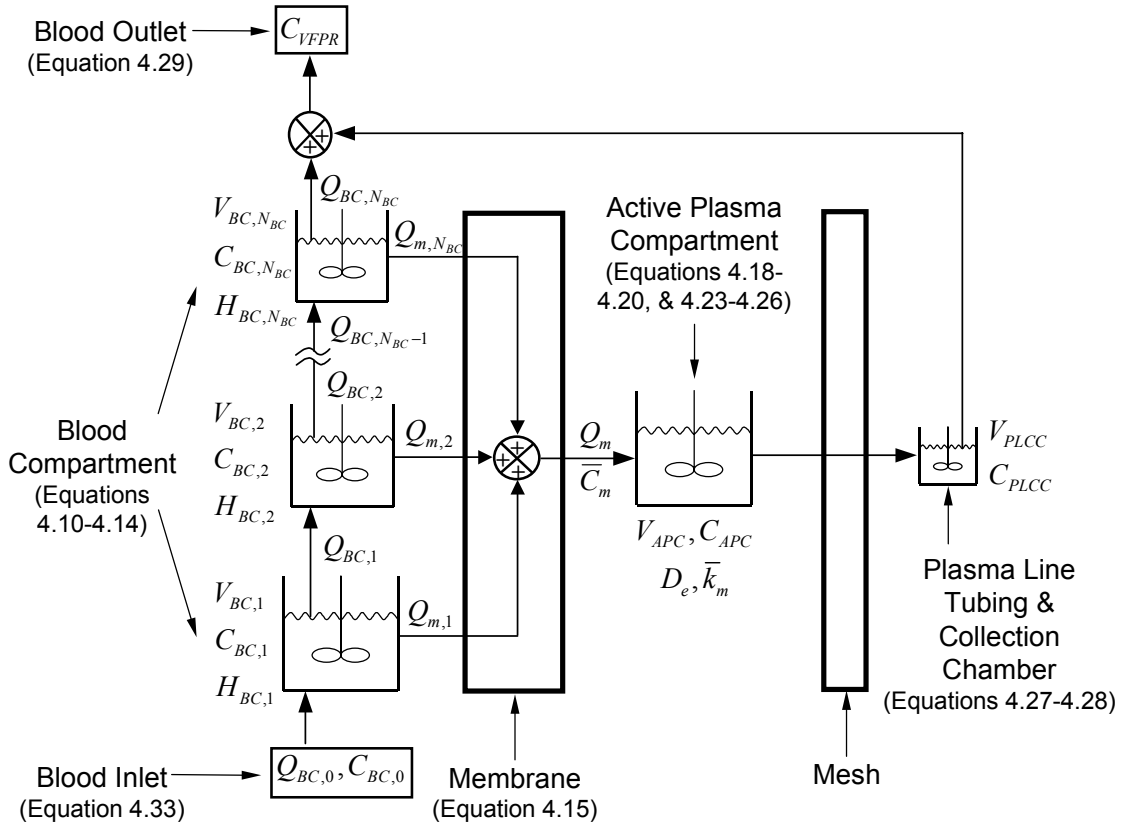


**Figure 4.1 Schematic diagram of the dynamic VFPR adsorption model.** The macroscopic mixing behavior of the blood compartment is described by a finite series of ideally well-mixed control volumes or “tanks.” The bulk fluid of the active plasma chamber and the lumped volume of the plasma line tubing & plasma collection chamber are each represented by a single tank.

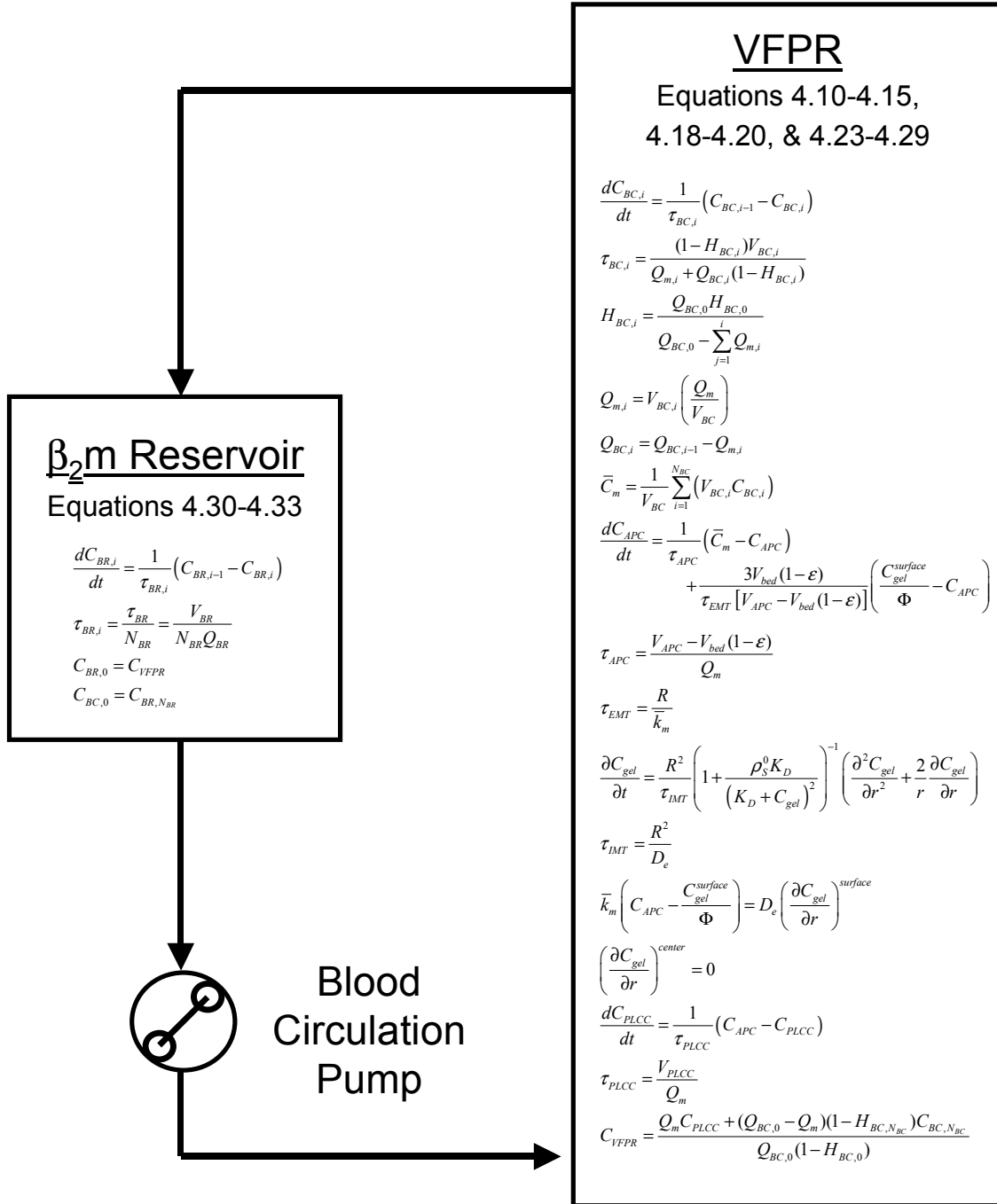


**Figure 4.2 Closed-loop blood detoxification with the VFPR.** The  $\beta_2m$  reservoir represents either a human patient or a substituted model (i.e. a bag of blood) and the circuit tubing. The equations shown are provided as a convenience to the reader and are described throughout the text.

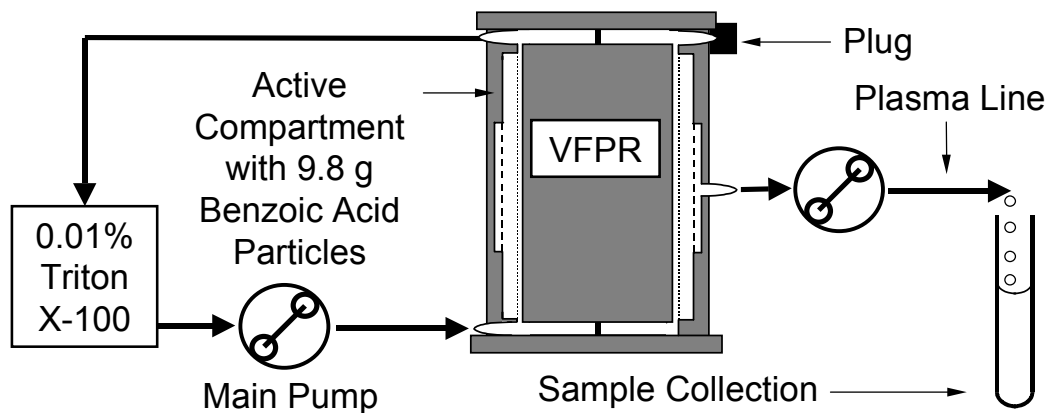


**Figure 4.3 Apparatus used to conduct the dissolution studies.** Agarose gel beads (40 mL Sepharose® CL-4B) were included in the active compartment in an attempt to duplicate the conditions of the dynamic  $\beta_2$ m-adsorption experiments. The main pump flowrate (200 mL/min), plasma pump flowrate (50 mL/min), and cylinder rotation rate ( $1.2 \times 10^3$  rpm) also matched those used during the  $\beta_2$ m-adsorption experiments. Aggregation of the benzoic acid particles was prevented by adding 0.01% Triton X-100 to the system. It has previously been reported that the use of a similar non-ionic surfactant during benzoic acid dissolution studies has a minimal effect (<5%) on the mass-transfer rate [Gondoh *et al.*, 1968].

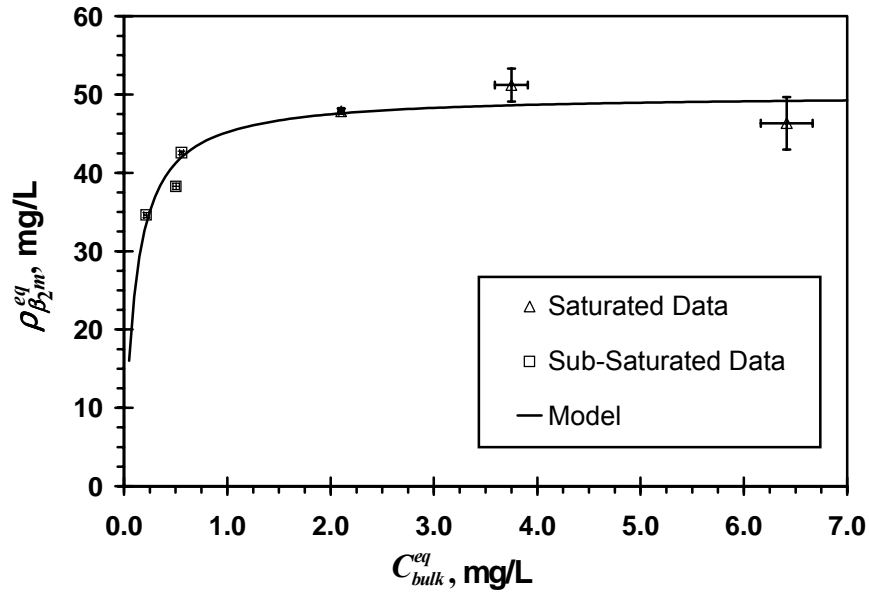


**Figure 4.4 Equilibrium adsorption behavior of the immunoadsorbent media.** Equations 4.7 and 4.8 were regressed to the saturated (Chapter 2) and sub-saturated data to determine the value of  $K_D$  ( $0.1 \pm 0.1$  mg- $\beta_2m$  /L  $\sim$  10 nmol- $\beta_2m$  /L). The value of  $\rho_s^0$  ( $50 \pm 3$  mg- $\beta_2m$ /L-gel) was calculated from the saturated data (reported as  $\rho_s' = 30 \pm 2$  mg- $\beta_2m$ /L-settled-bed in Chapter 2). The controls did not show significant fluorescence. Error bars and confidence intervals represent the standard error of the mean (SEM).

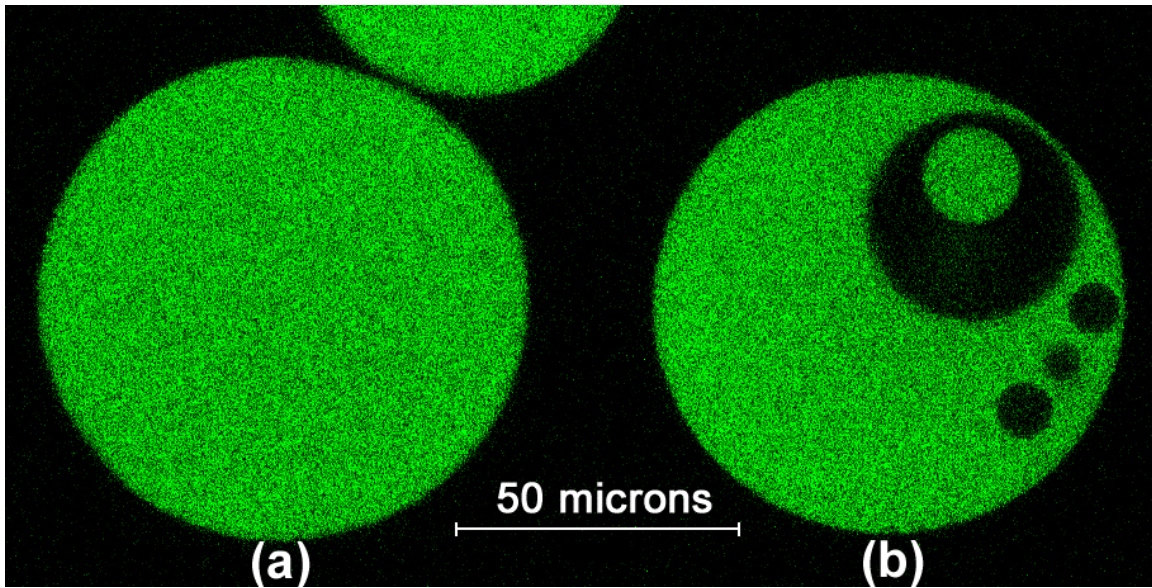


**Figure 4.5** Confocal micrograph of the immunoadsorbent gel: center cross-section of a typical bead (a) and an atypical bead (b).  $\beta_2m$  is shown in green. The controls showed no apparent adsorption of  $\beta_2m$  or intrinsic fluorescence of the immunoadsorbent. The thickness of the cross-section shown is  $0.40\ \mu\text{m}$  and the resolution is  $0.22\ \mu\text{m}$ .

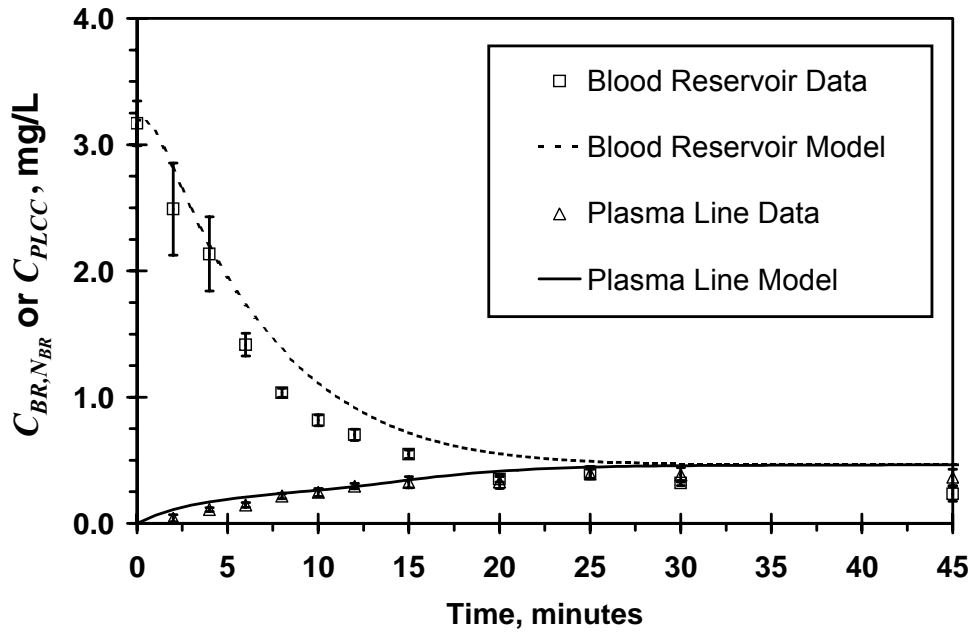
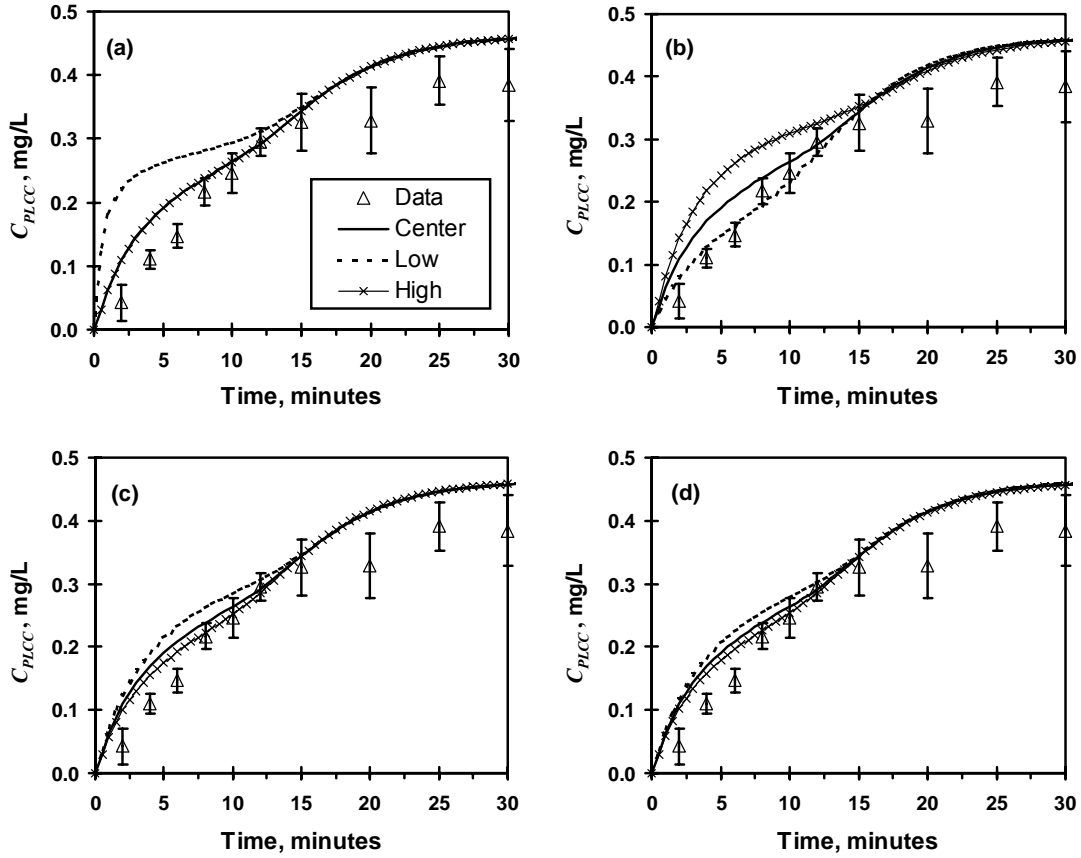


Figure 4.6 The predicted and observed dynamics of  $\beta_2m$  clearance from whole blood by an immunoabsorptive VFPR, *in vitro*. The model equations listed in Figure 4.2 and the input parameters listed in Table 2.1 were used to calculate the blood reservoir outlet and plasma line  $\beta_2m$  concentrations. The blood reservoir outlet and plasma line data was first presented in Chapter 2. Error bars represent the standard error of the mean (SEM).



**Figure 4.7 Sensitivity analysis results for the model parameters  $\bar{k}_m$  (a),  $R$  (b),  $D_e$  (c), and  $\Phi$  (d).** The plasma line data ( $\Delta$ ) was taken from Chapter 2 [Ameer *et al.*, 2001] and the error bars represent the standard error of the mean (SEM). The center values for the model parameters are listed in Table 4.1. The high and low values are as follows:  $\bar{k}_m = 10^{-2}$  &  $10^{-5}$  m/s,  $R = 58$  &  $34 \mu\text{m}(\pm\sigma)$ ,  $D_e = 1.8 \times 10^{-10}$  &  $0.7 \times 10^{-10} \text{ m}^2/\text{s} (\pm 20\%)$ ,  $\Phi = 1.00$  &  $0.75$  (the measured value reported Johnson and co-workers [1995] for lactalbumin in 6% agarose gel).

## 4.8 REFERENCES

- Ameer GA, EA Grovender, H Ploegh, D Ting, WF Owen, M Rupnick and R Langer (2001) "A Novel Immunoadsorption Device for Removing Beta2-Microglobulin from Whole Blood." *Kidney Int.* 59: 1544-50.
- Budavari S, MJ O'Neil, A Smith and PE Heckelman (1989) Merck & Company, Rahway, NJ: pp. 170.
- Cantor CR and PR Schimmel (1980) *Biophysical Chemistry: Techniques for the Study of Biological Structure and Function.*, W. H. Freeman and Company, New York.
- Djabourov M, AH A. H. Clark, DW Rowlands and SB Ross-Murphy (1989) "Small-Angle X-Ray Scattering Characterization of Agarose Sols and Gels." *Macromol Rev.* 22: 180.
- Floege J, A Bartsch, M Schulze, S Shaldon, KM Koch and LC Smeby (1991) "Clearance and Synthesis Rates of Beta-2-Microglobulin in Patients Undergoing Hemodialysis and in Normal Subjects." *J Lab Clin Med.* 118: 153-65.
- Floege J and M Ketteler (2001) "Beta-2-Microglobulin-Derived Amyloidosis: An Update." *Kidney Int.* 59 Suppl 78: S164-71.
- Fournier RL (1999) Taylor & Francis, Philadelphia: pp. 65.
- Gondoh S, M Shiozawa, K Kusunoki and I Nakamori (1968) "Effects of Surfactants on the Solution Rate of Single Benzoic Acid Spheres in Water." *Kagaku Kogaku.* 32: 919.
- Grovender EA, CL Cooney, R Langer and GA Ameer (2002) "Immunoadsorption Model for a Novel Fluidized-Bed Blood Detoxification Device." *AIChE Journal.* 48: 2357-65.
- Grovender EA, CL Cooney, RS Langer and GA Ameer (2001) "Modeling the Mixing Behavior of a Novel Fluidized Extracorporeal Immunoabsorber." *Chem Eng Sci.* 56: 5437-41.
- Johnson EM, DA Berk, RK Jain and WM Deen (1995) "Diffusion and Partitioning of Proteins in Charged Agarose Gels." *Biophysical Journal.* 68: 1561-8.
- Johnson EM, DA Berk, RK Jain and WM Deen (1996) "Hindered Diffusion in Agarose Gels: Test of Effective Medium Model." *Biophysical Journal.* 70: 1017-23.
- Leaver G, JA Howell and JR Conder (1992) "Adsorption Kinetics of Albumin on a Cross-Linked Cellulose Chromatographic Ion Exchanger." *J Chromatog.* 509: 101.
- Moore CMV (1994) *Characterization of a Taylor-Couette Flow Reactor.* Massachusetts Institute of Technology, Chemical Engineering: Cambridge.
- Ogston AG (1958) "The Spaces in a Uniform Random Suspension of Fibers." *Trans Faraday Soc.* 54: 1754.
- Polson A (1950) "Some Aspects of Diffusion in Solution and a Definition of a Colloid Particle." *J Phys Colloid Chem.* 54: 649.
- Press WH, S. A. , SA Teukolsky, WT Vetterling and BP Flannery (1992) *Numerical Recipes in Fortran 77: The Art of Scientific Computing*, Cambridge University Press, New York.
- Wolf AV, MG Brown and PG Prentiss (1984) In *Crc Handbook of Chemistry and Physics*(Eds, Weast, RC, MJ Astle and WH Beyer) CRC Press, Boca Raton, FL: pp. D-235.

## Chapter 5: ScFv-Based Immunoabsorbent

### 5.1 INTRODUCTION

In Chapter 2, a model anti- $\beta_2m$  immunoabsorbent was created by immobilizing whole BBM.1 antibodies onto porous agarose gel beads. While the molar binding activity of the immobilized BBM.1 antibody was lower than expected (6%), its  $\beta_2m$ -adsorption site density ( $\rho'_s = 0.030 \pm 0.002$  mg- $\beta_2m$ /mL-settled-gel) was sufficient to conduct preliminary *in vitro* research with a VFPR prototype. The ideal immunoabsorbent for this application should possess a high  $\beta_2m$ -adsorption site density ( $\rho'_s > 1$  mg- $\beta_2m$ /mL-settled-gel), so as to reduce the hold-up and/or loss of valuable plasma proteins during extracorporeal therapy. Single-chain variable region antibody fragments (scFv) should theoretically allow for higher effective  $\beta_2m$ -adsorption site densities because they are smaller in size than whole antibodies. ScFvs are also genetically defined and amenable to microbial expression and *in vitro* evolution. These potential advantages of scFvs over whole antibodies motivated the creation of the BBM.1 scFv-based immunoabsorbent that is described by this chapter.

### 5.2 METHODS

#### 5.2.1 Labeling of $\beta_2m$

Recombinant human  $\beta_2m$  was prepared as previously described [Ameer *et al.*, 2001] and biotinylated using the FluoReporter® Biotin-XX protein labeling kit (Molecular Probes, Eugene, OR). A 20 mg/mL working stock of biotin-XX (sulfosuccinimidyl ester, sodium salt) in DMSO (dimethylsulfoxide) was prepared and a 10-fold molar excess was added to 1.6 mg/mL  $\beta_2m$  in PBS 7.4 (phosphate buffered saline, pH 7.4: 10 mM  $PO_4$ , 138 mM NaCl, 2.7 mM KCl). The labeling reaction was performed at this pH to inhibit the reaction of the sulfosuccinimidyl ester with the primary amines of lysine residues, thereby favoring the labeling of the  $\beta_2m$  at the N-terminus. The reaction mixture was incubated on a rocker for 90 min at room temperature and subsequently dialyzed overnight into PBS 7.4 at 4°C to remove any unreacted biotin-XX using a 6-8 kD membrane (Spectrum Laboratories, Rancho Dominguez, CA). The final concentration of  $\beta_2m$  was determined using an extinction coefficient of 20,065 M<sup>-1</sup> cm<sup>-1</sup> at 280 nm as previously described [Ameer *et al.*, 2001], while the degree of biotinylation (0.93 mol-biotin/mol- $\beta_2m$ ) was determined following the kit instructions.

Recombinant human  $\beta_2m$  was labeled with Alexa Fluor® 488 (carboxylic acid, succinimidyl ester), a fluorophore that is spectrally similar to fluorescein, but possesses greater brightness and photostability (Molecular Probes). The protocol used was essentially that described above for the biotinylation of  $\beta_2m$ . However, 3-fold molar excess of a 5 mg/mL working stock of labeling agent was added to 1.1 mg/mL of  $\beta_2m$  in PBS 7.4 for the labeling reaction. The final concentration and degree of labeling (0.056 mole-fluorophore/mole- $\beta_2m$ ) was determined using the extinction coefficient previously described [Ameer *et al.*, 2001] and the protocol provided by Molecular Probes.

### 5.2.2 Cloning of $V_H$ and $V_L$ genes

The BBM.1 antibody-producing hybridoma cell line (HB-28) was purchased from ATCC (Manassas, VA) and grown in T-flask static culture at 37°C in a 5% CO<sub>2</sub> atmosphere. The growth media consisted of 90% RPMI 1640 medium (ATCC), 10% FBS (fetal bovine serum), 100 u/mL penicillin, and 0.1 mg/mL streptomycin. The total RNA from  $3 \times 10^7$  cells was isolated and RT-PCR was performed using the RNeasy® Midi and the OneStep RT-PCR kits from Qiagen (Valencia, CA). Various combinations of the primers (0.5  $\mu$ M each) provided in the Mouse Ig-Primer Set (Novagen, Madison, WI) were used along with 1  $\mu$ g of RNA and 40 units of RNase inhibitor (Promega, Madison, WI) in 50  $\mu$ L RT-PCR reaction volumes. The thermocycler was run for 1 reverse-transcription cycle of 30 min at 50°C, 1 DNA polymerase-activation cycle of 15 min at 95°C, 35 amplification cycles of 45 sec at 94°C, 1 min at 60°C, 1 min at 72°C and 1 final extension cycle of 10 min at 72°C.

The PCR products were run on 1.2 or 2.0% agarose gels stained with ethidium bromide. Those displaying bands characteristic of  $V_H$  and  $V_L$  genes (about 500 base pairs in length) were purified using the QIAquick kit (Qiagen) and ligated into the pSTBlue-1 plasmid (Novagen). The ligation products were used to transform NovaBlue Singles™ competent cells (included in the pSTBlue-1 Perfectly Blunt Cloning kit from Novagen), which were plated onto LB (Luria-Bertani medium) agar plates containing 50 mg/mL ampicillin. After incubating the plates overnight at 37°C, single colonies were each grown in 5 mL of LB containing 100-150 mg/L ampicillin at 37°C overnight, and their plasmids were purified using the QIAprep® Spin Miniprep kit (Qiagen). The DNA inserts of the plasmid clones were sequenced and translated into peptide sequences so that they could be compared

to the partial peptide sequences obtained through the N-terminal degradation of protein A-purified BBM.1 antibody.

Twenty-two cycles of N-terminal degradation were performed on a sample of whole BBM.1 antibody. For each degradation cycle, the two predominant residues were assigned to one of two peptide chains based on a match with the published sequence of the MOPC-21 myeloma  $\kappa$  light chain [Svasti and Milstein, 1972]. This was done because the BBM.1 hybridoma cell line (HB-28) was created by fusing an anti- $\beta_2m$  B-cell with the X63-Ag8 myeloma [Brodsky *et al.*, 1979], a descendent of the MOPC-21 myeloma [Kohler and Milstein, 1975]. Both the X63-Ag8 and MOPC-21 myeloma cell lines have been shown to secrete the MOPC-21  $\kappa$  light chain as well as an IgG<sub>1</sub> heavy chain [Kohler and Milstein, 1975].

### 5.2.3 Display of scFv fragment by yeast

The V<sub>H</sub> and V<sub>L</sub> genes cloned from the BBM.1 hybridoma were initially expressed as a scFv fragment in a yeast display system [Boder and Wittrup, 1997] (Figure 5.1). This approach was selected because the  $\beta_2m$ -binding affinity of the scFv could readily be characterized in a quantitative fashion and, if deemed necessary, would be in a vector that is amenable to *in vitro* evolution [Boder *et al.*, 2000].

#### 5.2.3.1 Insert Assembly

The scFv DNA insert was assembled in a V<sub>H</sub>-(Gly<sub>4</sub>Ser)<sub>4</sub>-V<sub>L</sub> configuration via the splicing by overlap extension (SOE) method [Horton *et al.*, 1989]. All of the PCR reactions were performed using Cloned Pfu DNA polymerase and Cloned Pfu Reaction Buffer (Stratagene, La Jolla, CA), following the manufacturer's instructions except where otherwise noted. During the first round of PCR, the V<sub>H</sub> and V<sub>L</sub> DNA inserts were amplified from the pSTBlue-1 plasmids (30 ng plasmid DNA in each 50  $\mu$ L reaction volume) using the custom primers shown in Figure 5.2 (0.2  $\mu$ M each). The thermocycler was run for 1 cycle of 45 sec at 98°C, 28 cycles of 45 at 98°C, 90 sec at 72°C, and 1 cycle of 10 min at 72°C. The resulting V<sub>H</sub> and V<sub>L</sub> PCR products were purified using the QIAquick® Kit and quantitated by measuring their absorbance at 260 nm.

The second round of PCR was initiated without primers and was performed in a single 50  $\mu$ L reaction volume with 77 ng of each  $V_H$  and  $V_L$  PCR product and 400  $\mu$ M of each dNTP (deoxynucleotide triphosphate). The thermocycler was run for 5 cycles of 1 min at 96°C, 1 min at 53°C, 2 min at 72°C, and 1 cycle of 10 min at 72°C. The 5'- $V_H$  and 3'- $V_L$  primers were then added (0.5  $\mu$ M each) and the thermocycler was run for 15 cycles of 1 min at 96°C, 1 min at 53°C, 1 min at 72°C, and 1 cycle of 10 min at 72°C. The resulting scFv DNA insert was purified and quantitated as above.

#### 5.2.3.2 Plasmid Construction

The purified scFv SOE PCR product and the pCTCON yeast display plasmid [Graff, 2002] (a derivative of the pCT302 plasmid [Boder and Wittrup, 1997] with a BamHI site added 5' to the c-myc sequence) were digested with BamHI and NheI restriction enzymes for more than 2 hours at 37°C, according to the manufacturer's instructions (New England Biolabs, Beverly, MA). The restriction digest products were purified using the QIAquick® Kit, combined in an equimolar ratio (500 ng plasmid, 4  $\mu$ g insert), and ligated using T4 DNA ligase (Stratagene) following the manufacturer's instructions. After incubating the ligation reaction mixture at room temperature for more than 2 hours, the reaction was heat deactivated at 65°C for 10 min. The ligation products were used to transform XL1-Blue Supercompetent *E. coli* (Stratagene), following the manufacturer's protocol, and plated on LB agar plates containing 50 mg/mL ampicillin. Single colonies were each grown in 5 mL of LB containing 100 mg/L ampicillin at 37°C overnight and their plasmid clones were purified using the QIAprep® Spin Miniprep Kit. A plasmid clone with the desired in-frame scFv insert was identified through DNA sequencing and labeled pEAG1.

#### 5.2.3.3 Yeast Transformation, Growth, and Induction

EBY100 strain yeast cells [Boder and Wittrup, 1997] were transformed with pEAG1 through electroporation, plated onto SD-CAA agar plates (7 g/L yeast nitrogen base, 5.4 g/L  $\text{NaH}_2\text{PO}_4$ , 8.6 g/L  $\text{Na}_2\text{HPO}_4$ , 5.0 g/L casamino acids, 20 g/L dextrose, Trp and Ura deficient) and incubated for 2.5 days at 30°C. Cells originating from a single colony were grown in 5 mL of SD-CAA media (7 g/L yeast nitrogen base, 2.7 g/L  $\text{NaH}_2\text{PO}_4$ , 5.0 g/L  $\text{Na}_2\text{HPO}_4$ , 5.0 g/L casamino acids, 20 g/L dextrose) at 30°C on an orbital shaker for about 16 hours ( $\text{OD}_{600}$

= 4.0). A volume of the yeast suspension containing  $5 \times 10^7$  cells ( $OD_{600}=1$  represents  $1 \times 10^7$  cells/mL [Boder and Wittrup, 2000]) was centrifuged, re-suspended in 5 mL of SG-CAA induction media (same as SD-CAA, but substituting galactose for dextrose), and incubated at 22°C on an orbital shaker for approximately 20 hours.

#### 5.2.3.4 *Yeast Labeling*

The labeling of the yeast cells for FACS analysis was performed in a fashion similar to that previously described [VanAntwerp and Wittrup, 2000]. Each of a series of 1.5 mL centrifuge tubes were loaded with  $1 \times 10^6$  EBY100 cells (transformed with pEAG1 and induced with galactose). The tubes were centrifuged and the yeast pellets were washed with 500  $\mu$ L of PBS/BSA (PBS 7.4 with 0.1% bovine serum albumin added as a carrier). Murine anti-HA tag antibody (12Ca5 MAb, Roche, Basel, Switzerland) and biotinylated recombinant human  $\beta_2m$  were used as primary labeling agents at concentrations of 2  $\mu$ g/mL and  $1 \times 10^{-11}$ – $1 \times 10^{-6}$  M, respectively. The primary labeling of each tube was carried out in 1.0 mL of PBS/BSA at room temperature on a rocker for 30 minutes. The cells were spun down and washed as above with ice-chilled PBS/BSA. Secondary labeling was conducted in 100  $\mu$ L of PBS/BSA on ice for 15 minutes, using 40  $\mu$ L/mL each of streptavidin-phycoerythrin (PharMingen, San Diego, CA) and FITC-conjugated anti-mouse IgG (Sigma, St. Louis, MO). The cells were centrifuged at 4°C and washed quickly with 500  $\mu$ L of ice-chilled PBS/BSA. The labeled cell pellets were stored on ice and protected from light until FACS analysis.

Four additional yeast pellets were labeled for FACS analysis, which served as controls. The labeling was performed as described above, except that: (1) the primary labels were omitted; (2) biotinylated recombinant human  $\beta_2m$  and streptavidin-phycoerythrin were omitted; (3) the murine anti-HA tag antibody and FITC-conjugated anti-mouse IgG were omitted, (4) un-biotinylated recombinant human  $\beta_2m$  was added in 100-fold molar excess to competitively inhibit the biotinylated  $\beta_2m$ .

#### 5.2.3.5 *FACS Analysis*

The labeled yeast cell pellets were each resuspended in approximately 1.0 mL of PBS/BSA and analyzed with an Epics® XL FACS (fluorescence activated cell sorter; Beckman Coulter, Fullerton, CA) in a fashion similar to those previously described [Boder

and Wittrup, 2000; VanAntwerp and Wittrup, 2000]. Samples were gated by light scattering and then by FITC signal in order to avoid consideration of particles other than un-clustered scFv-displaying yeast cells. The mean phycoerythrin (PE) signal for more than  $2 \times 10^4$  scFv-displaying cells labeled with each  $\beta_2m$  concentration was recorded. SPHERO™ Rainbow Calibration Particles (3.0-3.4  $\mu m$ , Spherotech, Libertyville, IL) with six different known densities of surface-immobilized FITC were also analyzed ( $>1 \times 10^3$  counted at each density) to allow for the correlation of the mean FITC signal per cell to the mean number of scFv fragments displayed by each cell.

### 5.2.3.6 Mathematical Modeling

Assuming a monovalent antibody-antigen binding interaction, the antibody-antigen equilibrium dissociation constant,  $K_D$ , is defined by Equation 5.1

$$K_D \equiv \frac{[scFv]_{eq} [\beta_2m]_{eq}}{[scFv * \beta_2m]_{eq}} \quad [5.1]$$

Here  $[scFv]_{eq}$ ,  $[\beta_2m]_{eq}$ , and  $[scFv * \beta_2m]_{eq}$  are the equilibrium concentrations (mole per L of cell suspension during primary labeling) of dissociated antibody fragment, dissociated antigen ( $\beta_2m$ ), and scFv fragment-antigen complex, respectively.

Assuming that the binding of  $\beta_2m$  by the scFv fragment is the only reaction consuming the dissociated species,  $[scFv]_{eq}$  and  $[\beta_2m]_{eq}$  can be expressed in terms of other variables as described by Equations 5.2 and 5.3.

$$[scFv]_{eq} = [scFv]_0 - [scFv * \beta_2m]_{eq} = P_0[Y]_0 - [scFv * \beta_2m]_{eq} \quad [5.2]$$

$$[\beta_2m]_{eq} = [\beta_2m]_0 - [scFv * \beta_2m]_{eq} \quad [5.3]$$

Here  $[scFv]_0$ ,  $[\beta_2m]_0$ , and  $[Y]_0$  are the initial molar concentrations of dissociated antibody fragment,  $\beta_2m$ , and yeast cells during the primary labeling step and  $P_0$  is the mean number of scFv fragments displayed per cell (mole-scFv/mole-yeast). The value of  $P_0$  was independently determined from the mean FITC signal and the calibration curve obtained from the FACS analysis of the SPHERO™ standards.

The mean PE signal of the scFv-displaying population,  $F$ , is assumed to be a linear function of  $[scFv * \beta_2m]_{eq}$  as described by Equation 5.4, where  $C_1$  and  $C_2$  are empirical constants.

$$F = c_1[scFv * \beta_2m]_{eq} + c_2 \quad [5.4]$$

Equations 5.1-5.4 can be combined and rearranged to yield Equation 5.5, which was used to regress the values of  $K_D$ ,  $c_1$ , and  $c_2$  from each set of  $F$  vs.  $[\beta_2m]_0$  data .

$$F = \frac{c_1}{2} \left[ (K_D + [\beta_2m]_0 + P_0[Y]_0) - \sqrt{(K_D + [\beta_2m]_0 + P_0[Y]_0)^2 - 4P_0[Y]_0[\beta_2m]_0} \right] + c_2 \quad [5.5]$$

#### 5.2.4 Secretion of scFv fragment by yeast

A His6-tag and a cysteine residue were added to the C-terminus of the secreted version of the BBM.1 scFv fragment to facilitate its purification and subsequent immobilization. This location was chosen to minimize the interference of the purification tag and the immobilization bond with the  $\beta_2m$ -binding site. It was deemed necessary to remove the Lys-Arg sequence near the C-terminus of the  $V_L$  gene because it is known to be cleaved by the Kex2 protease within the trans-Golgi network of *Saccharomyces cerevisiae* [Bevan *et al.*, 1998; Rockwell and Fuller, 1998].

##### 5.2.4.1 Plasmid Construction

The Lys-Arg sequence in the  $V_L$  was removed by changing the Arg residue to Asn. This was achieved through PCR (50  $\mu$ L reaction volume) with the 5'- $V_H$  and 3'-Lys-Asn primers (Figure 5.2, 0.25  $\mu$ M each) and the pEAG1 plasmid (1  $\mu$ L). Cloned Pfu DNA polymerase and Cloned Pfu Reaction Buffer were used to carry out the reaction, following the manufacturer's instructions. The thermocycler was run for 1 cycle of 1 min at 98°C, 28 cycles of 1 min at 98°C, 2 min at 72°C, and 1 cycle of 10 min at 72°C. The resulting scFv PCR product was ligated into the pCT302 plasmid essentially as described for the construction of the pEAG1 plasmid, except that a 2:1 molar ratio of scFv insert to plasmid DNA was used during the ligation reaction. A plasmid clone with the desired scFv insert, pEAG2, was obtained from the ligation reaction products in the same manner as pEAG1.

The Kex2 protease resistant form of the BBM.1 scFv insert was amplified from the pEAG2 plasmid through PCR with the 5'- $V_H$  and 3'-His6-Cys primers (Figure 5.2). The PCR was performed as described for the creation of pEAG2, except that the thermocycler was run for 1 cycle of 1 min at 98°C, 28 cycles of 1 min at 98°C, 1 min at 55°C, 1 min at 72°C and 1 cycle of 10 min at 72°C. The resulting scFv insert was ligated into the secretion

plasmid pRS-GALTwt [Shusta *et al.*, 1999] in frame with the synthetic pre pro signaling sequence [Clements *et al.*, 1991], under control of the GAL1,10 promoter. The ligation protocol was essentially that described for the construction of the pEAG1 from pCTCON, except that the BamHI restriction enzyme was replaced with XhoI (New England Biolabs) and a 4:1 molar ratio of scFv insert to plasmid DNA was used. A secretion plasmid clone with the desired scFv insert, pEAG3, was obtained from the ligation reaction products in the same manner as pEAG1 and pEAG2.

#### 5.2.4.2 Yeast Transformation, Growth, and Induction

YVH10 yeast, a protein disulfide isomerase overexpressing strain of *Saccharomyces cerevisiae* [Robinson *et al.*, 1994], were transformed with pEAG3 and pRS314 (to add Trp-resistance to allow selection on Trp deficient media) [Sikorski and Hieter, 1989] using the lithium acetate/single-stranded carrier DNA/polyethylene glycol method [Agatep *et al.*, 1998]. Cells were plated onto selective SD-SCAA plates (6.7 g/L yeast nitrogen base, 7.5 g/L NaH<sub>2</sub>PO<sub>4</sub>, 5.4 g/L Na<sub>2</sub>HPO<sub>4</sub>, 20 g/L dextrose, 15 g/L agar, 182 g/L sorbitol, and synthetic casamino acids: 40 mg/L adenine sulfate, 140 mg/L His, 190 mg/L Arg, 108 mg/L Met, 52 mg/L Tyr, 290 mg/L Ile, 440 mg/L Lys, 200 mg/L Phe, 1260 mg/L Glu, 400 mg/L Asp, 380 mg/L Val, 220 mg/L Thr, 130 mg/L Gly, deficient in Leu, Trp, and Ura) and incubated at 30°C for 3 days.

Expansion of the transformed YVH10 cells was initiated by inoculating 50 mL of SD-SCAA liquid media (same as SC-SCAA plates, but with agar and sorbitol omitted) with cells originating from a single colony. After incubating the starter culture on an orbital shaker at 30°C overnight (OD<sub>600</sub> = 3.6), 30 mL of the starter culture was used to inoculate 6 L of SD-SCAA. Each liter of SD-SCAA was placed into a 2.5 L fully baffled Tunair flask (Shelton Scientific, Shelton, CT) and incubated at 30°C for 1 day (OD<sub>600</sub> = 6.8). The yeast cells were then centrifuged and resuspended in 6 L of YPG induction media (10 g/L yeast extract, 20 g/L peptone, 20 g/L galactose) with 100 units/mL penicillin and 0.1 g/L streptomycin added to inhibit bacterial contamination. Each liter of YPG was placed in a 2 L, smooth-bottomed Erlenmeyer flask and incubated at room temperature (approximately 22°C) for about 3 days (OD<sub>600</sub> = 17.4). The cell suspension was then centrifuged and the

supernatant was 0.2  $\mu\text{m}$  filtered and concentrated to an approximate volume of 400 mL using a 10 kD Prep/Scale-TFF<sup>TM</sup> regenerated cellulose membrane (Millipore, Bedford, MA).

#### 5.2.4.3 Protein Purification

The His6-tagged scFv fragment was purified from the concentrated cell culture supernatant via nickel affinity chromatography, for which PBS 8.0 (phosphate buffered saline, pH 8.0: 50 mM phosphate, 300 mM sodium chloride) was used with varying imidazole concentrations. To remove metal contaminants, 5 mM sodium ethylenediaminetetraacetic acid (EDTA) was added to the concentrated culture supernatant, which was placed in a 400 mL stirred ultrafiltration cell with a 10 kD YM10 regenerated cellulose disk membrane (Millipore). The cell was subsequently flushed with 2.8 L of PBS 8.0 to facilitate buffer exchange. To minimize the binding of un-tagged protein, 10 mM imidazole was added and the protein was bound to a 5 mL column of Ni-NTA agarose gel beads (Qiagen). The resin was washed with 60 mL of 20 mM imidazole and eluted with 30 mL of 250 mM imidazole. The eluted protein was further purified by size-exclusion chromatography using Superose<sup>®</sup> 12 prep grade resin (Amersham Biosciences, Uppsala, Sweden) eluted with PBS 7.4. The desired fractions were pooled and the concentration of scFv was measured by reading the absorbance at 280 nm, using a molar extinction coefficient of 51,130 L/mol  $\text{cm}^{-1}$  and a molecular weight of 29,032 g/mole. These values were calculated from the amino acid sequence and the formula reported by Pace and co-workers [Pace *et al.*, 1995].

### 5.2.5 Immunoabsorbent based on scFv fragment

#### 5.2.5.1 Protein Immobilization

Immediately prior to immobilization, the purified scFv fragment was reduced with Immobilized TCEP (Tris[2-carboxyethyl] phosphine hydrochloride]) Disulfide Reducing Gel (Pierce, Rockford, IL). The reaction was performed for one hour at room temperature on a rocker in 3.5 mL of PBS 7.2 (phosphate buffered saline, pH 7.2: 100 mM  $\text{PO}_4$ , 150 mM NaCl) containing 15 mM EDTA, 33% TCEP gel by volume, and 2.0 mg/mL scFv fragment. During the same hour, lysine Sepharose<sup>®</sup> 4B (Amersham Biotech) was activated with sulfosuccinimidyl 4-(N-maleimidomethyl)cyclohexane-1-carboxylate (Sulfo-SMCC, Pierce).

Sulfo-SMCC is a heterobifunctional cross-linking agent that reacts with sulfhydryl and primary amine groups. This reaction was also performed for one hour at room temperature on a rocker, but in 4.5 mL of 150 mM sodium bicarbonate buffer (pH 8.8) containing 1.8 mg/mL Sulfo-SMCC and 22% swollen lysine Sepharose<sup>®</sup> 4B gel by volume.

Following the one-hour incubation, the activated lysine gel was rinsed (several times, totaling 30 volumes) and re-suspend with ice-cold PBS 7.2. Immediately thereafter, the reduced scFv fragment was removed from the TCEP gel by centrifuging it in a Micro Bio-Spin<sup>®</sup> (Bio-Rad, Hercules, CA) column. The TCEP gel was rinsed with 1.0 mL of PBS 7.2 to improve the recovery of the scFv fragment. The scFv fragment immobilization reaction was performed for 24 hours on a rocker at 4°C in 4.0 mL PBS 7.2 containing 4.4 mg scFv fragment and 0.45 mL Sulfo-SMCC activated gel (settled bed volume). The number free thiol groups per scFv fragment molecule, before and after contact with the TCEP gel, was measured using the Thiol and Sulfide Quantitation kit obtained from Molecular Probes. The kit instructions were followed except that the degassing performed by argon bubbling instead of using vacuum desiccator.

The following day, the soluble scFv fragment was removed from the gel by centrifuging it in a Micro Bio-Spin column and the gel was rinsed 4 times with 2.0 mL of PBS 7.2. The gel was re-suspended in 2.0 mL PBS 7.2, containing 1 mM L-cysteine as a quenching agent, and incubated overnight at 4°C on a rocker. After quenching, the gel was centrifuged, rinsed four times as before, and resuspended in PBS 7.4. Equal volumes of the reduced scFv fragment, the quenching buffer, and the eight rinses were assayed for protein by SDS-PAGE (sodium dodecyl sulfate-polyacrylamide gel electrophoresis). A control matrix was prepared by immobilizing L-cysteine onto lysine Sepharose<sup>®</sup> 4B gel following the above protocol, omitting the scFv-protein.

#### 5.2.5.2 Characterization

Alexa Fluor<sup>®</sup> 488-labeled recombinant human  $\beta_2m$  ( $\beta_2m$ -AF488, see Section 5.2.1) was used to determine the  $\beta_2m$ -adsorption capacity of the agarose-immobilized scFv antibody fragment and control matrix. A series of 0.5 mL centrifuge tubes were each loaded with 100  $\mu$ L of 10% gel suspension in FCS/PBS (75% fetal calf serum, 25% PBS 7.4 by volume), a saturating quantity of  $\beta_2m$ -AF488 (16, 12 or 10  $\mu$ g; 0.96 mg/mL stock), and

sufficient FCS/PBS to bring the total volume to 0.400 mL. The tubes were equilibrated at 37°C for 1 hour on a rocker and then centrifuged. From each tube, three 100 µL volumes of supernatant were loaded into individual wells of a 96-well plate, which was also loaded with calibration standards (0, 10, 20, 30, 40, and 50 mg/L of β<sub>2</sub>m-AF488 in FCS/PBS). The plate was read by a Mithras LB 940 plate reader (Berthold Technologies, Bad Wildbad, Germany), using excitation and emission wavelengths of 485 and 535 nm, respectively. A linear calibration curve was generated and was used to determine the β<sub>2</sub>m-AF488 concentrations of the experimental samples. The β<sub>2</sub>m-adsorption capacity of the agarose-immobilized scFv antibody fragment was calculated from this data, using Equation 5.6.

$$\rho'_s = \frac{V_{total}}{V_{gel}} (C_0 - C_{eq}) \quad [5.6]$$

Here  $\rho'_s$  is the adsorption site density (mg β<sub>2</sub>m per mL of settled gel),  $V_{total}$  is the total volume of each tube (mL),  $V_{gel}$  is the settled-volume of the gel (µL),  $C_0$  is the initial β<sub>2</sub>m concentration (mg/L), and  $C_{eq}$  is the concentration of desorbed β<sub>2</sub>m at equilibrium (mg/L).

For regeneration, the labeled gel was recovered from the centrifuge tubes, placed in a Micro Bio-Spin® column, and centrifuged. The immunoadsorptive media was regenerated by rinsing it four times with 2.0 mL of stripping buffer (300 mM glycine, pH 2.8). The regenerated media was rinsed four times with 2.0 mL of PBS 7.4, and then rinsed once and resuspended with FCS/PBS to make a 10% suspension. The adsorption capacity of the regenerated immunoadsorptive media was measured as above.

The affinity of the regenerated immunoadsorptive media for β<sub>2</sub>m was assessed by following the protocol used to determine the adsorption capacity, except that each tube was loaded with twice the amount of gel along with a sub-saturating quantity of β<sub>2</sub>m-AF488 (6 µg). The calibration standards also spanned a lower concentration range (0, 0.5, 1.0, 2.5, 5.0, 10, 15 mg/mL).

Leaching of the scFv fragment by the stripping buffer was assayed through Western blotting. Diluting it with 13 mL of 100 mM sodium phosphate, 1 mM EDTA, pH 8.0, neutralized each 2.0 mL volume of stripping buffer. Equal volume samples of the neutralized stripping buffer and similarly diluted scFv from the immobilization reaction were run on SDS-PAGE with 5% 2-mercaptoethanol added to the sample buffer as a reducing agent. A PVDF (polyvinylidene difluoride) membrane was used for blotting, which was

labeled with Anti-His HRP conjugate (using the included Anti-His HRP conjugate blocking buffer) following the manufacturer's instructions (Qiagen). However, PBS 7.4 was used instead of Tris buffered saline. Colorimetric detection was performed using the Opti-4CN™ substrate kit (Bio-Rad), again following manufacturer's instructions.

### 5.2.6 Statistical Analysis

Measured quantities are reported as the mean  $\pm$  the standard error of the mean (SEM), except for the scFv immobilization density and the mass ratio of adsorbed  $\beta_2m$  to immobilized antibody, for which the error estimates correspond to the accuracy of the gel volume measurement. The significance of the difference between two means was tested by ANOVA (analysis of variance) using a two-tailed p value of 0.05. Regressions were performed by minimizing the summed square error (SSE).

## 5.3 RESULTS

### 5.3.1 Cloning of $V_H$ and $V_L$ genes

As resolved by agarose gel electrophoresis, one combination of the Ig-Prime kit heavy chain primers (MuIgV<sub>H</sub>5'-D and MuIgV<sub>H</sub>3'-2) and three combinations of the light chain primers (MuIgκV<sub>L</sub>5'-B, MuIgκV<sub>L</sub>5'-C, and MuIgκV<sub>L</sub>5'-E, each with MuIgκV<sub>L</sub>3'-1) yielded RT-PCR products that were characteristic of  $V_H$  and  $V_L$  genes (approximately 400 base pairs in length). The DNA sequences of two of the  $V_L$  RT-PCR products (MuIgκV<sub>L</sub>5'-B and MuIgκV<sub>L</sub>5'-C) were found to match the aberrant light chain sequence listed in the Ig-Prime kit instructions [Carroll *et al.*, 1988] and were discarded. The sequences of the remaining  $V_H$  and  $V_L$  genes (Figure 5.3) were translated and compared to the peptide sequencing results of the protein A-purified BBM.1 antibody.

Three different peptide chains were detected by N-terminal degradation, where only two were expected for a pure monoclonal. The signal for one of the peptide chains was too weak to determine its sequence with a high level of confidence, while the two predominant peptide chains were found in approximately equal proportions. The sequence of the MOPC-21 κ light chain was used to infer the sequence of the second peptide chain in the BBM.1 antibody sample. This peptide sequence matched the cloned  $V_H$  sequence, but did not match that of the MOPC-21 heavy chain [Milstein *et al.*, 1974]. Meanwhile, the sequence of the

cloned  $V_L$  gene did not match the sequence of the MOPC-21  $\kappa$  light chain. These findings suggested that the cloned  $V_H$  and  $V_L$  genes belonged to the anti- $\beta_2m$  antibody secreted by the BBM.1 hybridoma.

### 5.3.2 Display of scFv fragment by yeast

The ability of the cloned  $V_H$  and  $V_L$  genes to bind  $\beta_2m$  was confirmed by expressing them as a scFv fragment in a yeast display format. The addition of 100-fold molar excess unbiotinylated  $\beta_2m$  effectively inhibited the binding of the biotinylated  $\beta_2m$ , while the average number of scFv fragments displayed by the pEAG1-transformed yeast was  $2 \times 10^4 \pm 0.3 \times 10^4$  mole-scFv/mole-yeast ( $P_0$ ). The three FACS titration curves that were used to determine the value of the scFv- $\beta_2m$  dissociation equilibrium constant are summarized by Figure 5.4 ( $K_D = 0.7 \pm 0.3$  nM =  $0.008 \pm 0.004$  mg- $\beta_2m$  /L). Based on these results, it was concluded that the cloned  $V_H$  and  $V_L$  genes belong to the anti- $\beta_2m$  antibody produced by the BBM.1 cell line.

### 5.3.3 Secretion of scFv fragment by yeast

Figure 5.5 gives the sequence of the secreted scFv fragment, while Figure 5.6 demonstrates the purity of the scFv fragment after purification by nickel affinity chromatography. One minor peak and two major peaks were eluted from the size-exclusion column (as resolved by monitoring the absorbance of at 280 nm). The minor peak corresponded to the exclusion-limit of the resin, while the two major peaks (approximately the same size) corresponded to the molecular weights of the scFv fragment and its dimer. The fractions from the two major peaks were pooled to improve the yield of scFv fragment preparation and used to produce the immunoabsorptive media. The yield of purified scFv fragment per unit volume of culture was 1.5 mg/L.

### 5.3.4 Immunoabsorbent based on scFv fragment

The TCEP reducing gel increased the molar ratio of free thiol groups to scFv fragments from less than 0.1% to 50%. At the end of the immobilization reaction, 25% of the total, or 50% of the reduced scFv fragment, had bound to the Sulfo-SMCC-activated gel. This corresponds to an immobilization density of  $2.4 \pm 0.2$  mg-scFv/mL-settled-gel. No leaching of the scFv fragment from the immunoabsorbent was detected in the PBS rinses

(SDS-PAGE), cysteine quenching buffer (SDS-PAGE), or in the neutralized stripping buffer (Western blot).

**Table 5.1  $\beta_2$ m-Adsorption Site Density of the Immunoabsorptive Media ( $\rho'_s$ ).**\*

	Initial $\beta_2$ m Concentration, $C_0$ [mg/L]				
	40	30	25	Mean	Significance
<b>Before Regeneration (<math>N = 3</math>) [mg-<math>\beta_2</math>m/mL-settled-gel]</b>	$0.33 \pm 0.04^\dagger$	$0.41 \pm 0.01$	$0.48 \pm 0.05$	$0.40 \pm 0.04$	$p > 0.2$
<b>After Regeneration (<math>N = 5</math>) [mg-<math>\beta_2</math>m/mL-settled-gel]</b>	$0.41 \pm 0.02$	$0.44 \pm 0.02$	$0.43 \pm 0.01$	$0.43 \pm 0.01$	$p > 0.6$
<b>Mean [mg-<math>\beta_2</math>m/mL-settled-gel]</b>					$0.41 \pm 0.01$
<b>Significance</b>					$p > 0.2$

The observed  $\beta_2$ m-adsorption site density ( $\rho'_s$ ) did not significantly depend on the  $\beta_2$ m-concentration under saturating conditions, nor did it significantly change after one round of regeneration (Table 5.1). The average measured value of  $\rho'_s$  was  $0.41 \pm 0.01$  mg- $\beta_2$ m/mL-settled-gel, which corresponds to a binding activity of 42% (molar ratio of adsorbed  $\beta_2$ m to immobilized scFv fragment) for the immobilized scFv fragment. Under sub-saturating conditions ( $C_0 = 15$  mg/mL), the regenerated immunoabsorbent possessed sufficient affinity to bring the concentration down to  $C_{eq} = 1.0 \pm 0.1$  mg/L ( $N = 5$ ).

\* Various initial concentrations ( $C_0$ ) of  $\beta_2$ m-AF488 were equilibrated with 10  $\mu$ L volumes of the immunoabsorptive media ( $V_{gel}$ ) in 0.400 mL of FCS/PBS ( $V_{total}$ ) at 37°C for 1 hour. The equilibrium concentration of desorbed  $\beta_2$ m-AF488 ( $C_{eq}$ ) was measured and used to calculate the  $\beta_2$ m-adsorption site density ( $\rho'_s$ ) using Equation 5.6. These experiments were conducted on the immunoabsorptive media before and after regeneration with 0.3 M glycine, pH 2.8.

<sup>†</sup>  $N = 2$

## 5.4 DISCUSSION

The removal of  $\beta_2m$  from human blood plasma has previously been investigated with immunoadsorbents consisting of whole anti- $\beta_2m$  antibodies immobilized onto porous beads [Mogi *et al.*, 1989; Nakano *et al.*, 1991; Vallar *et al.*, 1995; Shabunina *et al.*, 2001]. These small-scale affinity chromatography experiments have demonstrated that an immunoadsorbent can remove  $\beta_2m$  from human plasma with an affinity that has not been achieved with hydrophobic interaction-based adsorbents [Furuyoshi *et al.*, 1998; Davankov *et al.*, 2000]. Furthermore, these antibody-based adsorbents were found to be highly specific for  $\beta_2m$ , while the specificity of hydrophobic interaction-based adsorbents continues to be a concern [Tsuchida *et al.*, 1998; Reiter *et al.*, 2002]. To date, perhaps the most promising anti- $\beta_2m$  immunoadsorbent has been reported by Vallar and co-workers [Vallar *et al.*, 1995], which consisted of monoclonal antibodies immobilized onto Sepharose<sup>®</sup> CL-4B gel beads. This adsorbent was highly regenerable and possessed a  $\beta_2m$ -adsorption site density (0.9 mg- $\beta_2m$ /mL-settled-gel) that is expected to be sufficient, but not optimal for actual clinical application (i.e. 350 mL settled volume of adsorbent required to remove 315 mg of  $\beta_2m$ ).

While the results of these preliminary investigations are encouraging, the challenge of removing  $\beta_2m$  from whole blood in a single extracorporeal device has not been addressed until recently (Chapter 2, [Ameer *et al.*, 2001]). More specifically, low concentrations of  $\beta_2m$  (3.2 mg/L) were removed from whole human blood *in vitro* at a therapeutically relevant flowrate (200 mL-blood/min) using a novel, plasmapheretic extracorporeal device (the VFPR) and an immunoadsorbent based on whole BBM.1 antibodies. The concentration of  $\beta_2m$  that was cleared by the VFPR device was limited by a low  $\beta_2m$ -adsorption site density ( $\rho'_s = 0.030 \pm 0.002$  mg- $\beta_2m$ /mL-settled-gel), which was caused by the low molar binding activity of the immobilized BBM.1 antibody (only 6% of the immobilized antibody bound  $\beta_2m$ ). Nevertheless, the immobilized whole antibodies (BBM.1) that retained binding activity demonstrated a high affinity for  $\beta_2m$  ( $K_D = 0.1 \pm 0.1$  mg/L) as well as the ability to be regenerated repeatedly (>10x) without a detectable loss of binding activity. At the time, it was hypothesized that the low  $\beta_2m$ -adsorption site density was either caused by the excessive deactivation of the monoclonal antibody by the immobilization chemistry (cyanogen bromide

activation of agarose) and/or the expression of an additional, unwanted immunoglobulin chain (impurity) by the hybridoma cell line.

Research into the origin of the BBM.1 antibody-producing hybridoma cell line (HB-28) has revealed that it was created using the X63-Ag8 myeloma [Brodsky *et al.*, 1979], which has been shown to secrete the MOPC-21  $\kappa$  light and IgG<sub>1</sub> heavy chains [Milstein *et al.*, 1974; Kohler and Milstein, 1975]. In light of this fact, protein-A purified BBM.1 antibody was partially sequenced through N-terminal degradation. The results suggest that the protein sample primarily consisted of the MOPC-21 light chain and an IgG heavy chain other than the MOPC-21 IgG<sub>1</sub> chain (presumably the anti- $\beta_2$ m heavy chain), with a trace amount (<10%) of a third peptide chain (presumably the anti- $\beta_2$ m light chain). The apparent absence of MOPC-21 IgG<sub>1</sub> in the protein sample can be explained by the fact that protein A is known to bind to IgG<sub>2b</sub> with a higher affinity than IgG<sub>1</sub> [Ladisich, 2001] and that the BBM.1 antibody has been classified as IgG<sub>2b</sub> [Brodsky *et al.*, 1979].

The optimization of an immunoadsorbent for the extracorporeal removal of  $\beta_2$ m will require the maximization of the  $\beta_2$ m-adsorption site density to minimize the required volume of immunoadsorbent. The volume of immunoadsorbent contained within the extracorporeal device is an important parameter for the optimization of biocompatibility, as it is proportional to the amount of blood plasma retained during therapeutic operation. One strategy for achieving higher  $\beta_2$ m-adsorption site densities is to use scFv antibody fragments as immunoadsorption ligands instead of significantly larger whole antibodies (1 mg of scFv fragment can bind 0.4 mg of  $\beta_2$ m, whereas 1 mg of whole antibody can only bind 0.16 mg of  $\beta_2$ m). Another advantage of scFv fragments over whole antibodies is their ability to be expressed by microbial vectors. This makes scFv fragments amenable to *in vitro* evolution in a convenient yeast display format and provides more options for process optimization, potentially resulting in a significant reduction in production cost. ScFv fragments are also genetically defined, which offers the opportunity to eliminate the expression of unwanted peptide chains by the source hybridoma cell line.

Motivated by the potential advantages of scFv fragments, the desirable affinity and regeneration capacity of BBM.1, and the apparent MOPC-21  $\kappa$  light chain contamination, an immunoadsorbent for the removal of  $\beta_2$ m was created that is based on BBM.1 scFv fragments. The BBM.1 scFv was first expressed in a yeast display format to facilitate the

characterization of its phenotype and to enable the engineering of its properties (i.e. stability and/or regeneration capacity under various conditions) through *in vitro* evolution, if it is desired in the future.

The binding affinity of the yeast-displayed scFv fragment for  $\beta_2m$  was quantitated by FACS analysis. The measured value of  $K_D$  ( $0.7 \pm 0.3$  nM =  $0.008 \pm 0.004$  mg/L) is in agreement with that previously reported for the agarose-immobilized whole BBM.1 antibody ( $0.1 \pm 0.1$  mg/L) (Chapter 4, [Grovender *et al.*, 2002]). This result is noteworthy from an antibody engineering perspective, because the conversion of a whole antibody to a wild-type scFv fragment can result in a significant decrease in affinity [Maynard *et al.*, 2002]. Furthermore, our reported value for  $K_D$  is well below the  $\beta_2m$  concentration range expected in the blood plasma of healthy individuals (1.0-3.0 mg/L) [Floege and Ketteler, 2001]. Hence, the yeast-displayed wild-type BBM.1 scFv fragment possesses an affinity for recombinant human  $\beta_2m$  that is optimal for the clinical treatment of DRA through extracorporeal immunoadsorption.

Given the encouraging binding affinity of the yeast-displayed antibody fragment, the scFv gene\* was expressed by a yeast secretion vector. The selected protein expression and purification methods produced enough of the scFv fragment so that a small volume of a model scFv immunoadsorbent could be produced for investigational purposes. The molar binding activity (42%) and the  $\beta_2m$ -adsorption site density ( $\rho'_s = 0.41 \pm 0.01$  mg- $\beta_2m$ /mL-settled-gel) of the scFv-based adsorbent are significantly greater than those measured for the whole BBM.1 antibody-based adsorbent (molar binding activity of 6%,  $\rho'_s = 0.030 \pm 0.002$  mg- $\beta_2m$ /mL-settled-gel). This improvement can be attributed to the elimination of the production of the MOPC-21 light chain by the cloning procedure. Hence, this work demonstrates how the creation of a wild-type scFv fragment from an existing hybridoma cell line can be used to separate desired antibody genes from contaminating ones. Under saturating conditions ( $C_{eq} \gg K_D$ ), the mass ratio of adsorbed  $\beta_2m$  to immobilized antibody ( $0.17 \pm 0.02$  mg- $\beta_2m$ /mg-scFv) is roughly equivalent to the theoretical limit for 100% active, bivalent whole IgG antibody (0.16 mg- $\beta_2m$ /mg-antibody) and 70% higher than that actually achieved by Vallar and co-workers (0.1 mg- $\beta_2m$ /mg-antibody) [Vallar *et al.*, 1995].

---

\* A Kex2 protease-resistant version.

Shabunina and co-workers [Shabunina *et al.*, 2001] have immobilized whole, polyclonal anti- $\beta_2m$  antibodies onto Sepharose<sup>®</sup> CL-4B at densities that range from 2 to 16 mg/mL-settled-gel. Over this range the mass ratio of adsorbed  $\beta_2m$  to immobilized antibody remained constant (0.04 mg- $\beta_2m$ /mg-antibody). If this immobilization density can be achieved for the BBM.1 scFv while maintaining a molar binding activity of 42%, a new immunoabsorbent with a  $\beta_2m$ -adsorption site density of 2.7 mg- $\beta_2m$ /mL-settled-gel could theoretically be produced. This would represent a 3-fold increase over the  $\beta_2m$ -adsorption site density reported by Vallar and co-workers [Vallar *et al.*, 1995], which is the highest reliable value reported in the literature.\*

This is the first time that a scFv-based adsorbent for the extracorporeal removal of  $\beta_2m$  has been reported<sup>†</sup>. Under saturating conditions, this new type of immunoabsorbent binds a mass ratio of adsorbed  $\beta_2m$  to immobilized antibody that is above the theoretical limit obtainable with whole antibodies. Future work will involve the optimization of the scFv fragment expression, purification, and immobilization methods. A large volume (100-200 mL) of this scFv-based immunoabsorbent will be produced and used within a VFPR device to remove pathologic levels (20-70 mg/L [Gejyo *et al.*, 1986; Koch, 1992]) of  $\beta_2m$  from human blood. We expect that the immobilization density of the scFv fragment can be increased sufficiently such that, when combined with the high mass ratio of adsorbed  $\beta_2m$  to immobilized antibody, a  $\beta_2m$ -adsorption site density can be achieved that is significantly greater than the highest reported to date ( $\rho'_s = 0.9$  mg- $\beta_2m$ /mL-settled-gel [Vallar *et al.*, 1995]). This increase in the  $\beta_2m$ -adsorption site density should translate into a proportionate decrease in the volume of adsorbent needed for extracorporeal therapy and the blood plasma retained, thereby improving the biocompatibility of the device.

---

\* Mogi and co-workers [Mogi *et al.*, 1989] have reported a  $\beta_2m$ -adsorption site density of 4.3 mg/mL. However, this value is not reliable because their reported antibody immobilization density (18.8 mg-antibody/mL-gel) corresponds to a mass ratio of adsorbed  $\beta_2m$  to immobilized antibody (0.23 mg- $\beta_2m$ /mg-antibody) that is well above the theoretical limit (0.16 mg- $\beta_2m$ /mg-antibody).

<sup>†</sup> To the best knowledge of the author and Thesis Advisory Committee.



**5'-V<sub>H</sub>:**

/NheI

G ATC GAT CGA GCT AGC GAG GTT CAG CTG CAG CAG TC  
 I D R A S E V Q L Q Q  
 | -> V<sub>H</sub>

**3'-V<sub>H</sub>:**

CC TCA GTC ACC GTC TCC TCA GGT GGT GGT GGT TCT GGT GGT GGT GGT TCT GGC  
 S V T V S S G G G G S G G G G S G  
 V<sub>H</sub> <-|-> Linker

GGC GGC GGC TCC  
 G G G S

**5'-V<sub>L</sub>:**

GGC GGC GGC GGC TCC GGA GGA GGA GGA TCG GAC ATT CAG ATG ACC CAG  
 G G G G S G G G G S D I Q M T Q  
 Linker <-|-> V<sub>L</sub>

**3'-V<sub>L</sub>:**

/BamHI

TTC GGA GGG GGG ACC AAG CTG GAA ATA AAA CGG GCT GGA TCC GAT CGA TCG ATC  
 F G G G T K L E I K R A G S D R S I  
 V<sub>L</sub> <-|-

**3'-Lys-Asn:**

/BamHI

TTC GGA GGG GGG ACC AAG CTG GAA ATA AAA AAC GCT GAT GGA TCC GAT CGA TCG  
 F G G G T K L E I K N A D G S D R S  
 V<sub>L</sub> <-|-|Lys-Asn|

ATC  
 I

**3'-His6-Cys:**

/XhoI

CTT ATT TCT GAA GAG GAC TTG CAC CAC CAC CAC CAC CAC TGT TAG TGA CTC GAG  
 L I S E E D L H H H H H H C STP STP L E  
 C-myc-tag <-|-> His-tag <-|-|Cys| Stop |

GAT CGA TCG  
 D R S

**Figure 5.2 Custom primers used for PCR.** The assembly of the scFv insert by SOE was performed using 5'-V<sub>H</sub>, 3'-V<sub>H</sub>, 5'-V<sub>L</sub> and 3'-V<sub>L</sub>. The inserts for pEAG2 and pEAG3 were made using 5'-V<sub>H</sub>, 3'-Arg-Asn and 3'-His6-Cys. The 3'-V<sub>L</sub>-Arg-Asn also reintroduces the 110th amino acid in the BBM.1 V<sub>L</sub> gene, which was omitted from the 3'-V<sub>L</sub> primer. The sequences of the 3' primers listed are the reverse compliment of those actually used.

**V<sub>H</sub>:**

GAG GTT CAG CTG CAG CAG TCT GGG GCA GAG CTT GTG AAG CCA GGG GCC TCA **51**  
 E V Q L Q Q S G A E L V K P G A S **17**

GTC AAG TTG TCC TGC ACA CCT TCT GGC TTC AAT GTT AAA GAC ACC TAT ATA **102**  
 V K L S C T P S G F N V K D T Y I **34**

CAC TGG GTG AAA CAG AGG CCT AAA CAG GGC CTG GAG TGG ATT GGA AGG ATT **153**  
 H W V K Q R P K Q G L E W I G R I **51**

GAT CCT TCG GAT GGT GAT ATT AAA TAT GAC CCG AAG TTC CAG GGC AAG GCC **204**  
 D P S D G D I K Y D P K F Q G K A **68**

ACT ATA ACA GCA GAC ACA TCC TCC AAC ACA GTC TCC CTG CAG CTC AGC AGC **255**  
 T I T A D T S S N T V S L Q L S S **85**

CTG ACA TCT GAG GAC ACC GCC GTC TAT TAC TGT GCT AGA TGG TTT GGT GAC **306**  
 L T S E D T A V Y Y C A R W F G D **102**

TAC GGG GCT ATG AAC TAC TGG GGT CAA GGA ACC TCA GTC ACC GTC TCC TCA **357**  
 Y G A M N Y W G Q G T S V T V S S **119**

**V<sub>L</sub>:**

GAC ATT CAG ATG ACC CAG TCT CCT GCC TCC CAG TCT GCA TCT CTG GGA GAA **51**  
 D I Q M T Q S P A S Q S A S L G E **17**

AGT GTC ACC ATC ACA TGC CTG GCA AGT CAG ACC ATT GGT ACA TGG TTA GCT **102**  
 S V T I T C L A S Q T I G T W L A **34**

TGG TAT CAG CAG AAA CCA GGG AAA TCT CCT CAG CTC CTG ATT TAT GCG GCA **153**  
 W Y Q Q K P G K S P Q L L I Y A A **51**

ACC AGC TTG GCA GAT GGG GTC CCA TCA AGG TTC AGT GGT AGT GGA TCT GGC **204**  
 T S L A D G V P S R F S G S G S G **68**

ACA AAA TTT TCT CTC AAG ATC AGG ACC CTA CAG GCT GAA GAT TTT GTA AGT **255**  
 T K F S L K I R T L Q A E D F V S **85**

TAT TAC TGT CAA CAA CTT TAC AGT AAA CCG TAC ACG TTC GGA GGG GGG ACC **306**  
 Y Y C Q Q L Y S K P Y T F G G G T **102**

AAG CTG GAA ATA AAA CGG GCT GAT **330**  
 K L E I K R A D **110**

**Figure 5.3 V<sub>H</sub> and V<sub>L</sub> Genes Cloned from the BBM.1 Hybridoma.**

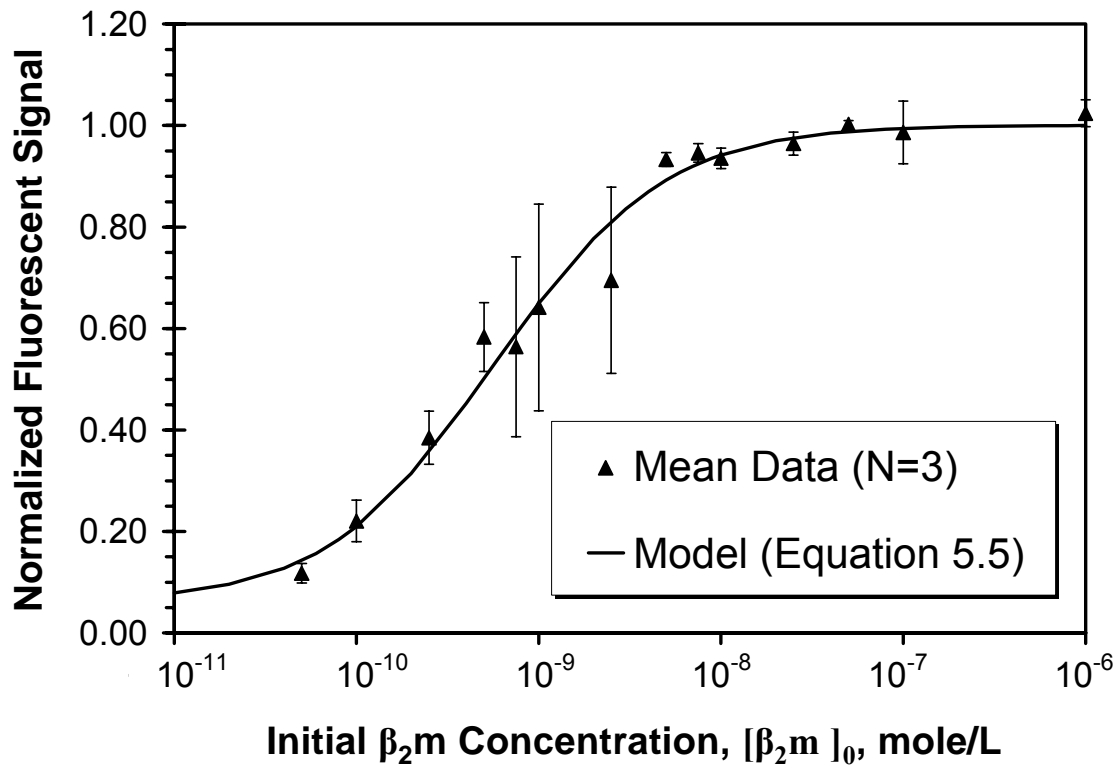


**Figure 5.4 Titration of BBM.1-scFv displaying yeast with fluorescent  $\beta_2m$ .** Aliquots of EBY100 cells transformed with pEAG1 and displaying wild-type BBM.1-scFv fragment were labeled with various concentrations of biotinylated  $\beta_2m$ . Streptavidin-PE was used to label the adsorbed  $\beta_2m$ . The mean PE signal of the scFv-displaying population of each yeast aliquot was measured by a fluorescence-activated cell sorter (FACS). Error bars represent standard error of the mean (SEM).

**N-terminal Flanking Sequence:**

```
                /NheI
GAA GCT CGG CCG GCT AGC GAG GTT CAG CTG CAG CAG TCT GGG GCA GAG
E  A  R  P  A  S  E  V  Q  L  Q  Q  S  G  A  E
    Spacer <- |           | -> VH
```

**C-terminal Flanking Sequence:**

```
                /BamHI
GAA ATA AAA AAC GCT GAT GGA TCC GAA CAA AAG CTT ATT TCT GAA GAG GAC TTG
E  I  K  N  A  D  G  S  E  Q  K  L  I  S  E  E  D  L
    |Lys-Asn| VL <- |           | ->           C-myc-tag           <- |

CAC CAC CAC CAC CAC CAC TGT
H  H  H  H  H  H  C
|->   His-tag   <- |Cys|
```

**Figure 5.5** The scFv fragment secreted by YVH10 yeast transformed with pEAG3. The full sequences of the V<sub>H</sub> and V<sub>L</sub> genes are given by Figure 5.3.

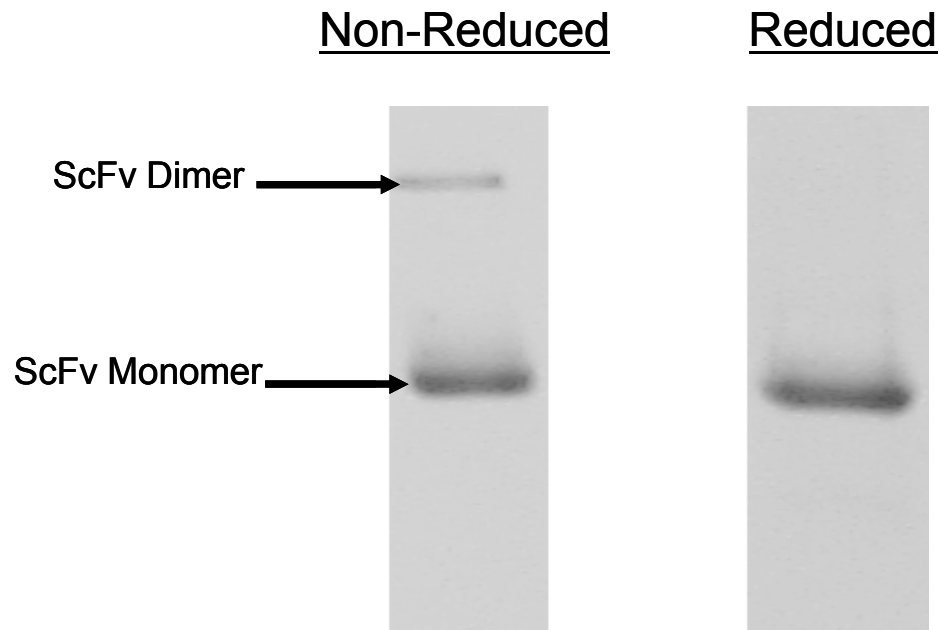


**Figure 5.6** SDS-PAGE of the secreted BBM.1-scFv fragment after nickel affinity purification. The reduced sample was treated with 5% betamercaptoethanol and boiled for 5 minutes to dissociate the scFv dimer.

## 5.5 REFERENCES

- Agatep R, RD Kirkpatrick, DL Parchaliuk, RA Woods and RD Gietz (1998) Technical Tips Online.
- Ameer GA, EA Grovender, H Ploegh, D Ting, WF Owen, M Rupnick and R Langer (2001) "A Novel Immunoadsorption Device for Removing Beta2-Microglobulin from Whole Blood." *Kidney Int.* 59: 1544-50.
- Bevan A, C Brenner and RS Fuller (1998) "Quantitative Assessment of Enzyme Specificity in Vivo: P-2 Recognition by Kex2 Protease Defined in a Genetic System." *Proceedings of the National Academy of Sciences of the United States of America.* 95: 10384-9.
- Boder ET, KS Midelfort and KD Wittrup (2000) "Directed Evolution of Antibody Fragments with Monovalent Femtomolar Antigen-Binding Affinity." *Proc Natl Acad Sci USA.* 97: 10701-5.
- Boder ET and KD Wittrup (1997) "Yeast Surface Display for Screening Combinatorial Polypeptide Libraries." *Nat Biotechnol.* 15: 553-7.
- Boder ET and KD Wittrup (2000) "Yeast Surface Display for Directed Evolution of Protein Expression, Affinity, and Stability." *Methods Enzymol.* 328: 430-44.
- Brodsky FM, WF Bodmer and P Parham (1979) "Characterization of a Monoclonal Anti-Beta-2-Microglobulin Antibody and Its Use in the Genetic and Biochemical Analysis of Major Histocompatibility Antigens." *Eur J Immunol.* 9: 536-45.
- Carroll WL, E Mendel and S Levy (1988) "Hybridoma Fusion Cell Lines Contain an Aberrant Kappa Transcript." *Molecular Immunology.* 25: 991-5.
- Clements JM, GH Catlin, MJ Price and RM Edwards (1991) "Secretion of Human Epidermal Growth Factor from *Saccharomyces Cerevisiae* Using Synthetic Leader Sequences." *Gene.* 106: 267-71.
- Davankov V, L Pavlova, M Tsyurupa, J Brady, M Balsamo and E Yousha (2000) "Polymeric Adsorbent for Removing Toxic Proteins from Blood of Patients with Kidney Failure." *J Chromatogr B Biomed Sci Appl.* 739: 73-80.
- Floege J and M Ketteler (2001) "Beta-2-Microglobulin-Derived Amyloidosis: An Update." *Kidney Int.* 59 Suppl 78: S164-71.
- Furuyoshi S, M Nakatani, J Taman, H Kutsuki, S Takata and N Tani (1998) "New Adsorption Column (Lixelle) to Eliminate Beta-2-Microglobulin for Direct Hemoperfusion." *Ther Apher.* 2: 13-7.
- Gejyo F, S Odani, N Yamada, N Honma, H Saito, M Suzuki and e al. (1986) "Beta-2-Microglobulin: A New Form of Amyloid Protein Associated with Chronic Hemodialysis." *Kidney Int.* 30: 385.
- Graff C (2002) *Antibody Engineering for Tumor Immunotherapy.* MIT, Chemical Engineering: Cambridge.
- Grovender EA, CL Cooney, R Langer and GA Ameer (2002) "Immunoadsorption Model for a Novel Fluidized-Bed Blood Detoxification Device." *AIChE Journal.* 48: 2357-65.
- Horton RM, HD Hunt, SN Ho, JK Pullen and LR Pease (1989) "Engineering Hybrid Genes without the Use of Restriction Enzymes: Gene Splicing by Overlap Extension." *Gene.* 77: 61-8.
- Koch KM (1992) "Dialysis-Related Amyloidosis." *Kidney Int.* 41: 1416.
- Kohler G and C Milstein (1975) "Continuous Cultures of Fused Cells Secreting Antibody of Predefined Specificity." *Nature.* 256: 495-7.

- Ladisch MR (2001) *Bioseparations Engineering: Principles, Practice, Economics*, Wiley-Interscience, New York.
- Maynard JA, CBM Maassen, SH Leppla, K Brasky, JL Patterson, BL Iverson and G Georgiou (2002) "Protection against Anthrax Toxin by Recombinant Antibody Fragments Correlates with Antigen Affinity." *Nat Biotechnol.* 20: 597-601.
- Milstein C, K Adetugbo, NJ Cowan and DS Secher (1974) In *Progress in Immunology II*. Vol. 1 (Eds, Brent, L and J Holborow) North-Holland Publishing Company: pp. 157-68.
- Mogi M, M Harada, T Adachi, K Kojima and T Nagatsu (1989) "Selective Removal of Beta-2-Microglobulin from Human Plasma by High-Performance Immunoaffinity Chromatography." *J Chromatogr B Biomed Sci Appl.* 496: 194-200.
- Nakano H, H Gomi, T Shibasaki, F Ishimoto and O Sakai (1991) "An Experimental Study on Selective Elimination of Beta-2-Microglobulin Using Immunoabsorption Method in Patients with Chronic Renal Failure." *Biomater Artif Cells Immobilization Biotechnol.* 19: 61-9.
- Pace CN, F Vajdos, L Fee, G Grimsley and T Gray (1995) "How to Measure and Predict the Molar Absorption Coefficient of a Protein." *Protein Sci.* 4: 2411-23.
- Reiter K, V Bordoni, G Dall'Olio, MG Ricatti, M Soli, S Ruperti, G Soffiati, E Galloni, V D'Intini, R Bellomo and C Ronco (2002) "In Vito Removal of Therapeutic Drugs with a Novel Adsorbent System." *Blood Purification.* 20: 380-8.
- Robinson AS, V Hines and KD Wittrup (1994) "Protein Disulfide-Isomerase Overexpression Increases Secretion of Foreign Proteins in *Saccharomyces-Cerevisiae*." *Bio-Technology.* 12: 381-4.
- Rockwell NC and RS Fuller (1998) "Interplay between S-1 and S-4 Subsites in Kex2 Protease: Kex2 Exhibits Dual Specificity for the P-4 Side Chain." *Biochemistry.* 37: 3386-91.
- Shabunina IV, OI Afanas'eva and SN Pokrovskii (2001) "Immunsorbent for Removal of Beta-2-Microglobulin from Human Blood Plasma." *Bulletin of Experimental Biology and Medicine.* 4: 984-6.
- Shusta EV, MC Kieke, E Parke, DM Kranz and KD Wittrup (1999) "Yeast Polypeptide Fusion Surface Display Levels Predict Thermal Stability and Soluble Secretion Efficiency." *J Mol Biol.* 292: 949-56.
- Sikorski RS and P Hieter (1989) "A System of Shuttle Vectors and Yeast Host Strains Designed for Efficient Manipulation of DNA in *Saccharomyces-Cerevisiae*." *Genetics.* 122: 19-27.
- Svasti J and C Milstein (1972) "The Complete Amino Acid Sequence of a Mouse Kappa Light Chain." *Biochem J.* 128: 427-44.
- Tsuchida K, Y Takemoto, T Nakamura, O Fu, C Okada, S Yamagami and T Kishimoto (1998) "Lixelle Adsorbent to Remove Inflammatory Cytokines." *Artif Organs.* 22: 1064-7.
- Vallar L, PM Costa, A Teixeira, M Pfister, R Barrois, PP Costa and C Rivat (1995) "Immunoabsorption Procedure as a Potential Method for the Specific Beta 2-Microglobulin Removal from Plasma of Patients with Chronic Renal Failure." *J Chromatogr B Biomed Appl.* 664: 97-106.
- VanAntwerp JJ and KD Wittrup (2000) "Fine Affinity Discrimination by Yeast Surface Display and Flow Cytometry." *Biotechnol Prog.* 16: 31-7.



## Chapter 6: Afterword

### 6.1 SUMMARY AND CONCLUSIONS

The body of work presented in this thesis supports the feasibility of using an extracorporeal immunoabsorptive VFPR to specifically remove  $\beta_2m$  from blood for the prevention and/or treatment of DRA (dialysis-related amyloidosis). Furthermore, this blood detoxification technology platform could potentially be used to treat other diseases that are caused by circulating molecules that are otherwise difficult to remove (sepsis, liver failure, autoimmune disease, drug overdoses, and genetic disorders). The biocompatibility and efficacy of the proposed therapy was evaluated with a model immunoabsorbent consisting of whole BBM.1 antibodies immobilized onto porous agarose gel beads (Chapter 2). Concurrently, a dynamic immunoabsorption model was developed for the VFPR that was based upon the independent characterization of the mass-transfer processes within the VFPR and the thermodynamic behavior of the model immunoabsorbent (Chapter 4). The molar binding activity of the immobilized BBM.1 antibody was lower than expected (6%), but its  $\beta_2m$ -adsorption site density ( $0.030 \pm 0.002$  mg- $\beta_2m$ /mL-settled-gel) was sufficient for preliminary research. Hence, this model immunoabsorbent was used in a VFPR prototype to remove  $\beta_2m$  from donated bags of human blood in a closed-loop circuit at a clinically relevant flowrate (200 mL/min blood circulation rate). Over a two-hour operating period, no significant change was detected in the complete blood count and the total mass of soluble blood protein. Meanwhile, the plasma free hemoglobin increased at a rate deemed acceptable for hemodialysis [Ameer *et al.*, 1999]. This preliminary safety data supports the feasibility of using an immunoabsorptive VFPR for the extracorporeal removal of  $\beta_2m$ .

The high-affinity of the proposed  $\beta_2m$  removal system was demonstrated by the ability of the immunoabsorptive VFPR to bring the concentration of native donor baseline  $\beta_2m$  ( $1.3 \pm 0.1$  mg/L) to a level that was below the detectable limit of the assay (0.1 mg/L). The immunoabsorbent was successfully regenerated and used to remove controlled amounts ( $3.2 \pm 2$  mg/L) of recombinant human  $\beta_2m$  from the same donated bags of human blood. The dynamics of  $\beta_2m$  clearance from the blood bags was predicted by the mathematical immunoabsorption model, without using adjustable parameters. The predicted and experimentally observed time-scales of  $\beta_2m$  removal from the blood were in agreement with

that calculated by dividing the total cell-free blood path (445 mL) by the hemofiltration rate (50 mL-plasma/min). This finding led to the conclusion that the mass-transfer processes within the active plasma compartment of the VFPR prototype were not rate-limiting. Furthermore, the process controlling the rate of  $\beta_2m$  removal from the blood was the hemofiltration rate, which was on the order of the supply rate of  $\beta_2m$  into the circulation (approximately 70 mL/min [Floege *et al.*, 1991]). Both of these mass-transfer processes are expected to be rate-controlling should this specific device design be used for the extracorporeal removal of  $\beta_2m$ .

The ideal extracorporeal  $\beta_2m$  removal technology would detoxify blood at a rate that is much faster than the supply rate of  $\beta_2m$  to the circulation. In light of this, a new VFPR prototype with a 22% longer microporous membrane was constructed. The macroscopic mixing patterns within this new prototype were characterized using the same experimental and mathematical methods that were used in the development of the dynamic immunoadsorption model (Chapter 3). The compartmental macroscopic mixing model was able to describe the residence-time distribution data ( $r^2 > 0.94$ ) over the range of process conditions considered. This suggests that the plasma flux across the microporous membrane was not a function of position, which was an assumption of the model derivation. Therefore, the new VFPR prototype is expected to allow for a proportionate increase in the rate of  $\beta_2m$  removal (hemofiltration rates of 70-85 mL-plasma/min).

In order to reduce the hold-up and/or loss of valuable plasma proteins during extracorporeal therapy, the ideal immunoadsorbent for the removal of  $\beta_2m$  should possess a high  $\beta_2m$ -adsorption site density ( $>1$  mg- $\beta_2m$ /mL-settled-gel). ScFv antibody fragments should theoretically allow for higher effective  $\beta_2m$ -adsorption site densities because they are smaller in size than whole antibodies. This theoretical basis motivated the creation of the BBM.1 scFv fragment and a scFv-based immunoadsorbent for a feasibility study (Chapter 5). The molar binding activity (42%) and the  $\beta_2m$ -adsorption site density ( $\rho'_s = 0.41 \pm 0.01$  mg- $\beta_2m$ /mL-settled-gel) of the scFv-based adsorbent were dramatically improved from that of the whole BBM.1 antibody-based adsorbent (described above). This improvement was attributed to the elimination of the expression of a non- $\beta_2m$ -binding immunoglobulin chain by the cloning procedure. Under saturating conditions, the mass ratio of adsorbed  $\beta_2m$  to

immobilized antibody is roughly equivalent to the theoretical limit for 100% active, bivalent whole IgG antibody and 70% higher than the highest value reported in the literature for immobilized anti- $\beta_2$ m whole antibodies (0.1 mg- $\beta_2$ m/mg-antibody) [Vallar *et al.*, 1995].

Whole anti- $\beta_2$ m antibodies have been immobilized onto agarose gel beads at densities ranging from 2 to 16 mg/mL-settled-gel, without a detectable decrease in the mass ratio of adsorbed  $\beta_2$ m (under saturating conditions) to immobilized antibody [Shabunina *et al.*, 2001]. If this immobilization density can be achieved for the BBM.1 scFv fragment through the optimization of the immobilization process while maintaining a molar binding activity of 42%, a new immunoabsorbent could be produced with a  $\beta_2$ m-adsorption site density of 2.7 mg- $\beta_2$ m/mL-settled-gel. This would represent a 3-fold improvement over the highest  $\beta_2$ m-adsorption site density reported to date [Vallar *et al.*, 1995]. The ability of this hypothetical adsorbent to remove  $\beta_2$ m from whole blood was predicted using the VFPR immunoabsorption model (Chapter 4) and a set of input parameters (Table 6.1) corresponding to the large VFPR prototype (Chapter 3). According to the model calculations (Figure 6.1), this immunoabsorptive VFPR should be able to reduce a pathologically elevated  $\beta_2$ m concentration of 60 mg/L\* to a level that is within normal the normal range of healthy individuals (1.0-3.0 mg/L [Floege and Ketteler, 2001]) over the 5-hour period. This corresponds to 313 mg of  $\beta_2$ m removed from the blood reservoir or twice the amount reported to be removed by the kidneys daily (150 mg [Vincent *et al.*, 1980]).

Increasing the adsorption site density of the immunoabsorbent should theoretically allow for a proportionate decrease in the volume of adsorbent required for extracorporeal therapy, thereby enhancing biocompatibility. In existing direct hemoperfusion devices such as the Lixelle® [Furuyoshi *et al.*, 1998] and Betasorb® [Ronco *et al.*, 2001] columns, the rate of  $\beta_2$ m removal is directly proportional to the volume of adsorbent contained within them. This is due to the low surface area to volume ratio of the relatively large (>400  $\mu$ m) adsorbent particles that are required for biocompatibility with whole blood for this application. Therefore, a decrease in the adsorbent volume of these direct hemoperfusion columns would come at the expense of a proportionate decrease in the  $\beta_2$ m removal rate.

---

\* Plasma  $\beta_2$ m concentrations of chronic hemodialysis patients typically range 20-70 mg/L [Gejyo *et al.*, 1986; Koch, 1992].

This is not expected to be the case for the VFPR, in which the relatively small adsorbent particles should allow for a 3-fold decrease in the volume of the adsorbent without a significant decrease in efficacy.

**Table 6.1 Immunoabsorption model input parameters for the large VFPR prototype loaded with the hypothetical scFv-based adsorbent.**

Parameter	Value	Units	Parameter	Value	Units
$C_{APC}^{t=0}$	0	mg/L	$Q_m$	75 <sup>§</sup>	mL/min
$C_{BC,i}^{t=0}$	0	mg/L	$R$	46 <sup>‡</sup>	
$C_{BR,i}^{t=0}$	60 <sup>*</sup>	mg/L	$V_{BC}$	52.4 <sup>†</sup>	mL
$C_{gel}^{t=0}$	0	mg/L	$V_{BC,i}$	8.0, 7.5, 7.1, 6.7,	mL
$C_{PLCC}^{t=0}$	0	mg/L		6.3, 6.0, 5.6, 5.3 <sup>†</sup>	
$D_e$	1.1 x 10 <sup>-10</sup> <sup>‡</sup>	m <sup>2</sup> /s	$V_{APC}$	175 <sup>†</sup>	mL
$H_{BR}$	0.31 <sup>‡</sup>	-	$V_{bed}$	120 <sup>†</sup>	mL
$K_D$	0.008 <sup>§</sup>	mg/L	$V_{BR}$	7.7 <sup>**</sup>	L
$\bar{k}_m$	10 <sup>-3</sup> <sup>‡</sup>	m/s	$V_{PLCC}$	20	mL
$N_{BC}$	8 <sup>††</sup>	-	$\epsilon$	0.4 <sup>‡</sup>	-
$N_{BR}$	3 <sup>‡</sup>	-	$\Phi$	0.87	-
$Q_{BR}$	200 <sup>§</sup>	mL/min	$\rho'_s$	2.7 <sup>‡‡</sup>	mg/mL

\* Plasma  $\beta_2m$  concentrations of chronic hemodialysis patients typically range 20-70 mg/L [Gejyo *et al.*, 1986; Koch, 1992].

† From Table 3.6.

‡ From Table 4.1.

§ Value determined for yeast-displayed BBM.1 scFv in Chapter 5.

\*\* This value was chosen so that the blood reservoir would contain 318 mg of  $\beta_2m$  at a clinically expected  $\beta_2m$  concentration. This blood volume is larger than that which would actually be found in an actual patient (~5 L).

†† From Table 3.4.

‡‡ Value for the hypothetical BBM.1 scFv-based immunoabsorbent described in Section 6.1.

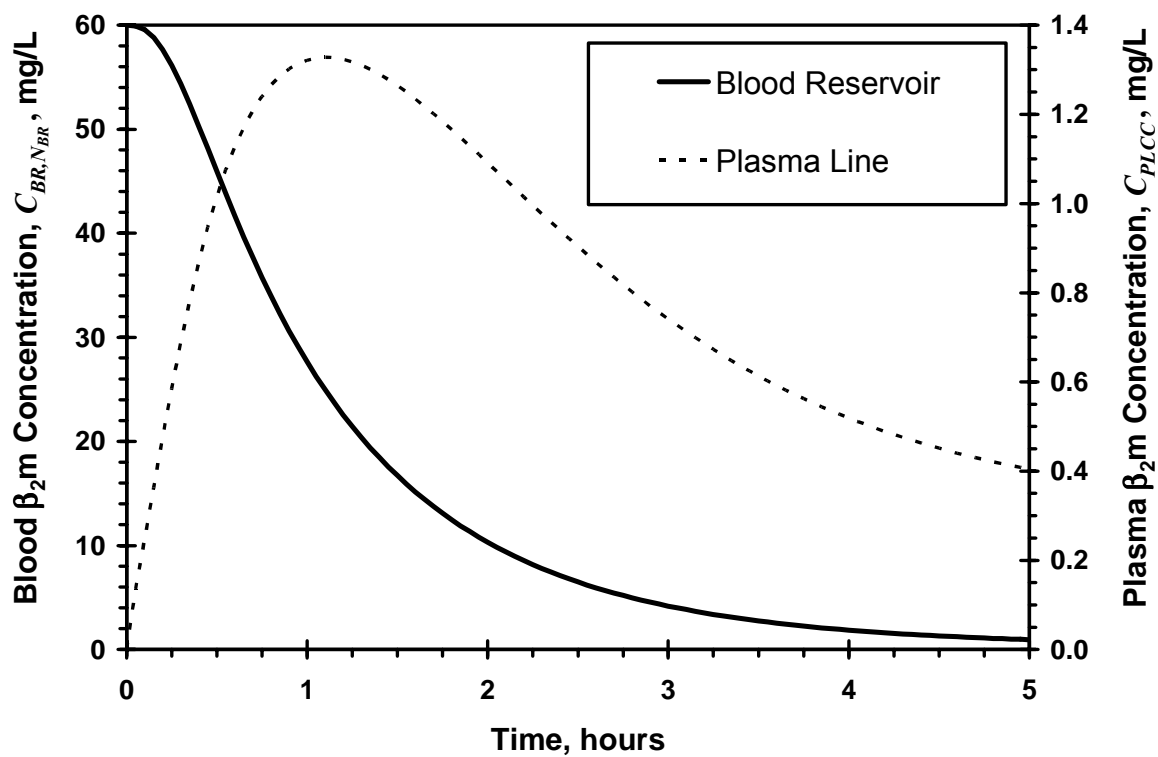


**Figure 6.1** Immunoabsorption model-predicted clearance of  $\beta_2m$  from whole blood by the large VFPR prototype loaded with the hypothetical scFv-based adsorbent. Chapter 4 describes the mathematical model in detail, Table 6.1 provides a complete listing of the input parameters used, and Chapter 3 describes the large VFPR prototype.

## 6.2 RECOMMENDATIONS FOR FUTURE WORK

The next milestone for this research project should be the production of 0.1-1.0 L of a new scFv-based adsorbent that possesses a  $\beta_2$ m-adsorption site density greater than 2 mg- $\beta_2$ m/mL-settled-gel. Based on the logic presented in Section 6.1, this is a reasonable goal that will require the optimization of the production, purification, and immobilization methods for the scFv fragment.

### 6.2.1 Optimization of ScFv Production

A greater than six-fold increase in the secretion level of recombinant glucose oxidase by *S. cerevisiae* has been reported by changing from a shaker flask to a stirred tank batch fermentor and optimizing the rates of agitation and aeration [Kapat *et al.*, 1998]. Therefore, the effect of varying several culture parameters (mixing pattern, temperature, media composition, oxygen level) on the secretion level of BBM.1 scFv (g-scFv/L-culture) by YVH10 *S. cerevisiae* should be studied in a stirred tank batch fermentor. Furthermore, *in vitro* evolution of the BBM.1 scFv fragment could be performed to increase the expression level of the BBM.1 scFv in a yeast display format, which often correlates with secretion efficiency [Shusta *et al.*, 1999; Boder and Wittrup, 2000]. The secretion level of the wild-type BBM.1 scFv fragment without the His6-tag should be studied to determine its effect on the secretion efficiency. This type of purification tag has inhibited the secretion of certain scFv fragments by yeast in the Wittrup Laboratory at MIT.\*

It is possible that expressing the BBM.1 scFv fragment as inclusion bodies or as soluble active protein in bacteria could be more efficient than the optimized yeast secretion system [Datar *et al.*, 1993; Martineau *et al.*, 1998]. Therefore, bacterial expression systems for the scFv fragment should also be investigated. Moving to a bacterial vector would also open up the possibility of expressing the scFv as an intein fusion protein, which would offer more alternatives for purification and subsequent immobilization through an N-terminal cysteine residue or a C-terminal thioester group [Xu and Evans, 2001].

---

\* Personal communication with Katarina Midelfort.

### 6.2.2 Optimization of ScFv Purification

The purification of the His6-tagged scFv fragment by nickel affinity chromatography proved to be effective (Chapter 5). However, the fact that this purification method is patented would present a definite drawback if the immunoabsorbent were to be commercialized. Other affinity chromatography ligands that could potentially replace nickel include thiol groups and recombinant human  $\beta_2m$ . Activated Thiol Sepharose® 4B is commercially available from Amersham Biosciences and recombinant human  $\beta_2m$  could be immobilized onto Sepharose® CL-4B (following the protocol used to immobilize BBM.1 in Section 2.2.2). Alternatively, recombinant human  $\beta_2m$  could be biotinylated (Section 5.2.1) and bound to Streptavidin Sepharose® HP (Amersham Biosciences).

Following the initial purification of the scFv fragment by one of the above affinity chromatography methods, one or two additional rounds of chromatographic purification should be performed on the scFv fragment before it is used to treat a patient or animal model. It is suggested that ion exchange be used to concentrate the scFv fragment followed by size-exclusion chromatography, which will re-dilute the purified product.

### 6.2.3 Optimization of ScFv Immobilization

It is possible that the state of aggregation of the BBM.1 scFv fragment affects its amenability for active immobilization. Therefore, the thermodynamics and kinetics of dimerization should be characterized under various buffer conditions (salt concentration, scFv concentration, pH, reducing agent concentration). Size-exclusion chromatography could be used to obtain fractions rich in either monomers or dimers and to subsequently determine the effect of changes in buffer conditions on the state of aggregation [Pavlinkova *et al.*, 1999]. Furthermore, the effect of varying several parameters on the immobilization density and molar binding activity for the maleimide-thiol immobilization reaction should be studied, including:

1. The length and hydrophobicity of the spacer arm, either expressed as part of the scFv peptide or included in the chemical cross-linking agent.
2. The reducing conditions of the scFv fragment immediately prior to immobilization. Ideally, 100% of the C-terminal free cysteine residues of the scFv fragments should

be reduced without reducing the disulfide bridges within the immunoglobulin folds. Reducing agents such as immobilized TCEP gel (Section 5.2.5.1), soluble TCEP, DTT (dithiothreitol), reduced glutathione, cysteine, or  $\beta$ -mercaptoethanol could be used in various amounts and buffers. Soluble TCEP is reported to have an advantage over other types of soluble reducing reagents in that it does not interfere with maleimide-thiol reactions [Haugland and Blalgt, 1998]. This reaction should also be performed in an oxygen-free environment (degassed buffers in a nitrogen or argon-filled glove box).

3. The time, temperature, pH, salt concentration, and reducing agent concentration of the maleimide-thiol immobilization reaction.
4. The scFv concentration and contacting scheme during the immobilization reaction. Performing the immobilization reaction at low scFv concentrations could minimize spontaneous dimerization (if it is not desired). Meanwhile, a high scFv concentration could increase the conversion of the immobilization reaction. Therefore, performing the immobilization reaction in a plug-flow format with a low concentration of scFv could potentially be optimal, as it could minimize dimerization and back-mixing.

### 6.3 REFERENCES

- Ameer GA, G Barabino, R Sasisekharan, W Harmon, CL Cooney and R Langer (1999) "Ex Vivo Evaluation of a Taylor-Couette Flow, Immobilized Heparinase I Device for Clinical Application." *Proc Natl Acad Sci USA*. 96: 2350-5.
- Boder ET and KD Wittrup (2000) "Yeast Surface Display for Directed Evolution of Protein Expression, Affinity, and Stability." *Methods Enzymol*. 328: 430-44.
- Datar RV, T Cartwright and CG Rosen (1993) "Process Economics of Animal Cell and Bacterial Fermentations: A Case Study Analysis of Tissue Plasminogen Activator." *Bio-Technology*. 11: 349-57.
- Floege J, A Bartsch, M Schulze, S Shaldon, KM Koch and LC Smeby (1991) "Clearance and Synthesis Rates of Beta-2-Microglobulin in Patients Undergoing Hemodialysis and in Normal Subjects." *J Lab Clin Med*. 118: 153-65.
- Floege J and M Ketteler (2001) "Beta-2-Microglobulin-Derived Amyloidosis: An Update." *Kidney Int*. 59 Suppl 78: S164-71.
- Furuyoshi S, M Nakatani, J Taman, H Kutsuki, S Takata and N Tani (1998) "New Adsorption Column (Lixelle) to Eliminate Beta-2-Microglobulin for Direct Hemoperfusion." *Ther Apher*. 2: 13-7.
- Gejyo F, S Odani, N Yamada, N Honma, H Saito, M Suzuki and e al. (1986) "Beta-2-Microglobulin: A New Form of Amyloid Protein Associated with Chronic Hemodialysis." *Kidney Int*. 30: 385.
- Haugland RP and MK Blagat (1998) In *Immunological Protocols*. Vol. 80 (Ed, Pound, JD) Humana Press Inc., Totowa, NJ: pp. 189-90.
- Kapat A, JK Jung, YH Park, SY Hong and HK Choi (1998) "Effects of Agitation and Aeration on the Production of Extracellular Glucose Oxidase from a Recombinant *Saccharomyces Cerevisiae*." *Bioprocess Engineering*. 18: 347-51.
- Koch KM (1992) "Dialysis-Related Amyloidosis." *Kidney Int*. 41: 1416.
- Martineau P, P Jones and G Winter (1998) "Expression of an Antibody Fragment at High Levels in the Bacterial Cytoplasm." *Journal of Molecular Biology*. 280: 117-27.
- Pavlinkova G, GW Beresford, BJM Booth, SK Batra and D Colcher (1999) "Pharmacokinetics and Biodistribution of Engineered Single-Chain Antibody Constructs of Mab Cc49 in Colon Carcinoma Xenografts." *Journal of Nuclear Medicine*. 40: 1536-46.
- Ronco C, A Brendolan, JF Winchester, E Golds, J Clemmer, HD Polaschegg, TE Muller, G La Greca and NW Levin (2001) "First Clinical Experience with an Adjunctive Hemoperfusion Device Designed Specifically to Remove Beta-2-Microglobulin in Hemodialysis." *Blood Purification*. 19: 260-89.
- Shabunina IV, OI Afanas'eva and SN Pokrovskii (2001) "Immunosorbent for Removal of Beta-2-Microglobulin from Human Blood Plasma." *Bulletin of Experimental Biology and Medicine*. 4: 984-6.
- Shusta EV, MC Kieke, E Parke, DM Kranz and KD Wittrup (1999) "Yeast Polypeptide Fusion Surface Display Levels Predict Thermal Stability and Soluble Secretion Efficiency." *J Mol Biol*. 292: 949-56.
- Vallar L, PM Costa, A Teixeira, M Pfister, R Barrois, PP Costa and C Rivat (1995) "Immunoabsorption Procedure as a Potential Method for the Specific Beta 2-Microglobulin Removal from Plasma of Patients with Chronic Renal Failure." *J Chromatogr B Biomed Appl*. 664: 97-106.

Vincent C, N Pozet and JP Revillard (1980) "Plasma Beta-2 Microglobulin Turnover in Renal-Insufficiency." *Acta Clinica Belgica*. 35: 2-13.

Xu MQ and TC Evans (2001) "Intein-Mediated Ligation and Cyclization of Expressed Proteins." *Methods*. 24: 257-77.

# Appendix: Immunoadsorption Model FORTRAN 77 Program

```
PROGRAM CIRCUIT

C      KM:          MASS-TRANSFER COEFFICIENT [m/sec]
C      NRSTEP:     NUMBER OF RADIAL STEPS [-]
C      RADIUS:     AVERAGE BEAD RADIUS [micron]
C      TTIME:     TOTAL INTEGRATION TIME [minutes]
C      C0:         INITIAL PATIENT B2M CONCENTRATION [mg/L]
C      DT:         SCALED TIME STEP [-]
C      DE:         EFFECTIVE DIFFUSIVITY [m^2/sec]
C      PA1:        OLD SCALED PATIENT CONCENTRATION
C      PA2:        NEW SCALED PATIENT CONCENTRATION
C      KPA:        PATIENT RUNGE-KUTTA PARAMETER
C      BL0:        INITIAL SCALED BLOOD CHAMBER CONCENTRATION
C      BL1:        OLD SCALED BLOOD CHAMBER CONCENTRATION
C      BL2:        NEW SCALED BLOOD CHAMBER CONCENTRATION
C      KBL:        BLOOD CHAMBER RUNGE-KUTTA PARAMETER
C      MEM1:       OLD SCALED AVERAGE MEMBRANE CONCENTRATION
C      MEM2:       NEW SCALED AVERAGE MEMBRANE CONCENTRATION
C      KMEM:       MEMBRANE RUNGE-KUTTA PARAMETER
C      PL0:        INITIAL SCALED PLASMA CHAMBER CONCENTRATION
C      PL1:        OLD SCALED PLASMA CHAMBER CONCENTRATION
C      PL2:        NEW SCALED PLASMA CHAMBER CONCENTRATION
C      KPL:        PLASMA CHAMBER RUNGE-KUTTA PARAMETER
C      BE1:        OLD SCALED BEAD CONCENTRATION
C      BE2:        NEW SCALED BEAD CONCENTRATION
C      KBE:        BEAD RUNGE-KUTTA PARAMETER
C      CC1:        OLD SCALED COLLECTION CHAMBER CONCENTRATION
C      CC2:        NEW SCALED COLLECTION CHAMBER CONCENTRATION
C      KCC:        COLLECTION CHAMBER RUNGE-KUTTA PARAMETER
C      VFPR1:      OLD SCALED VFPR EXIT CONCENTRATION
C      VFPR2:      NEW SCALED VFPR EXIT CONCENTRATION
C      KVFPR:      VFPR EXIT RUNGE-KUTTA PARAMETER
C      KD:         ANTIBODY-B2M DISSOCIATION CONSTANT, BASED ON
C      ==>>>>    BULK CONCENTRATION/SETTLED VOLUME
C      ==>>>>>> [mg-B2m/L-total fluid]
C      DS:         DENSITY OF B2M BINDING SITES [mg-B2m/settled-L-gel]
C      PHI:        PARTITION COEFFICIENT [pore conc./surface conc.]
C      EPS:        GEL BED VOID FRACTION [EMPTY VOL/BED VOL]
C      SPHI:       GEL BEAD PORE VOLUME FRACTION [L-pores/L-bead]
C      VPLASMA:    TOTAL PLASMA CHAMBER VOLUME [ml]
C      VBLOOD:     WET GEL BEAD VOLUME [ml]
C      VBLOOD():  BLOOD CHAMBER VOLUMES (INCL. CELLS) [ml]
C      VPATIENT:   CELL-FREE PATIENT VOLUME (INCL. CELLS) [ml]
C      VCC:        VOLUME OF PLASMA COLLECTION CHAMBER (ml)
C      Q:          CELL-FREE CIRCUIT FLOWRATE [ml/min]
C      QM:         PLASMA FLOWRATE THROUGH MEMBRANE [ml/min]
C      XB:         PLASMA FLOW BYPASS FRACTION [-]
C      TPROC:      PROCESS TIME SCALE [sec]
C      TPAT:       PATIENT SPACE-TIME [sec]
C      TBLOOD():  PLASMA RESIDENCE TIME OF BLOOD COMPARTMENT TANKS [sec]
C      TPLAS:     PLASMA CHAMBER SPACE-TIME [sec]
```

```

C      TBEXT:      BEAD EXTERNAL MASS-TRANSFER TIME SCALE [sec]
C      TBEINT:     BEAD INTERNAL MASS-TRANSFER TIME SCALE [sec]
C      ERROR:      RELATIVE ERROR IN MASS BALANCE
C      TOLER:      MASS BALANCE ERROR TOLERANCE
C      INBEAD:     TOTAL B2M IN AND ON THE BEADS [mg]
C      ADSORBED:   TOTAL B2M ADSORBED AT THE END OF SIMULATION
C      MAXERROR:   THE MAXIMUM AMOUNT OF ERROR IN THE MASS BALANCE
C      MAXERRJ:    THE TIME STEP NUMBER AT WHICH MAXERROR OCCURS
C      NPA:        NUMBER OF PATIENT "TANKS-IN-SERIES"
C      NBL:        NUMBER OF BLOOD COMPARTMENT "TANKS-IN-SERIES"
C      NPL:        NUMBER OF PLASMA COMPARTMENT "TANKS-IN-SERIES"
C      PAMASS:     MASS OF B2M IN PATIENT AT TIME T [MG]
C      BLMASS:     MASS OF B2M IN BLOOD CHAMBER AT TIME T [MG]
C      PLMASS:     MASS OF B2M IN PLASMA CHAMBER AT TIME T [MG]
C      MASS0:      INITIAL MASS OF B2M IN THE SYSTEM [MG]
C      HCT0:       PATIENT HEMATOCRIT
C      HCT():      BLOOD COMPARTMENT TANK HEMATOCRITS
C      TOTALVOL:   TOTAL CELL-FREE, POLYMER-FREE, VOLUME OF SYSTEM [L]

      INTEGER I, J, M, NTSTEP, COUNT, NWRITE, MAXERRJ, NPA, NBL, NPL,
X      NRSTEP

      REAL*8 RADIUS, C0, KM, DT, KD, DS, PHI, INBEAD, TOLER, ERROR,
X      MAXERROR, DR, VPLASMA, VBEAD, VPATIENT,Q, XB, TPROC,
X      TPAT, TPLAS, TCC, TBEXT, BL0, PL0, PAMASS, BLMASS,
X      PLMASS, DE, TBEINT, EPS, SPHI, VBLTOTAL, CC1, CC2,
X      MEM1, MEM2, VFPR1, VFPR2, KVFPR, KMEM, KCC, HCT0,
X      QMUPTOI, MASS0, TOTALVOL

      REAL*8, ALLOCATABLE :: BE1(:, :), BE2(:, :), PA1(:), PA2(:),
X      BL1(:), BL2(:), PL1(:), PL2(:), VBLOOD(:), TBLOOD(:),
X      KPA(:), KBL(:), KPL(:), KBE(:, :), ADSORBED(:),
X      DESORBED(:), HCT(:)

C      READ INPUT FILE

      OPEN(UNIT = 5, FILE='INPUT.DAT', STATUS = 'OLD')
      READ(5,*) BL0, PL0
      READ(5,*) NPA, NBL, NPL
      READ(5,*) RADIUS
      READ(5,*) NRSTEP
      READ(5,*) TTIME
      READ(5,*) NWRITE
      READ(5,*) C0
      READ(5,*) KM
      READ(5,*) DE
      READ(5,*) KD
      READ(5,*) DS
      READ(5,*) PHI
      READ(5,*) SPHI
      READ(5,*) EPS
      READ(5,*) VPATIENT
      VPATIENT = VPATIENT*1000

C      DIMENSION ARRAYS ACCORDINGLY
      ALLOCATE ( PA1(1:NPA), PA2(1:NPA), BL1(1:NBL), BL2(1:NBL),

```

```

X          PL1(1:NPL), PL2(1:NPL), BE1(1:NPL,0:NRSTEP),
X          BE2(1:NPL,0:NRSTEP), KPA(1:NPA), KBL(1:NBL),
X          KPL(1:NPL), KBE(1:NPL,0:NRSTEP), ADSORBED(1:NPL),
X          DESORBED(1:NPL), VBLOOD(1:NBL), HCT(1:NBL),
X          TBLOOD(1:NBL) )

      READ(5,*) HCT0
      READ(5,*) (VBLOOD(I), I=1,NBL)
      READ(5,*) VPLASMA
      READ(5,*) VBEAD
      READ(5,*) VCC
      READ(5,*) Q
      READ(5,*) QM
      READ(5,*) XB
      READ(5,*) TOLER

      CLOSE(5)

C      CALCULATE TOTAL BLOOD CHAMBER VOLUME
      VBLTOTAL = 0
      DO 5 I= 1,NBL
        VBLTOTAL = VBLTOTAL + VBLOOD(I)
5      CONTINUE

C      CALCULATE TIME SCALES
      TPAT = VPATIENT/Q*60
      TPLAS = (VPLASMA-(1-EPS)*VBEAD)/((1-XB)*QM)*60

      QMUPTOI = 0
      DO 7 I = 1, NBL
        QMUPTOI = QMUPTOI + QM/VBLTOTAL*VBLOOD(I)
        HCT(I) = Q*HCT0/(Q-QMUPTOI)
        TBLOOD(I) = 60 * (1-HCT(I))*VBLOOD(I) /
X          (QM/VBLTOTAL*VBLOOD(I)+(1-HCT(I))*(Q-QMUPTOI))
7      CONTINUE

      TBEEEXT = (RADIUS*1E-6)*(VPLASMA-(1-EPS)*VBEAD)/
X          (3*(1-EPS)*VBEAD*KM*SPHI)
      TBEINT = (RADIUS*1E-6)**2/DE
      TCC = VCC/QM*60

C      DEFINE THE PROCESS TIME-SCALE
      TPROC = (VPATIENT+VBLTOTAL*BL0)/(1-XB)/QM*60

C      CALCULATE THE SCALED TIME STEP
      IF ((TBEINT/(2.2*REAL(NRSTEP)**2)).LT.(TBEEEXT*0.05)) THEN
        DT = TBEINT/TPROC/(2.2*REAL(NRSTEP)**2)
        PRINT*, 'INTERNAL DIFFUSION LIMITED.'
      ELSE
        DT = TBEEEXT/TPROC*0.05
        PRINT*, 'EXTERNAL DIFFUSION LIMITED.'
      END IF

C      CALCULATE THE SCALED RADIAL STEP

```

```

DR = 1/REAL(NRSTEP)

C      CALCULATE THE INITIAL MASS OF B2M IN SYSTEM
      MASS0 = C0/1000 * ( VPATIENT*(1-HCT0) +
X          PL0*(VPLASMA-VBEAD*(1-EPS)) )
      TOTALVOL = (VPATIENT*(1-HCT0) + VPLASMA
X          - (1-SPHI)*(1-EPS)*VBEAD + VCC)/1000
      DO 8 I = 1, NBL
          MASS0 = MASS0 + C0/1000 * BL0 * VBLOOD(I) * (1-HCT(I))
          TOTALVOL = TOTALVOL + VBLOOD(I) * (1-HCT(I))/1000
8      CONTINUE

C      BEGIN WRITING THE PARAMETER OUTPUT FILE

      OPEN(UNIT = 7, FILE='PARAMETER.DAT', STATUS='UNKNOWN')
      WRITE(7,20) 'INITIAL BLOOD CHAMBER CONCENTRATION: ', BL0
      WRITE(7,20) 'INITIAL PLASMA CHAMBER CONCENTRATION: ', PL0
      WRITE(7,20) 'PARTICLE RADIUS: ', RADIUS, ' MICRONS'
      WRITE(7,25) 'NUMBER OR RADIAL STEPS: ', NRSTEP
      WRITE(7,20) 'TOTAL INTEGRATION TIME: ', TTIME, ' MINUTES'
      WRITE(7,20) 'INITIAL B2M CONCENTRATION: ', C0, ' MG/L'
      WRITE(7,20) 'SCALED TIME STEP: ', DT
      WRITE(7,20) 'TIME STEP: ', DT*TPROC, ' SECONDS'
      WRITE(7,20) 'MASS-TRANSFER COEFFICIENT: ', KM, ' M/SEC'
      WRITE(7,20) 'EFFECTIVE DIFFUSIVITY: ', DE, ' M^2/SEC'
      WRITE(7,20) 'BULK DISSOCIATION CONSTANT: ', KD, ' MG-B2M/L'
      WRITE(7,20) 'BINDING SITE DENSITY: ', DS, ' MG-B2M/SETTLED-L'
      WRITE(7,20) 'PARTITION COEFFICIENT: ', PHI
      WRITE(7,20) 'PORE VOLUME FRACTION: ', SPHI,
X      ' PORE/BEAD VOLUME'
      WRITE(7,20) 'SETTLED-BED VOID FRACTION: ', EPS
      WRITE(7,20) 'PATIENT VOLUME (CELLS INLC.): ',
X          VPATIENT/1000, ' L'
      DO 10 I = 1, NBL
          WRITE(7,15) 'BLOOD CHAMBER TANK ',I,
X          ' VOLUME: ', VBLOOD(I), ' ML'
10      CONTINUE
      WRITE(7,20) 'TOTAL BLOOD CHAMBER VOLUME: ', VBLTOTAL, 'ML'
      WRITE(7,20) 'TOTAL PLASMA CHAMBER VOLUME: ', VPLASMA, ' ML'
      WRITE(7,20) 'TOTAL BEAD VOLUME: ', VBEAD, ' ML'
      WRITE(7,20) 'TOTAL INITIAL CELL-FREE VOLUME: ', TOTALVOL, ' L'

      WRITE(7,20) 'INITIAL TOTAL B2M IN SYSTEM: ', MASS0, ' MG'
      WRITE(7,20) 'MASS ERROR TOLERANCE: ', TOLER
      WRITE(7,20) 'CIRCULATION FLOWRATE (CELL INCL.): ',
X      Q, ' ML/MIN'
      WRITE(7,20) 'PATIENT HEMATOCRIT: ', HCT0, ' HCT'
      DO 11 I = 1, NBL
          WRITE(7,15) 'BLOOD CHAMBER HCT,', I, ': ', HCT(I), 'HCT'
11      CONTINUE
      WRITE(7,20) 'MEMBRANE PLASMA FLOWRATE: ', QM, ' ML/MIN'
      WRITE(7,20) 'PLASMA CHAMBER BYPASS FRACTION: ', XB
      WRITE(7,20) 'PATIENT SPACE-TIME: ', TPAT/60, ' MIN'
      DO 12 I = 1, NBL
          WRITE(7,15) 'BLOOD CHAMBER TAU,', I, ': ', TBLOOD(I), 'SEC'

```

```

12      CONTINUE
        WRITE(7,20) 'PLASMA CHAMBER SPACE-TIME:  ', TPLAS, ' SEC'
        WRITE(7,20) 'INTERNAL BEAD TIME-SCALE:  ', TBEINT, ' SEC'
        WRITE(7,20) 'EXTERNAL BEAD TIME-SCALE:  ', TBEXT, ' SEC'
        WRITE(7,20) 'PROCESS TIME-SCALE:  ', TPROC/60, ' MIN'
        WRITE(7,25) 'NUMBER OF PATIENT TANKS:  ', NPA
        WRITE(7,25) 'NUMBER OF BLOOD CHAMBER TANKS:  ', NBL
        WRITE(7,25) 'NUMBER OF PLASMA CHAMBER TANKS:  ', NPL
15      FORMAT(A19, I1, A10, E12.4, A20)
20      FORMAT(A30, E12.4, A20)
25      FORMAT(A30, I12, A20)

C      CONVERT KD AND DS FROM A BULK BASIS TO A PORE BASIS
      KD = KD * PHI
      DS = DS/SPHI/(1-EPS)

C      SPECIFY INITIAL CONDITIONS

      DO 30 I = 1, NPA
        PA1(I) = 1.0
30     CONTINUE
      DO 35 I = 1, NBL
        BL1(I) = BL0
35     CONTINUE
      DO 40 I = 1, NPL
        PL1(I) = PL0
        DO 37 M = 0, NRSTEP
          BE1(I,M) = 0.0
37     CONTINUE
40     CONTINUE

      CC1 = 0
      MEM1 = BL0
      VFPR1 = 1/Q/(1-HCT0) * ( (1-XB)*QM*CC1 + XB*QM*MEM1 +
X          (Q-QM)*BL1(NBL)*(1-HCT(NBL)) )

C      OPEN PROCESS OUTPUT FILE

      OPEN(UNIT=9, FILE='SYSTEM.OUT', STATUS = 'UNKNOWN')
      WRITE(9,'(8A14)') 'TIME, MIN', 'PATIENT', 'BLOOD',
X          'PL CHAMB', 'LST BD CNTR', 'PL LINE', 'INBEAD, MG',
X          'ERROR'
      WRITE(9,'(8E14.5)') 0.0, PA1(NPA), BL1(NBL), PL1(1),
X      BE1(NPL,NRSTEP), (XB*MEM1+(1-XB)*CC1), 0.0, 0.0

C      INITIALIZE COUNTER AND MAXERROR
      COUNT = 0
      MAXERROR = 0.0
      MAXERRJ = 0

C      CALCULATE THE NUMBER OF TIMESTEPS IN THE SIMULATION
      NTSTEP = INT(TTIME*60/TPROC/DT)+1
      PRINT*, 'NUMBER OF TIMESTEPS CALCULATED'

C      PERFORM NUMERICAL INTEGRATION USING SECOND ORDER RUNGE-KUTTA

```

```

DO 200 J = 1, NTSTEP

C      CALCULATE THE RUNGE-KUTTA PARAMETERS FOR THE PATIENT

      KPA(1) = PA1(1) + REAL(NPA)*0.5*DT*TPROC/TPAT*(VFPR1-PA1(1))
      IF (NPA.GT.1) THEN
        DO 50 I = 2, NPA
          KPA(I) = PA1(I) +
X          REAL(NPA)*0.5*DT*TPROC/TPAT*(PA1(I-1)-PA1(I))
50      CONTINUE
      END IF

C      CALCULATE THE RUNGE-KUTTA PARAMETERS FOR THE BLOOD CHAMBER

      KBL(1) = BL1(1) +
X          0.5*DT*TPROC/TBLOOD(1)*(PA1(NPA)-BL1(1))

      IF (NBL.GT.1) THEN
        DO 60 I = 2, NBL
          KBL(I) = BL1(I) +
X          0.5*DT*TPROC/TBLOOD(I) * (BL1(I-1)-BL1(I))
C          PRINT*, 'KBL(', I,') CALCULATED AS: ', KBL(I)
60      CONTINUE
      END IF

C      CALCULATE THE RUNGE-KUTTA PARAMETER FOR THE MEMBRANE
      KMEM = 0
      DO 62 I = 1, NBL
        KMEM = KMEM + VBLOOD(I)*KBL(I)/VBLTOTAL
C        PRINT*, 'KMEM CALCULATED THROUGH TANK ', I, ' AS: ', KMEM
62      CONTINUE

C      CALCULATE THE RUNGE-KUTTA PARAMETERS FOR THE PLASMA CHAMBER

      KPL(1) = PL1(1) +
X          REAL(NPL)*0.5*DT*TPROC/TPLAS*(MEM1-PL1(1)) +
X          0.5*DT*TPROC/TBEXT*(BE1(1,0)/PHI-PL1(1))

      IF (KPL(1).LT.0) THEN
        PRINT*, 'KPL(1) IS LESS THAN ZERO'

        PRINT*, 'TIME COUNTER (J) = ', J
        CLOSE (7)
        CLOSE (9)
        STOP
      END IF

C      SPECIFY BEAD SURFACE BOUNDARY CONDITION
      KBE(1,0) = (KM*PL1(1)+(DE/(DR*RADIUS*1E-6))*BE1(1,1)) /
X          (KM/PHI+DE/(DR*RADIUS*1E-6))

      IF ((J.GT.10).AND.(KBE(1,0).EQ.0)) THEN

```

```

        PRINT*, 'ERROR:  KBE(1,0) = ', KBE(1,0), ' J = ', J
        CLOSE(7)
        CLOSE(9)
        STOP
    END IF

    DO 65 M = 1, NRSTEP-1
        KBE(1,M) = BE1(1,M) + 0.5*TPROC/TBEINT*
X          ((BE1(1,M+1)-2*BE1(1,M)+BE1(1,M-1))*DT/(DR)**2
X          -DT*(BE1(1,M+1)-BE1(1,M-1))/(DR*(1-REAL(M)*DR)))
X
X          / (1+DS*KD/(KD+C0*BE1(1,M))**2)
65    CONTINUE

C      SPECIFY NO-FLUX AT THE CENTER
        KBE(1,NRSTEP) = BE1(1,NRSTEP) + TPROC/TBEINT *
X          (BE1(1,NRSTEP-1)-BE1(1,NRSTEP))*DT/(DR)**2
X          / (1+DS*KD/(KD+C0*BE1(1,NRSTEP))**2)

        IF (NPL.GT.1) THEN
        DO 70 I = 2, NPL
            KPL(I) = PL1(I) +
X              REAL(NPL)*0.5*DT*TPROC/TPLAS*(PL1(I-1)-PL1(I)) +
X              0.5*DT*TPROC/TBEEEXT*(BE1(I,0)/PHI-PL1(I))

C      SPECIFY BEAD SURFACE BOUNDARY CONDITION
        KBE(I,0) = (KM*PL1(I)+(DE/(DR*RADIUS*1E-6))*BE1(I,1)) /
X          (KM/PHI+DE/(DR*RADIUS*1E-6))

        DO 67 M = 1, NRSTEP-1
            KBE(I,M) = BE1(I,M) + 0.5*TPROC/TBEINT*
X          ((BE1(I,M+1)-2*BE1(I,M)+BE1(I,M-1))*DT/(DR)**2
X          -DT*(BE1(I,M+1)-BE1(I,M-1)) /
X          (DR*(1-REAL(M)*DR))) /
X          (1+DS*KD/(KD+C0*BE1(I,M))**2)
67    CONTINUE

C      SPECIFY NO-FLUX AT THE CENTER
        KBE(I,NRSTEP) = BE1(I,NRSTEP) + TPROC/TBEINT *
X          (BE1(I,NRSTEP-1)-BE1(I,NRSTEP))*DT/(DR)**2
X          / (1+DS*KD/(KD+C0*BE1(I,NRSTEP))**2)
70    CONTINUE
        END IF

C      CALCULATE THE RUNGA-KUTTA PARAMETER FOR THE COLLECTION CHAMBER
AND VFPR
        KCC = CC1 + 0.5*DT*TPROC/TCC*(PL1(NPL)-CC1)
        KVFPR = ( (1-XB)*QM*KCC + XB*QM*KMEM +
X          (Q-QM)*KBL(NBL)*(1-HCT(NBL)) ) / Q/(1-HCT0)

C      CALCULATE THE PATIENT CONCENTRATIONS

        PA2(1) = PA1(1) + REAL(NPA)*DT*TPROC/TPAT*(KVFPR-KPA(1))
        IF (NPA.GT.1) THEN
        DO 80 I = 2, NPA
            PA2(I) = PA1(I) + REAL(NPA)*DT*TPROC/TPAT*(KPA(I-1)-KPA(I))
80    CONTINUE

```

```

END IF

C      CALCULATE THE BLOOD COMPARTMENT CONCENTRATIONS

BL2(1) = BL1(1) + DT*TPROC/TBLOOD(1) * (KPA(NPA)-KBL(1))
IF (NBL.GT.1) THEN
DO 100 I = 2, NBL
    BL2(I) = BL1(I) +
X      DT*TPROC/TBLOOD(I) * (KBL(I-1)-KBL(I))
100  CONTINUE
END IF

C      CALCULATE THE NEW MEMBRANE CONCENTRATION
MEM2 = 0
DO 102 I = 1, NBL
    MEM2 = MEM2 + VBLOOD(I)*BL2(I)/VBLTOTAL
102  CONTINUE

C      CALCULATE THE PLASMA CHAMBER AND BEAD CONCENTRATIONS

PL2(1) = PL1(1) + REAL(NPL)*DT*TPROC/TPLAS*(KMEM-KPL(1))+
X      DT*TPROC/TBEXT*(KBE(1,0)/PHI-KPL(1))

IF (PL2(1).LT.0) THEN
    PRINT*, 'PL2(1) IS LESS THAN ZERO'
    PRINT*, 'TIME COUNTER (J) = ', J
    PRINT*, 'KMEM = ', KMEM
    PRINT*, 'KPL(1) = ', KPL(1)
    CLOSE (7)
    CLOSE (9)
    STOP
END IF

C      SPECIFY BEAD SURFACE BOUNDARY CONDITION
BE2(1,0) = (KM*KPL(1)+(DE/(DR*RADIUS*1E-6))*KBE(1,1)) /
X      (KM/PHI+DE/(DR*RADIUS*1E-6))

IF ((J.GT.10).AND.(BE2(1,0).EQ.0)) THEN
    PRINT*, 'ERROR: BE2(1,0) = ', BE2(1,0), ' J = ', J
    CLOSE(7)
    CLOSE(9)
    STOP
END IF

DO 105 M = 1, NRSTEP-1
    BE2(1,M) = BE1(1,M) + TPROC/TBEINT*
X      ((KBE(1,M+1)-2*KBE(1,M)+KBE(1,M-1))*DT/(DR)**2
X      -DT*(KBE(1,M+1)-KBE(1,M-1))/(DR*(1-REAL(M)*DR)))
X      / (1+DS*KD/(KD+C0*KBE(1,M))**2)
105  CONTINUE

C      SPECIFY NO-FLUX AT THE CENTER
BE2(1,NRSTEP) = KBE(1,NRSTEP) + TPROC/TBEINT * 2 *
X      (KBE(1,NRSTEP-1)-KBE(1,NRSTEP))*DT/(DR)**2
X      / (1+DS*KD/(KD+C0*KBE(1,NRSTEP))**2)

```

```

IF (NPL.GT.1) THEN

DO 110 I = 2, NPL
  PL2(I) = PL1(I) +
X      REAL(NPL)*DT*TPROC/TPLAS*(KPL(I-1)-KPL(I)) +
X      DT*TPROC/TBEEEXT*(KBE(I,0)/PHI-KPL(I))

C      SPECIFY BEAD SURFACE BOUNDARY CONDITION
X      BE2(I,0) = (KM*KPL(I)+(DE/(DR*RADIUS*1E-6))*KBE(I,1))/
              (KM/PHI+DE/(DR*RADIUS*1E-6))

DO 107 M = 1, NRSTEP-1
  BE2(I,M) = BE1(I,M) + TPROC/TBEINT*
X          ((KBE(I,M+1)-2*KBE(I,M)+KBE(I,M-1)) *
X          DT/(DR)**2-DT*(KBE(I,M+1)-KBE(I,M-1)) /
X          (DR*(1-REAL(M)*DR))) /
X          (1+DS*KD/(KD+C0*KBE(I,M))**2)
107  CONTINUE
C      SPECIFY NO-FLUX AT THE CENTER
X      BE2(I,NRSTEP) = KBE(I,NRSTEP) + TPROC/TBEINT *
X          (KBE(I,NRSTEP-1)-KBE(I,NRSTEP))*DT/(DR)**2
          / (1+DS*KD/(KD+C0*KBE(I,NRSTEP))**2)

110  CONTINUE
      END IF

C      CALCULATE THE COLLECTION CHAMBER AND VFPR CONCENTRATIONS
      CC2 = CC1 + DT*TPROC/TCC*(KPL(NPL)-KCC)
      VFPR2 = ( (1-XB)*QM*CC2 + XB*QM*MEM2 + (Q-QM)*BL2(NBL)*
X          (1-HCT(NBL)) ) / Q / (1-HCT0)

C      RESET CONCENTRATION VARIABLES AND CALCULATE COMPARTMENT MASSES

      PAMASS = 0.0
      BLMASS = 0.0
      PLMASS = 0.0
      INBEAD = 0.0

DO 120 I = 1, NPA
  PA1(I) = PA2(I)
  PAMASS = PAMASS + PA1(I)*VPATIENT*(1-HCT0)*C0/1000/REAL(NPA)
120  CONTINUE

DO 130 I = 1, NBL
  BL1(I) = BL2(I)
  BLMASS = BLMASS + BL1(I)*VBLOOD(I)*(1-HCT(I))*C0/1000
130  CONTINUE

DO 140 I = 1, NPL
  PL1(I) = PL2(I)
  PLMASS = PLMASS +
X      PL1(I)*(VPLASMA-(1-EPS)*VBEAD)*C0/1000/REAL(NPL)

      BE1(I,NRSTEP) = BE2(I,NRSTEP)
      ADSORBED(I) = 0.0

```

```

        DESORBED(I) = 0.0
        DO 135 M = 0, NRSTEP-1
            BE1(I,M) = BE2(I,M)
            ADSORBED(I) = 3*VBEAD*(1-EPS)/1000*DR*C0*(DS*(BE1(I,M) +
X                BE1(I,M+1))/2
X                /(KD+C0*(BE1(I,M)+BE1(I,M+1))/2))/REAL(NPL)
X                * (1-(M+0.5)*DR)**2 * SPHI + ADSORBED(I)
            DESORBED(I) = 3*VBEAD*(1-EPS)/1000*DR*C0 *
X                (SPHI*(BE1(I,M)+BE1(I,M+1))/2)
X                / REAL(NPL) * (1-(M+0.5)*DR)**2 + DESORBED(I)
135    CONTINUE

        INBEAD = INBEAD + ADSORBED(I) + DESORBED(I)

140    CONTINUE

        MEM1 = MEM2
        CC1 = CC2
        VFPR1 = VFPR2

C        CONFIRM THE B2M MASS BALANCE

        ERROR = 1 - ( PAMASS + BLMASS + PLMASS + INBEAD +
X                C0*VCC*CC1/1000 )/MASS0

        IF ((ABS(ERROR)).GT.(ABS(MAXERROR))) THEN
            MAXERROR = ERROR
            MAXERRJ = J
        END IF

C        WRITE THE CONCENTRATION PROFILE TO THE OUTPUT FILES

        IF (INT((DBLE(NTSTEP)/DBLE(NWRITE))).EQ.
X        (INT(DBLE(J)-DBLE(COUNT) *
X        DBLE(NTSTEP)/DBLE(NWRITE))))
X        THEN
            WRITE(9, '(8E14.5)') REAL(J)*DT*TPROC/60,
X            PA1(NPA), BL1(NBL), PL1(NPL), BE1(NPL, NRSTEP),
X            ((1-XB)*CC1+XB*MEM1),
X            INBEAD, ERROR

145        FORMAT(A35,E14.5)
            COUNT = COUNT + 1
        END IF

C        WRITE MASS BALANCE ERROR MESSAGE AND QUIT

        IF (ABS(ERROR).GT.(TOLER)) THEN
            PRINT*, 'ERROR:  B2M MASS BALANCE VIOLOATION.'

            WRITE(9, *) 'ERROR: B2M MASS BALANCE VIOLOATION.'
            WRITE(9, *) 'J = ', J, ' (NUMBER OF TIME STEPS)'
            WRITE(9, *) 'PERCENT ERROR: ', ERROR*100
            CLOSE(7)
            CLOSE(9)

```

```
STOP
END IF
```

```
200 CONTINUE
```

```
C FINISH WRITTING THE PARAMTER OUTPUT FILE
```

```
WRITE(7,*)
WRITE(7,20) 'TOTAL B2M IN THE BEADS: ', INBEAD, 'MG'
WRITE(7,20) 'MAXIMUM MASS BALANCE ERROR: ',MAXERROR*100,
X      'PERCENT'
WRITE(7,25) 'TIME STEP NO. AT MAXERROR: ',MAXERRJ, ' '
WRITE(7,20) 'TIME AT MAX ERROR: ',
X      MAXERRJ*DT*TPROC/60, ' MIN'
WRITE(7,20) 'FINAL TOTAL SYSTEM B2M: ', PAMASS + BLMASS +
X      PLMASS + INBEAD + C0*VCC*CC1/1000, ' MG'
WRITE(7,20) 'FINAL MASS BALANCE ERROR: ', ERROR*100, 'PERCENT'
WRITE(7,20) 'FINAL MEAN PATIENT CONCENTRATION: ',
X      PAMASS/(1-HCT0)/VPATIENT*1000, 'MG/L'
WRITE(7,20) 'FINAL MEAN PLASMA CHAMBER CONC.: ',
X      PLMASS/(1-EPS)/VPLASMA*1000, 'MG/L'
WRITE(7,20) 'FINAL PLASMA LINE CONC.: ',
X      (XB*MEM1+(1-XB)*CC1)*C0, 'MG/L'
WRITE(7,20) 'FINAL BEAD CENTER CONC.S (MG/L): '
WRITE(7,300) (C0*BE1(I,NRSTEP), I=1,NPL)
300 FORMAT(10E14.5)
```

```
C CLOSE OUTPUT FILES
```

```
CLOSE(7)
CLOSE(9)
```

```
END
```

